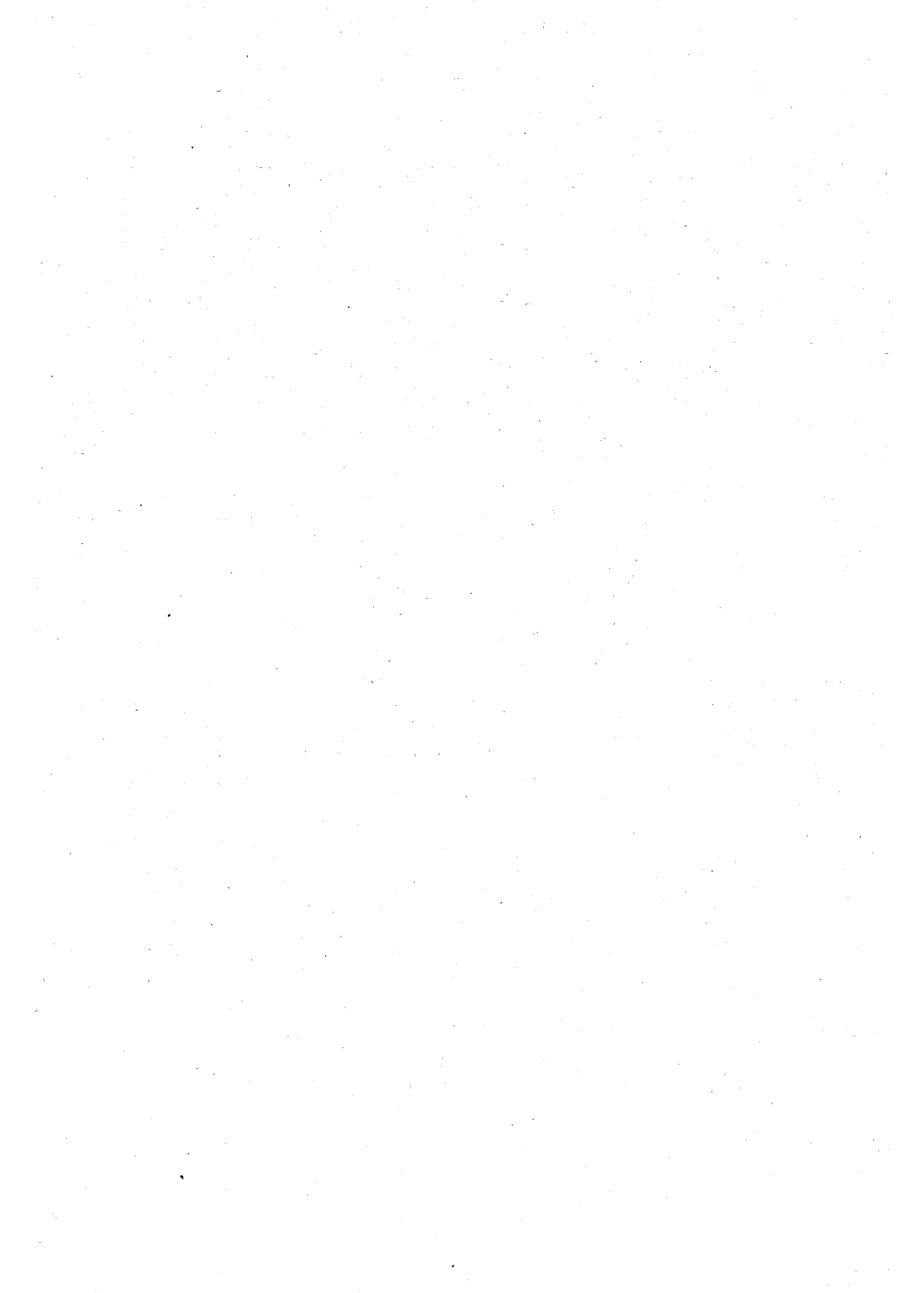
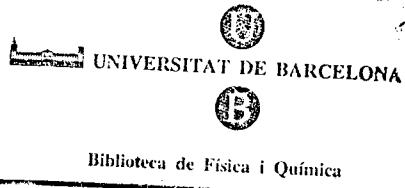


Universitat de Barcelona
Departament de Física Fonamental
Facultat de Física

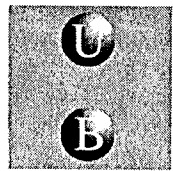
Search for Monochromatic
Gravitational-Wave Signals in Data of the
Cryogenic Detector “Explorer”

Miquel Montero Torralbo





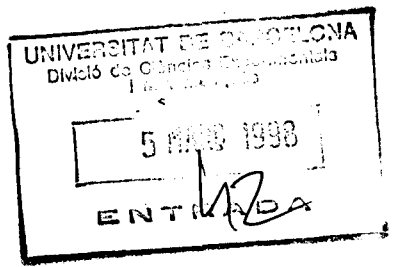
Biblioteca de Física i Química



Universitat de Barcelona
Departament de Física Fonamental
Facultat de Física

Search for Monochromatic
Gravitational-Wave Signals in Data of the
Cryogenic Detector “Explorer”

Miquel Montero Torralbo



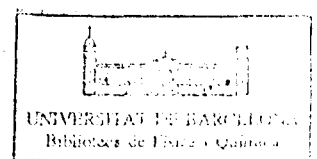
Programa de doctorat: *Mètodes Estadístics en la Física*
Bienni 1993-1995

Memòria presentada per Miquel Montero Torralbo per optar al títol de
Doctor en Ciències Físiques.

Certifico que la present tesi doctoral ha estat realitzada
sota la meva direcció. Barcelona, Març de 1998.

A handwritten signature in black ink, appearing to read 'Lobo' or 'Lobos'.

José Alberto Lobo Gutiérrez
Professor Titular
Departament de Física Fonamental
Universitat de Barcelona



A l'Ester, perquè al cap-davall la tesis només m'ha ocupat un terç dels darrers quatre anys i escaig. Ella en canvi m'ha hagut de suportar la resta del temps.

I

Nunca persegui la gloria,
ni dejar en la memoria
de los hombres mi canción;
yo amo los mundos sutiles,
ingrávidos y gentiles,
como pompas de jabón.
Me gusta verlos pintarse
de sol y grana, volar
bajo el cielo azul, temblar
súbitamente y quebrarse.

IV

Nuestras horas son minutos
cuando esperamos saber,
y siglos cuando sabemos
lo que se puede aprender.

VIII

En preguntar lo que sabes
el tiempo no has de perder...
Y a preguntas sin respuesta
¿quién te podrá responder?

XXIX

Caminante, son tus huellas
el camino y nada más;
caminante, no hay camino,
se hace camino al andar.
Al andar se hace camino,
y al volver la vista atrás
se ve la senda que nunca
se ha de volver a pisar.
Caminante, no hay camino,
sino estelas en la mar.

XLIV

Todo pasa y todo queda,
pero lo nuestro es pasar;
pasar haciendo caminos,
caminos sobre la mar.

—Antonio Machado,
Proverbios y Cantares

Agraïments

Com és evident que la realització d'una tesi no es qüestió de quatre dies, sinó més aviat de quatre anys (i escaig) el nombre de persones involucrades no es pot reduir a una, sinó que frega la cinquantena.

En primer lloc és de justícia agrair al meu director de tesi, José Alberto Lobo tot allò que ha fet perquè aquest treball que teniu a les mans hagi vist finalment la llum. En segon lloc, manifestar la meva gratitud cap a les persones que tan gentilment han acceptat de participar en l'evaluació de la meva feina. Per una banda els membres del tribunal, tant els titulars com els suplents: Chus Martín, Enric Verdaguer, Pia Astone, Josep Llosa i Paco Fayos, Jaume Massoliver i Domènech Espriu, respectivament. Per altra banda, aquells que amb els seus informes faran possible l'obtenció del grau de doctor europeu: Guido Pizzella i Bernard Schutz.

A molts d'aquests, però, no només els he d'agrair el fet puntual de jutjar el meu treball. Guido Pizzella i Pia Astone van fer possible en l'aspecte professional, que jo tingués accés a les dades de l'*Explorer*, sense les quals, com diu el tòpic, tot això no hauria estat possible. A més, en l'aspecte personal, la meva gratitud no té límits després de l'exquisit tracte rebut de part seva, i de la resta dels membres del grup *ROG* —Enzo Silvestri, Eugenio Coccia, Viviana Fafone, Gianni Federici, Carlo Cosmelli, i Giovanni Pallottino, entre d'altres— al llarg dels quatre mesos llargs que jo i l'Ester, la meva dona (què estrany que em sona!), vam passar a cavall de Roma i Frascati (a càrec de l'*INFN*), i per fer molt més fàcil la nostra existència en aquelles meravelloses terres. L'Enric Verdaguer, així com en José M. M. Senovilla, l'Eduard Salvador i en Ramón Canal, em van posar les coses senzilles amb els seus cursos de doctorat en aquells temps, mentre jo era fora. En Paco Fayos ha estat el meu company de despatx *de facto* durant els darrers mesos en què, de manera lenta però implacable, he anant prenent possessió del *fismat*, l'ordinador que ha fet la feina fosca de la meva tesi. La resta del temps, el Josep Llosa i l'Alfred Molina han estat primer magnífics veïns, i amb el temps han esdevingut bons amics.

Encara que si d'amics he de parlar, cal començar pels companys de *gàbia*, el Jordi i el Carlos, que ja hi eren dins quan jo vaig caure el 1993 (tant de temps fa?) pel departament, i el Raiül i el Miguel Ángel, que en aparèixer van ser *lo que faltaba para el duro*. Han estat molts dies de veritable (i agradable) convivència, la qual cosa no és sempre senzilla quan té lloc en un espai relativament reduït —i sense finestres!

D'aquells primers dies d'*iniciació* hem queda el bon regust dels altres *aprenents de bruixot relativista* amb els que, cadascun portat pel seu camí, fa temps que només comparteixen l'alegria del retrobament: en José Antonio, la Mercè i en Marc.

Amb el temps d'altres companys s'han anant afegint a la llista. Són molts i de tots ells m'enduré per sempre un bon record. Com que reconec que la meva memòria minva d'una manera que comença a ser alarmant (serà que m'estic fent vell?), prefereixo no fer cap llista on sempre hi mancarà per força un o dos noms. Així et dic a tu, sí, sí, a tu que estàs llegint això, que també comptes amb la meva gratitud, si més no per mostrar interès en la meva feina.

Un interès que sempre han manifestat l'Alícia i l'Álvaro, tot i que ens veiem de congrés en congrés.

En l'aspecte administratiu he de reconèixer que sempre m'he tobat recolzat (i qui no?) per l'eficàcia de l'Olga i l'atenció de la Carme, les secretàries del departament. Elles han contribuït també amb la seva dedicació a fer de la meva tesi allò que és.

Finalment, però no en darrer lloc, he d'agrair a la Direcció General de Recerca de la Generalitat de Catalunya que em concedí l'any 1994 una beca de formació d'investigadors, renovada consecutivament fins a finals de 1997. Segurament sense el seu ajut econòmic tot això hauria estat ben diferent.

M. M., Barcelona, Març de 1998.

Contents

1	Introduction	1
1.1	Historical background	1
1.2	Motivation	4
1.3	Overview of this work	6
1.4	Miscellaneous notation	8
2	The gravitational waves	11
2.1	Introduction	11
2.2	Gravitational waves	12
2.2.1	The weak-field limit of General Relativity	12
2.2.2	The Transverse-Traceless gauge	15
2.2.3	A very simple example of a monochromatic source	17
2.2.4	The effect of a plane wave on a set of test particles	21
2.3	The Doppler effect	24
2.3.1	The rotational term	25
2.3.2	The orbital term	27
2.4	The orientation	29
2.5	The overall waveform	32
3	The antenna	35
3.1	Introduction	35
3.2	Elastic bars and gravitational waves	36
3.2.1	The elastic model	37
3.2.2	The spring-like model	40
3.3	The experimental device	42
3.3.1	The resonant bar	42
3.3.2	The transducer	44

3.3.3	The amplifier	46
3.4	The resonator coupling	48
3.5	The antenna response to a gravity wave	52
3.5.1	The exact calculation	52
3.5.2	The approximate calculation	54
3.6	The noise	56
3.7	The data acquisition system	59
4	Data analysis	63
4.1	Introduction	63
4.2	Data filtering	64
4.2.1	Linear filters	65
4.2.2	The matched filter	68
4.2.3	Sampled data of finite length	69
4.3	Non-leaking signals embedded in noise with known spectrum .	72
4.3.1	A non-leaking pure monochromatic signal	72
4.3.2	The filter performance and the role of \mathcal{B}	74
4.3.3	Data splitting and averages	77
4.3.4	Probability distribution of $\bar{\mathbf{z}}(k)$	79
4.3.5	Mean and variance of $p(\bar{\mathbf{z}})$. A new SNR	81
4.4	Non-leaking signals embedded in noise of unknown spectrum .	83
4.4.1	Replacing $S(k; N)$	83
4.4.2	The actual filter output \mathbb{Z} and its distribution	84
4.4.3	A practical example	86
4.5	Leaking signals embedded in known spectrum noise	90
4.5.1	A leaking signal	90
4.5.2	Phase-varying filter	91
4.5.3	Statistical properties of $\bar{\mathbf{z}}$	92
4.6	Leaking signals embedded in noise of unknown spectrum	94
4.6.1	A spectral estimator	94
4.6.2	A single filtering process	96
4.6.3	Massive data processing	98

<i>Contents</i>	xiii
Appendix A	107
A.1 Overview	107
A.2 The angle Υ	107
Appendix B	109
B.1 Overview	109
B.2 The R87 data format.	109
Appendix C	115
C.1 Overview	115
C.2 The auxiliary functions	116
C.3 The “non-leaking” data processor	124
C.4 The massive data processor	133
C.5 The auxiliary programs	150
Resum	163
R.1 Introducció	163
R.1.1 Rerefons històric	163
R.1.2 Motivació	166
R.1.3 Sumari d'aquest treball	168
R.1.4 Notació miscel.lània	170
R.2 Les ones gravitatories	171
R.2.1 Introducció	171
R.2.2 Ones gravitatories	172
R.2.3 L'efecte Doppler	173
R.2.4 L'orientació	173
R.2.5 La forma global d'ona	174
R.3 L'antena	174
R.3.1 Introducció	174
R.3.2 Barres elàstiques i ones gravitatories	175
R.3.3 L'aparell experimental	176
R.3.4 L'acoblament dels ressonadors	176
R.3.5 La resposta de l'antena a una ona gravitòria	176
R.3.6 El soroll	177
R.3.7 El sistema d'adquisició de dades	177
R.4 L'anàlisi de dades	178
R.4.1 Introducció	178

R.4.2 Filtrat de dades	179
R.4.3 Els senyals monocromàtics i l'espectre del soroll	180
R.5 Conclusions	181
Bibliography	185

Chapter 1

Introduction

Shall quips and sentences and these paper bullets of the brain awe a man from the career of his humour? No, the world must be peopled. When I said I would die a bachelor, I did not think I should live till I were married.

—William Shakespeare, *Much Ado About Nothing*

1.1 Historical background

The first work on gravitational waves, i.e. the existence of radiative solutions, within the framework of General Relativity [28], is almost so old as the theory itself, and it is also due to A. Einstein [29].

Nevertheless, unlike other predictions of Einstein's theory of gravity, such as the bending of the light rays, the red shift in the emission spectra or the complete understanding of the previously-observed precession of the perihelion of Mercury, the experimental confirmation of the presence of gravity waves in Nature has been a challenge for many years. The reason for this elusive behaviour can be found in the conjunction of two facts. One the one hand gravitational radiation is not the predominant mechanism for releasing energy¹ even in the case of the most intense sources, those related to cosmic catastrophic events [84, 78]. The precise value, however, of the ratios determining the relative importance of the different effects (gravitational radiation, electro-magnetic

¹This simple statement assuming that gravitational waves carry energy, was indeed argued for decades. The idea began to be widely accepted after the work of H. Bondi [13].

radiation or mass ejection, for example) that contribute to the emission of energy by the system, remains today an open question in Astrophysics. On the other hand, these sources are distant astronomic objects which therefore will not strongly affect any human-size detector, almost irrespective of its intrinsic working principle.

According to that, it is not surprising that the scientific community had to wait more than fifty years until the first result claiming *evidence for discovery of gravitational radiation* was announced. It was J. Weber who, exploiting his original idea of monitoring the vibrations that a gravitational wave must cause in a massive elastic object [90], performed several tests [91] employing metallic cylinders —generically named thereafter Weber’s bars in his honour. Two of these room-temperature detectors were placed in distant locations (one at the Argonne National Laboratory of Chicago and the other at the University of Maryland) to search for coincidences in their outputs within the maximum delay in respective times of arrival of the events [92]. The registered elapsed time also informed on the possible location of the source and even the polarization of the radiation [93].

The positive outcomes published by Weber impelled other research groups to try to reproduce the experiment independently. Unfortunately, the new results not only did not confirm the previous conclusions but suggested the possibility that the events reported in the works of Weber were not produced by gravity waves —see, for instance, the articles of J. L. Levine and R. Garwin [49, 33, 50]. These contradictory results also encouraged the theoretical study of the ultimate sensitivity limit of those resonant gravitational-wave antennæ [34, 35], and thence the importance of the detector temperature.

Contemporary to this slightly deceptive scene we find one apparently disconnected event that had to become with the years the next milestone pointing to the presence of gravity waves in the Universe: the discovery of the binary pulsar PSR 1913+16 reported in 1975 by R. A. Hulse and J. H. Taylor [41]. This binary system brings together two interesting features: one of the two stars is a pulsar [79], an accurate natural clock, and its orbiting frequency (and thus the involved velocity) is quite high. Also, it was verified that its unseen companion is a second neutron star, and hence very intense gravitational fields fill the system. That explains why it was proposed as a possible astronomic gravitational laboratory by its discoverers. One of the most remarkable observations was the secular decay of the revolution period in the binary, which could be very accurately explained (within 1% of error) in terms of the energy

loss due to gravitational radiation, according to the predictions of General Relativity for this precise system [81, 82]. This is sometimes called an *indirect proof* of the existence of gravitational radiation but, in our opinion, what is really relevant in any proof is not its direct or indirect condition, but its correctness and its degree of accuracy. So, from our point of view, the existence of gravitational waves in Nature is no longer a polemic question.

In any case the interest in designing and constructing an operative gravitational wave antenna with the aim of obtaining a *direct* evidence was not reduced by the results derived from the study of the binary pulsar PSR 1913+16, but probably enhanced. During all these years passed from the Weber's experiments other room-temperature resonant detectors, like GEOGRAV [18], were designed, built and operated with technical success but yielding no relevant signs on the presence of gravitational signals in the data they recorded. Since it was clear to the experimental research groups that the thermal noise affecting the metallic cylinder strongly limited the sensitivity of these antennæ they concentrated in the development of the first *cryogenic* prototypes —the ALTAIR detector [15], for instance, was already operative in the late seventies.

Within this new generation of detectors [10], cooled down to the temperature of liquid helium and equipped with matched resonant transducers and quantum-effect based amplifiers, is where we find the antenna EXPLORER [6], owned by the *ROG* group at Rome but installed within *CERN* premises in Geneva. Other cryogenic resonant bars, however, are also operating in the present day in Legnaro —AURIGA [22]—, Louisiana —ALLEGRO [58]—, Perth —NIOBE [40]—, and Tokyo —the CRAB project [80]. Even the ultracryogenic detector of the *ROG* group —NAUTILUS [9]— placed in the Frascati *INFN* Laboratories (Rome) is currently operating with continuity at such a low temperature as 0.1 K.

Parallel to the growing of the resonant detectors, the possibility of using a two-arm interferometer as a gravitational-wave detector was proposed. The underlying idea is somehow similar to the historic Michelson-Morley experiment, but instead of trying to observe changes in the velocity of light, they are intended to monitor the differences between the length of the arms that a gravitational wave shall cause when crossing the device. Several *small-scale* prototypes, like those in Glasgow and Garching [66], were considered as a previous step of the hectometer and also kilometer-long new detectors, currently in advanced stages of construction: TAMA300 [44], GEO600 [56], LIGO [1] and VIRGO [20].

The future of the interferometric detectors seems to rely in the use of even larger arms, of about astronomical magnitudes —the LISA project [25]—, whereas the next generation of resonant antennæ may adopt spheric-like shapes. The convenience of using a sphere in the core of a cryogenic gravitational-wave antenna (due to its better cross-section and its omnidirectionality when compared with a cylinder) is not a new idea [5, 88]. The subject, however, has recently experienced an important thrust, both in the theoretical field [24, 55, 68], and in the applied one, with the ultra-cryogenic GRAIL detector in the Netherlands [32], and the SFERA and TIGA [42, 61, 62] projects.

1.2 Motivation

We have previously mentioned that it is generally believed that the most intense sources of gravitational radiation are related with astronomical catastrophic events. The magnitude of the processes that play a fundamental role in the temporal evolution of these dramatic scenarios also predict their brief duration. This is specially true in the case of the very short bursts (of about one millisecond) of gravitational energy released in the explosion of a supernova [84], but also applies to inspiralling compact binary systems [73] where the mechanism of gravitational-wave emission is more effective in the last few seconds, previous to the coalescence itself [76, 26].

The relatively large intensity of the bursts of gravitational radiation generated when a massive star collapses, or in a gamma-ray burster [75], but also their short duration when compared with the characteristic time-scales of the resonant detectors (the decay times of the mechanical oscillations) make these the preferred events [34] to be searched by the cryogenic antennæ —with the only remarkable exception of the CRAB detector series, as we shall explain later. In fact, the data-acquisition system of those detectors is usually designed in such a way that they perform *on-line* analyses, based on the lock-in procedure [14], of the information recorded by the experimental device, with the explicit aim of detecting impulsive signals. Therefore, it is usually found —see again, for instance, [6] or [58]— in the reports describing the first stages of the continuous acquisition of data by the detector, a section devoted to the discussion of the results obtained with that systematic filtering process.

This does not mean that no further *off-line* analysis is performed in the stored data stream. New filtering strategies based again in the search for

coincidences, like those performed by Weber, have been developed and applied when at least two antenæ have been simultaneously operating [7, 59]. Indeed, here relies the most important disadvantage of the search for the signals coming from these short duration sources: the possibility of missing the one important event in many years because no detector was working with optimum sensitivity (or maybe not working at all) at that precise moment.

This is not the case when searching for monochromatic waves. These signals are probably generated by the rotation of asymmetric stars, such as a pulsar or a neutron star [85]. As mentioned before, pulsars are known by their stable rotational motion, and thus they are gravitational-wave sources that continuously radiate for aeons. This stability, however, implies that the energy cannot be carried away by the emitted gravity waves at a very significant rate, because that should affect the star's rotational period. The precise amount of the outgoing flux of gravitational energy depends on several properties of the source, but specially on the degree of asymmetry of the spinning star, because it is in this parameter where it can be found the wider range of possible values. The most reasonable estimations of the gravitational radiation arriving at the Earth coming from monochromatic sources, even in the case of the so-called *millisecond* pulsars [83, 27], give results several orders of magnitude smaller than the typical burst amplitudes [84].

Nevertheless, the lower intensity of those waves can be largely counteracted with the increase of the observation time which we may, in principle, achieve thanks to the referred stability of the monochromatic source. Therefore, we must face the complexity that implies the study of such signals over long periods of time. Since the source is an astronomic object and our detector is planted on the Earth's surface, the received signal widely differs from the monochromatic emitted one: the Doppler shift due to the relative velocity between source and detector affects the observed frequency of the wave, and the change in their mutual orientation introduces time-dependent variations in the sensitivity of the antenna. Thence, some search strategy must be developed to compensate for these disturbing effects. Two main different approaches have been considered in the literature of the last decade [51, 31].

The first option needs of previous knowledge about the location of the source and also its rotational frequency, because the temporal behaviour of the preceding effects strongly depends on those parameters. When this precise information is available it is feasible to remove all these contributions in a previous step, and then to apply a more standard filtering algorithm oriented

to find *pure* monochromatic signals [66, 60]. Moreover, if the target of the search procedure is firmly settled, it is possible, not only tuning the filtering strategy to the source properties, but the *antenna* itself. In this scenario we find all the CRAB detectors: they are designed and built with the purpose of detecting the gravitational waves emitted by the rotating neutron star located in the very centre of the *Crab* nebula.

The latter possibility, in turn, implies the design of filtering algorithms that shall not be affected by the non-monochromatic behaviour of the wave [8, 17]. This will reduce its chances to reveal other cosmic signals but, since it assumes no information about the source, any so-implemented procedure will be useful (and necessary) when performing an all-sky search. The methods we are going to present in this work are included in this category.

1.3 Overview of this work

The structure of this essay relays in three fundamental mainstays: the study of the expected gravitational signal, the analysis of the antenna we intend to use for detecting it, and the description of the filtering procedures we have developed with the purpose of revealing its very presence in the collected experimental data.

With this aim we begin Chapter 2 with a summary of the fundamental topics of the linear approximation of General Relativity: we derive the wave equation, we discuss the physical meaning of the transverse-traceless gauge, and we introduce the quadrupole formula when computing the emitted waveform of a rigid homogeneous rotating ellipsoid, a very simple model for describing a spinning neutron star. The effect of a plane wave on a set of test particles is also presented in this chapter, postponing the study of the interaction between gravitational radiation and extended bodies, until Chapter 3.

Then we centre our attention in the problem of the description of the received wave, studying the two main disturbing processes we have mentioned in the preceding section: the Doppler shift in the observed frequency of the wave and the time-dependent sensitivity of the detector. We shall derive the explicit contributions of those effects to the waveform of the incoming perturbation, in terms of the astronomic location of the source and the geographical site of our detector. Therefore, the final expression we obtain for the gravitational strain shall be very convenient not only when we compute in Chapter 3 the

theoretical response of a resonant antenna to this precise driving force, but in practical data-analysis problems, because the formulæ can be easily restricted to concrete examples using a simple table of ephemeris.

Indeed, in Chapter 3 are described all the subjects specifically concerning the experimental detecting device: the cryogenic resonant antenna *Explorer*. We review, in the first place, the way in which a metallic cylinder couples to gravitational radiation. We present and solve the equations that the theory of elasticity assigns to such a system, and show how it can be rightfully modelled by a simple harmonic oscillator, a well-known result. Once we have argued why an elastic bar can be used as the core of a gravity-wave detector, we dissect the two main components of the *Explorer*, besides the aluminium cylinder itself: the resonant capacitive transducer, that efficiently turns the cylinder vibrations into electric voltages, and the d. c. SQUID, a quantum-effect based electro-magnetic amplifier. Then, we extend the commonly used harmonic-oscillator model to include the intentionally designed mechanical coupling that appears between the bar and the transducer. As mentioned before, we shall solve the new equations describing the whole detector, in the case in which the external force is due a Doppler-shifted monochromatic gravitational wave with time-dependent amplitude.

We also describe the data-acquisition system of the antenna, which finally records, in the form of computer files, those bar-end oscillations, together with other useful experimental information coming from different built-in sensors of the *Explorer*: two seismographs, a detector of electro-magnetic radiation, and several *on-line* analogical filters. Finally we study the presumed features of the noise that certainly disturbs this process of data acquisition, and therefore shall be present in the detector outcome, hopefully mixed with the response of the detector to the gravitational radiation impinging on it.

This approximation to the topic of the noise can be somehow thought as a small preface of Chapter 4, where we develop the problem of the analysis of the experimental data stream. In this chapter is where it can be found most of the original contributions to the subject of gravitational-wave detection we have presented in this essay. Our starting point is the well-established theory of the matched filter, which determines the optimum linear filter for a given signal, embedded in noise with known spectral density. In our case the filtering procedure obtained with this approach is equivalent to a simple discrete Fourier transform. Then we face the consequences that implies the practical impossibility of performing the analysis of the complete stream in a single filter

pass, but in several blocks. Unlike the usual procedure of averaging the square moduli of the Fourier transform of each piece, we develop a method that also uses the phase information contained in the different processed stretches of data, yielding in this way a non-linear filtering procedure.

In a first step we assume that the frequency of the hidden signal corresponds to a single bin of the spectral template we use, the naturally related one when the fast Fourier transform algorithm is applied. We consider the two possible scenarios depending on the information we have about the noise: its spectral density may be known or unknown. In both cases a detailed probabilistic study of the filter output is performed and the conclusions we draw are compared with the result obtained after the application of the second algorithm on true experimental data, with an external signal added. Since the method proves to be reliable (it unveils the presence of the control signal in the data series) and works in accordance of our statistical predictions, we relax the imposed frequency constraint. Therefore, two new general-frequency filtering methods (the first for known-spectrum noises, the second for unknown-spectrum ones) are developed. We discuss again the probabilistic behaviour of our search algorithms, what allow us to make statistical statements about the outstanding outcomes we obtain after a massive application of the filtering procedure upon a stretch of six month of data, recorded by the *Explorer* detector in 1991.

1.4 Miscellaneous notation

- In tensorial and tensor-like objects, the Greek indices run from zero to three, whereas Latin indices range from one to three.
- The metric tensor of the space-time, $g_{\mu\nu}$, has signature -++-.
- Einstein summation convention is used, both for three and four-dimensional quantities.
- Partial derivatives with respect to x^μ appear in the text in the form of a colon $_{,\mu}$.
- Partial derivatives with respect to x appear in the text in the form of $\partial/\partial x$ or ∂_x .
- \square denotes the D'Alembertian operator of the Minkowski's space-time.

- Indices within a parenthesis express symmetrization with respect to them, e.g. $\epsilon^{(\mu,\nu)} \equiv (\epsilon^{\mu,\nu} + \epsilon^{\nu,\mu})/2$.
- The hat ($\hat{\cdot}$) is always placed over the unitary Cartesian vectors.
- Complex-conjugation operation is represented by an asterisk ($*$).
- The real and imaginary part of A are $\Re\{A\}$ and $\Im\{A\}$ respectively.
- The (discrete or continuous) Fourier transform of A is denoted by \tilde{A} .
- We represent the angular frequency related to f_x by means of ω_x , i.e. $\omega_x = 2\pi f_x$.
- G is the Newtonian gravitational constant, c is the speed of light in the vacuum, and K_B is the Boltzmann's constant.

Chapter 2

The gravitational waves

I felt that I must scream or die! And now. Again. Hark!
louder! louder! louder! LOUDER!

Villains! —I shrieked—, dissemble no more! I admit the
deed! Tear up the planks! Here, here! It is the beating of
his hideous heart!

—Edgar Allan Poe, *The Tell-Tale Heart*

2.1 Introduction

This chapter is devoted to the study of the physical processes we have planned to address, the gravitational waves, with special attention to those that are monochromatic: their prediction [29] by General Relativity [28], their properties, the generation of that kind of radiation [30], its propagation and the foreseeable effects that may produce on an extended object that eventually can act as a detector [64].

We shall begin with the linear approximation of Einstein's theory of gravitation, in which gravity can be thought of as a small metric perturbation of flat space-time. We shall follow the standard procedure that leads to a wave equation which those quantities (a measurement of deviation of the actual metric from Minkowski's one) have to fulfill. We shall also see how the gravitational waves that are described by a symmetric matrix with, in principle, ten independent terms, can be fully (and locally) characterized just with two functions. We will display the explicit form of these functions, under some particular conditions, when the source is a spinning body, like a pulsar.

Once we have shown how the emitted wave looks like, we will move into the problem of the description of the received wave. Our interest is concerned with the case in which the gravitational observatory is placed in a fixed location on the surface of the Earth, a situation that will distort, from its point of view, the incoming wave [65, 43]. On one hand, the existence of a relative velocity between the source and the detector, due mainly to the orbital and rotational motions of the Earth, will produce a frequency shift: the well-known Doppler effect. On the other hand, this very rotational motion of our planet causes the alignment of any directional antenna with the source to vary. The sum of all these contributions will be the target of our search procedure.

2.2 Gravitational waves

In a metric theory of gravitation, like General Relativity, the gravitational forces are explained as geometry, geometry of space-time [64]. The gravitational waves are then nothing but ripples traveling in this space-time, which change geometric quantities, such as proper distances, when they pass through a place. This distortion of the geometry will be reflected in a trend to modify the shape and dimensions of material objects, that are then said to be affected by *tidal forces*, in reference to those that make raise and recess the oceanic waters.

In this section we are going to review how, in the frame of the weak-field limit of Einstein's gravity, a wave equation arises. We will try to cover most of the fundamental aspects of that kind of radiation, including an *a posteriori* test of the accuracy degree of the approximation that we have considered: we shall compute the amplitude of the gravitational waves coming from a distant slowly-spinning rigid object, and we will see how weak they are. This source model will also tell us about the explicit waveform of the outgoing radiation.

We shall end this point with a quantitative example of the effect of a monochromatic plane wave on a set of non-interacting point-like particles, stressing the resemblances and differences in their behaviour depending on the actual wave polarization.

2.2.1 The weak-field limit of General Relativity

We are going to recall here the appearance of a wave equation in the linear limit of General Relativity, leaving aside the *exact* gravitational waves, radiative

solutions to the whole Einstein's equations. We shall check afterwards the sufficiency of the approximation.

In any metric theory of gravitation, not only in General Relativity, a set of field equations must be solved before the values of the metric coefficients $g_{\mu\nu}$, which in their turn determine the structure of the space-time, are known. In the weak-field approximation, as it can be found in the standard literature [48, 64, 94], it is assumed that this tensor can be split in two parts

$$g_{\mu\nu} = \eta_{\mu\nu} + h_{\mu\nu}. \quad (2.1)$$

one of them, $\eta_{\mu\nu}$, the Minkowski's metric¹, that characterizes a flat space-time, and the other, $h_{\mu\nu}$, so small that we can neglect any second and higher order terms in this object. If we want, for instance, to raise one of its indices we need to use no longer $g^{\mu\nu}$, but² $\eta^{\mu\nu}$,

$$h^\mu{}_\nu = \eta^{\mu\alpha} h_{\alpha\nu}. \quad (2.2)$$

Now, we only have to substitute that particular decomposition of the metric tensor in the Einstein's equations

$$R_{\mu\nu} - \frac{1}{2} g_{\mu\nu} R^\alpha{}_\alpha = \frac{8\pi G}{c^4} T_{\mu\nu}, \quad (2.3)$$

keeping only the terms that are linear in $h_{\mu\nu}$; then we will obtain a new set of equations,

$$h_{\mu\alpha,\nu}{}^\alpha + h_{\nu\alpha,\mu}{}^\alpha - h_{\mu\nu,\alpha}{}^\alpha - h^\alpha{}_{\alpha,\mu\nu} - \eta_{\mu\nu}(h_{\alpha\beta}{}^{\alpha\beta} - \square h^\alpha{}_\alpha) = \frac{16\pi G}{c^4} T_{\mu\nu}, \quad (2.4)$$

that can be formally shortened if we introduce

$$\bar{h}_{\mu\nu} \equiv h_{\mu\nu} - \frac{1}{2} \eta_{\mu\nu} h^\alpha{}_\alpha, \quad (2.5)$$

leaving only four terms in the left-hand side of the equations:

$$-\square \bar{h}_{\mu\nu} - \eta_{\mu\nu} \bar{h}_{\alpha\beta}{}^{\alpha\beta} + \bar{h}_{\mu\alpha,\nu}{}^\alpha + \bar{h}_{\nu\alpha,\mu}{}^\alpha = \frac{16\pi G}{c^4} T_{\mu\nu}. \quad (2.6)$$

¹In all the following derivations it is implicitly assumed that we use a coordinate system in which $\eta_{\mu\nu} = \text{diag}(-1, 1, 1, 1)$.

² $\eta^{\mu\nu}$ is the inverse of $\eta_{\mu\nu}$, in the sense that $\eta^{\mu\alpha} \eta_{\alpha\nu} = \delta^\mu{}_\nu$.

The last expression shows us that a major simplification of the problem could be achieved if

$$\bar{h}_{\mu\nu}{}^\nu = 0, \quad (2.7)$$

a condition that it is absolutely feasible to fulfill. We have imposed no constraint on the coordinate system, other than the validity of the equation (2.1) in the sense we have explained before, what allow us to do a change of coordinates like

$$x'^\mu = x^\mu + \epsilon^\mu, \quad (2.8)$$

which will lead us to a new first-order metric tensor,

$$g'^{\mu\nu} = \eta^{\mu\nu} - h'^{\mu\nu} = \eta^{\mu\nu} - h^{\mu\nu} + \epsilon^{\mu,\nu} + \epsilon^{\nu,\mu}, \quad (2.9)$$

whenever

$$\epsilon^{(\mu,\nu)} \sim h^{\mu\nu}. \quad (2.10)$$

The four-dimensional divergence of the new metric perturbation, in terms of the old one and the coordinate differences, is given by

$$\bar{h}'^{\mu\nu}{}_\nu = \bar{h}^{\mu\nu}{}_\nu - \square \epsilon^\mu, \quad (2.11)$$

what tells us that we have only to set

$$\square \epsilon^\mu = \bar{h}^{\mu\nu}{}_\nu, \quad (2.12)$$

and the new $\bar{h}'_{\mu\nu}$ will show the property stated in (2.7). It seems clear that the coordinates, which are said to be *harmonic*, are not fully fixed by the condition (2.12), because after any change involving subsequently another ϵ'^μ with

$$\square' \epsilon'^\mu = 0, \quad (2.13)$$

the new version of expression (2.7) will still hold.

Summing up, the equations which finally verify the quantities $\bar{h}_{\mu\nu}$ are

$$\begin{cases} \square \bar{h}_{\mu\nu} &= -\frac{16\pi G}{c^4} T_{\mu\nu}, \\ \bar{h}_{\mu\nu}{}^\nu &= 0, \end{cases} \quad (2.14)$$

whose general solution is

$$\bar{h}_{\mu\nu}(t, \vec{x}) = \frac{4G}{c^4} \int_V \frac{T_{\mu\nu}(t - |\vec{x} - \vec{x}'|/c, \vec{x}')}{|\vec{x} - \vec{x}'|} d\vec{x}'. \quad (2.15)$$

Nevertheless, the most important feature of the upper expression in (2.14), within the scope of our particular interest, is that it reduces to the wave equation when we consider any region outside the source, where the energy-momentum tensor vanishes,

$$\square \tilde{h}_{\mu\nu} = 0, \quad (2.16)$$

what, in its turn, tells us that, in the weak-field limit, $\tilde{h}_{\mu\nu}$ propagates itself in vacuum, in the form of waves, *gravitational waves*. Finally, we have found how the radiation appears in the linear approximation to General Relativity. We must point out that, if we could calculate the integral that appears in the right-hand side of equation (2.15) we should get, up to our order of approximation, the complete solution of the problem, including, not only radiative terms, but also the monopolar gravitational field and so on. Then, whenever we use in this essay $h_{\mu\nu}$ as a synonymous of *gravitational wave*, we will have in mind not the whole $h_{\mu\nu}$ but that part which we can really identify as a gravitational wave thanks, for instance, to its properties, like the next one.

2.2.2 The Transverse-Traceless gauge

Let us take a closer look at the case in which the gravitational perturbation is a (locally, at least) plane wave,

$$h_{\mu\nu} = h_{\mu\nu}(\omega t - \vec{k} \cdot \vec{x}) \quad (2.17)$$

where \vec{k} , the wave vector, is constant both in modulus,

$$|\vec{k}| = \frac{\omega}{c}, \quad (2.18)$$

and orientation. We will take advantage of these properties just arranging the coordinate system in such a way that the third axis marks the propagation direction of the wave,

$$h_{\mu\nu} = h_{\mu\nu}(\omega\{t - z/c\}). \quad (2.19)$$

For the sake of simplicity we will restrict our study to (complex) monochromatic plane waves, what will not result, however, in a loose of generality. We must recall that we are dealing with a *linear* approximation of General Relativity. This means that we can treat any arbitrary plane wave as it was a superposition of many, maybe an infinity of, monochromatic plane waves, and

that the sum of their individual properties will determine the whole behaviour of the original perturbation.

We shall start writing down the explicit form of a monochromatic plane wave travelling upward along the z axis,

$$h^{\mu\nu} = H^{\mu\nu} e^{i\omega\{t-z/c\}}. \quad (2.20)$$

The $H^{\mu\nu}$ coefficients are constants, in the sense that they depend neither on t nor on z , and they can be thought as the elements of a symmetric matrix of rank four. But the invariance respect to the permutation of its two indexes is not the unique condition that the object $H^{\mu\nu}$ must satisfy. The choice of a particular gauge, in our case the harmonic one, will reduces the number of independent terms in the metric tensor, and hence in $h^{\mu\nu}$, from ten to six. Explicitly, equation (2.7), when dealing with a monochromatic plane wave, yields the following conditions for $H^{\mu\nu}$,

$$H_{\mu\nu} k^\nu = \frac{1}{2} H^\alpha{}_\alpha k_\mu, \quad (2.21)$$

which, in our wave-oriented frame of reference, finally imply

$$(H^{\mu\nu}) = \begin{pmatrix} H^{00} & H^{01} & H^{02} & \frac{H^{00}+H^{33}}{2} \\ H^{01} & \boxed{H^{11}} & H^{12} & H^{01} \\ H^{02} & H^{12} & -H^{11} & H^{02} \\ \frac{H^{00}+H^{33}}{2} & H^{01} & H^{02} & H^{33} \end{pmatrix}. \quad (2.22)$$

As we have mention in the preceding section, we have not yet completely exhausted the gauge freedom with the requirement of (2.7), because we are able to perform any first-order change of coordinates, in the terms marked by (2.10), just taking care of preserving their harmonic condition, or, what is the same, fulfilling the equation (2.13). On the other hand, this formula also tells us that, like $h_{\mu\nu}$, each component of ϵ^μ must follow itself a wave equation. It seems that the most convenient functional form for them is just

$$\epsilon^\mu = q^\mu e^{i\omega\{t-z/c\}}, \quad (2.23)$$

with q^μ also constant, since we plan to use this remanent freedom in the gauge choice to cancel some components of the new $H'^{\mu\nu}$. The transformation rule

between these components and the old ones comes from (2.11),

$$H'^{00} = H^{00} - 2\frac{\omega}{c}q^0, \quad (2.24)$$

$$H'^{01} = H^{01} - \frac{\omega}{c}q^1, \quad (2.25)$$

$$H'^{02} = H^{02} - \frac{\omega}{c}q^2, \quad (2.26)$$

$$H'^{33} = H^{33} - 2\frac{\omega}{c}q^3. \quad (2.27)$$

$$H'^{11} = H^{11}, \quad (2.28)$$

$$H'^{12} = H^{12}; \quad (2.29)$$

notoriously, it leaves invariant the elements inside the box in (2.22), whereas the rest of them can be made equal to zero at our discretion. This feature can be extended, as it has been argued, to any $h_{\mu\nu}$ representing a plane gravitational wave and thus we must conclude that all the physical information of such a wave will be condensed in two functions, called the “+” and “×” polarizations³, h_+ and h_\times ,

$$(h_{\mu\nu}) = \begin{pmatrix} 0 & 0 & 0 & 0 \\ 0 & h_+ & h_\times & 0 \\ 0 & h_\times & -h_+ & 0 \\ 0 & 0 & 0 & 0 \end{pmatrix}. \quad (2.30)$$

This matrix-like arrangement clearly shows that the metric perturbation is transverse (all non-null components of the wave lie in a plane orthogonal to its propagation direction) and traceless, both traits that give name to this particular instance of the harmonic gauge.

In the next section we will apply the theory we have exposed up to this point, in the practical case of finding the value of h_+ and h_\times when the source of the radiation is a *far* neutron star.

2.2.3 A very simple example of a monochromatic source

Let us compute the gravitational radiation emerging from a rigid homogeneous ellipsoid with semi-axes R_1, R_2, R_3 , that rotates with angular velocity Ω_P around its third axis.

³The reason for that peculiar notation will be clarified in Section 2.2.4.

Obviously, this is a naïve model [11, 12] for describing a spinning neutron star [79], but it will bring us a glimpse of the properties of the signals we want to detect. We will also use as a tool of calculus the quadrupole formula [30, 48] that follows from (2.15),

$$h_{ij} = \frac{2G}{c^4 D} \bar{I}_{ij}(t - D/c), \quad (2.31)$$

whose validity is subject to the fulfillment of further conditions⁴. Here, \bar{I}_{ij} is the trace-free part of I_{ij} , the second moment of the mass distribution $\varrho(\vec{x}')$,

$$\bar{I}_{ij} = I_{ij} - \frac{1}{3} \delta_{ij} I^k_k \quad (2.32)$$

$$I_{ij} = \int_V \varrho(\vec{x}') x'_i x'_j d^3 x' \quad (2.33)$$

and, hence, the bar should not be moved from I_{ij} to h_{ij} in expression (2.31). On the other hand, D , the distance between the source and the observational point, must be much larger than the wavelength of radiation. Now, we have to choose a set of three vectors $\{\hat{p}_1, \hat{p}_2, \hat{p}_3\}$ that can ease the task of obtaining the second moment of the mass distribution. The unit-length version of the angular-momentum vector seems to be a natural selection for, let us say, \hat{p}_3 , whereas, at this moment, we will not demand of \hat{p}_1 and \hat{p}_2 other properties than the orthonormality ones. This leaves us with some amount of freedom that will be useful later, as we shall see.

After some algebra, the non-vanishing components of I_{ij} appear to be

$$I_{11} = \frac{4\pi}{15} \varrho R_1 R_2 R_3 [R_1^2 \cos^2(\Omega_P t + \varphi_g) + R_2^2 \sin^2(\Omega_P t + \varphi_g)], \quad (2.34)$$

$$I_{12} = \frac{2\pi}{15} \varrho R_1 R_2 R_3 [R_1^2 - R_2^2] \sin(2\Omega_P t + 2\varphi_g), \quad (2.35)$$

$$I_{22} = \frac{4\pi}{15} \varrho R_1 R_2 R_3 [R_2^2 \cos^2(\Omega_P t + \varphi_g) + R_1^2 \sin^2(\Omega_P t + \varphi_g)], \quad (2.36)$$

$$I_{33} = \frac{4\pi}{15} \varrho R_1 R_2 R_3^3, \quad (2.37)$$

⁴In addition to the restrictions it inherits from the parent formula, we must demand that the velocities of the inner components of the source are small, compared to c , and that their motions are not self-gravity driven. This last condition can be surmounted [4, 89] adding to $T_{\mu\nu}$ the so-called *pseudotensor of stress-energy* for the gravitational field. In any case we need not bother here about this particular limitation.

where φ_g will not be rightfully settled as long as we do not specify \hat{p}_1 and \hat{p}_2 . The values of h_{ij} are now

$$h_{11} = h_0 \cos(\omega_g t - \omega_g \mathcal{D}/c + 2\varphi_g), \quad (2.38)$$

$$h_{12} = h_0 \sin(\omega_g t - \omega_g \mathcal{D}/c + 2\varphi_g), \quad (2.39)$$

$$h_{22} = -h_{11}, \quad (2.40)$$

$$h_{3i} = 0, \quad (2.41)$$

with

$$\omega_g \equiv 2\Omega_P, \quad (2.42)$$

and

$$h_0 \equiv \frac{4\pi G \omega_g^2}{15c^4 \mathcal{D}} \varrho R_1 R_2 R_3 (R_2^2 - R_1^2). \quad (2.43)$$

This last quantity can be rewritten in this way,

$$h_0 = \frac{G \omega_g^2}{c^4 \mathcal{D}} I \varepsilon, \quad (2.44)$$

in terms of the moment of inertia (with respect to the rotation axis) of the body, I , and the *equatorial ellipticity*, ε , which in our case reduces to

$$\varepsilon = \frac{R_2^2 - R_1^2}{R_1^2 + R_2^2}. \quad (2.45)$$

Looking at the expressions ranging from (2.38) to (2.41) we could conclude that we have naturally obtained the result in the **Transverse-Traceless** form: only $h_{11} = -h_{22}$ and h_{12} are different from zero!

Nevertheless, the **TT** gauge corresponds to a *local* choice of coordinates in which the line of sight defines the vector \hat{k} . This means that, incidentally, when considering observers *on the rotation axis*, (2.38) and (2.39) are the true h_+ and h_\times polarizations, and no further calculation is needed; but if we observe the source in a different direction we will have to perform a rotation in h_{ij} that leaves the actual \vec{k} on the new *third* axis, and then obtain the **TT** part. Since we can freely choose \hat{i} and \hat{j} in order to complete the adapted-to-the-wave basis, we will fix them at the same time of \hat{p}_1 and \hat{p}_2 in such a way that

$$\hat{p}_2 \cdot \hat{k} \leq 0, \quad (2.46)$$

$$\hat{i} \equiv \hat{p}_1, \quad (2.47)$$

$$\hat{j} \equiv \hat{k} \times \hat{i}, \quad (2.48)$$

what allows us to characterize the change of basis with just one parameter, ι , the angle that forms \hat{k} with \hat{p}_3 or, in other words, the line of sight with the axis of rotation (a display of the relationship between this two set of vectors, among others, can be found in Figure 2.1). In this situation the calculation of the **TT** components of the wave yields,

$$h_+ = h_0 \frac{1 + \cos^2 \iota}{2} \cos(\omega_g t + \varphi_g), \quad (2.49)$$

$$h_x = h_0 \cos \iota \sin(\omega_g t + \varphi_g), \quad (2.50)$$

with a suitable redefinition of φ_g .

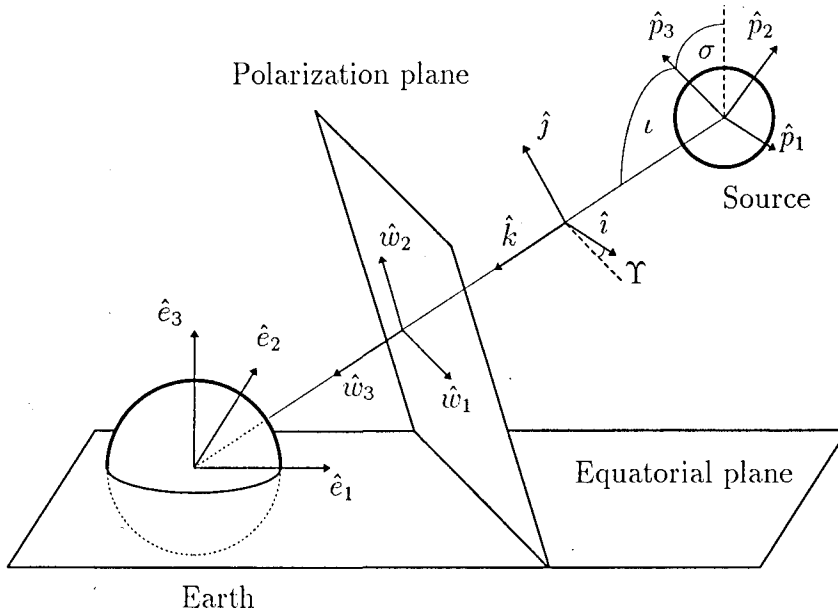


Figure 2.1: Design with several sets of vectors well-adapted to: the source, $\{\hat{p}_i\}$, the Earth, $\{\hat{e}_i\}$, the wave, $\{\hat{w}_i\}$ and $\{\hat{i}, \hat{j}, \hat{k}\}$; together with some relevant angles Υ , ι and σ .

This is only an orientative example of monochromatic gravitational radi-

ation coming from an astronomical spinning object, but we could finish this section giving values to the parameters [84, 12], in order to realize the order of magnitude of the metric perturbation we are planning to look for,

$$h_0 \simeq 1 \times 10^{-24} \left(\frac{f_g}{1000 \text{Hz}} \right)^2 \left(\frac{I}{10^{38} \text{kg m}^2} \right) \left(\frac{1 \text{kpc}}{\mathcal{D}} \right) \left(\frac{\varepsilon}{10^{-6}} \right); \quad (2.51)$$

it is clear that the weak-field approximation we have decided to adopt here is fully justified. Note that, whereas tentative values of f_0 , \mathcal{D} and I can be those typical of a millisecond galactic pulsar, the ellipticity can vary drastically from one source to another, leaving open the unfavourable possibility of values below 10^{-6} [87].

2.2.4 The effect of a plane wave on a set of test particles

Once we have consider the problem of the generation of plane gravitational waves in a very particular but representative case, we are going to review the detectable effects that may produce their interaction with other objects.

All the existing, or even projected, gravitational wave antennæ are designed to register in a suitable way the effects of the *tidal force*, a differential force that appears between two particles or, in general, any two points placed in the bosom of a non-uniform gravitational field. This also applies to elastic bodies: the tidal force which acts upon every element of mass simply adds to other external perturbations, providing, together with the inner tensions, the overall force. The mutual acceleration that this force produces can be written, when the field is weak enough, in terms of the second time derivative of the spatial components of the metric perturbation, and the undisturbed relative position of the two points, $\vec{\ell}_0$,

$$\ddot{\ell}_i = \frac{\ell_0}{2} \ddot{h}_{ij} n^j, \quad (2.52)$$

where ℓ_0 is the modulus of $\vec{\ell}_0$, and \hat{n} is its unitary vector.

In the present section we shall restrict the discussion to the behaviour of a set of free point-like test particles, leaving aside the study of extensive solid bodies until the next chapter. Furthermore, we will assume that those particles are originally arranged in a circular disposition on the polarization plane of the wave, whose orthogonal direction will define, as usual, the third or z axis. So

we can characterize the primary location of each bead using a single angular variable,

$$n_x = \cos \phi, \quad (2.53)$$

$$n_y = \sin \phi; \quad (2.54)$$

and compute its later position respect to the center of the circle simply integrating equation (2.52) for a TT gravitational wave like that in (2.30),

$$\ell_x(t) = \ell_0 \cos \phi + \frac{\ell_0}{2} (h_+(t) \cos \phi + h_x(t) \sin \phi), \quad (2.55)$$

$$\ell_y(t) = \ell_0 \sin \phi + \frac{\ell_0}{2} (h_x(t) \cos \phi - h_+(t) \sin \phi); \quad (2.56)$$

where we have used that the particles were originally at rest.

If we restrict the radiation to be “+” polarized, which means that $h_x = 0$, we easily realize that the set of the test particles lies on an ellipse whose principal axes follow the x and y directions,

$$\ell_x(t) = \ell_0 \left(1 + \frac{h_+(t)}{2} \right) \cos \phi, \quad (2.57)$$

$$\ell_y(t) = \ell_0 \left(1 - \frac{h_+(t)}{2} \right) \sin \phi. \quad (2.58)$$

The length of those elliptic semi-axes will change along the time, depending on the functional form of $h_+(t)$. Assuming, once again, a sinusoidal behaviour for the polarization, i.e.

$$h_+(t) \sim A_0 \sin(\omega_g t), \quad (2.59)$$

we shall get a time-dependent deformation of the kind shown in Figure 2.2.a. The cross-like shape of the superposition of the particle arrangement after a quarter of a period, and after three quarter of a period, explains the label “+” for this first polarization. The origin for the “ \times ” subscript can be argued in a similar way. Let us cancel $h_+(t)$ in formulæ (2.55) and (2.56),

$$\ell_x(t) = \ell_0 \cos \phi + \frac{\ell_0}{2} h_x(t) \sin \phi, \quad (2.60)$$

$$\ell_y(t) = \ell_0 \sin \phi + \frac{\ell_0}{2} h_x(t) \cos \phi. \quad (2.61)$$

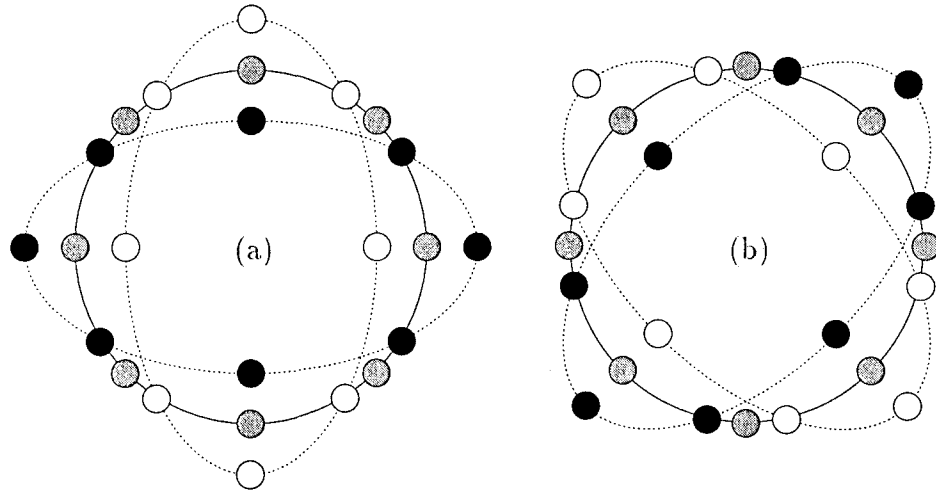


Figure 2.2: Effect of the “+” polarization (a) and the “x” polarization (b) of a monochromatic plane wave on a set of eight free point-like particles circularly distributed. The gray beads show the unperturbed disposition of the particles, while the black and white ones are placed marking the maximum displacements that they undergo, temporally separated by half a period. Notice that the particles lying on the “+” (“x”) positions experience radial displacements, while those on the “x” (“+”) locations only move tangentially in the first (second) case.

We can newly recognize an elliptic pattern in the distribution of the beads just performing a simple rotation of $\pi/4$ radians around the propagation direction of the wave:

$$\ell_{x'} \equiv \frac{\ell_x + \ell_y}{\sqrt{2}} = \ell_0 \left(1 + \frac{h_x(t)}{2} \right) \cos \left(\phi - \frac{\pi}{4} \right), \quad (2.62)$$

$$\ell_{y'} \equiv \frac{-\ell_x + \ell_y}{\sqrt{2}} = \ell_0 \left(1 - \frac{h_x(t)}{2} \right) \sin \left(\phi - \frac{\pi}{4} \right). \quad (2.63)$$

If we choose the same temporal evolution for the polarization,

$$h_x(t) \sim A_0 \sin(\omega_g t), \quad (2.64)$$

the result, which is represented in Figure 2.2.b, repeats up to the rotation that was already depicted in Figure 2.2.a.

Finally note that the displacements introduced in both graphs of Figure 2.2 have been enhanced for clarity reasons. We have seen in expression (2.51) how small is the amplitude of the monochromatic gravitational waves, emitted by an object so dense and spinning so fast such as a pulsar is, when they reach the Earth. We can then conclude that probably we shall never see a warning sign like that one in Figure 2.3 near a gravitational wave detector!

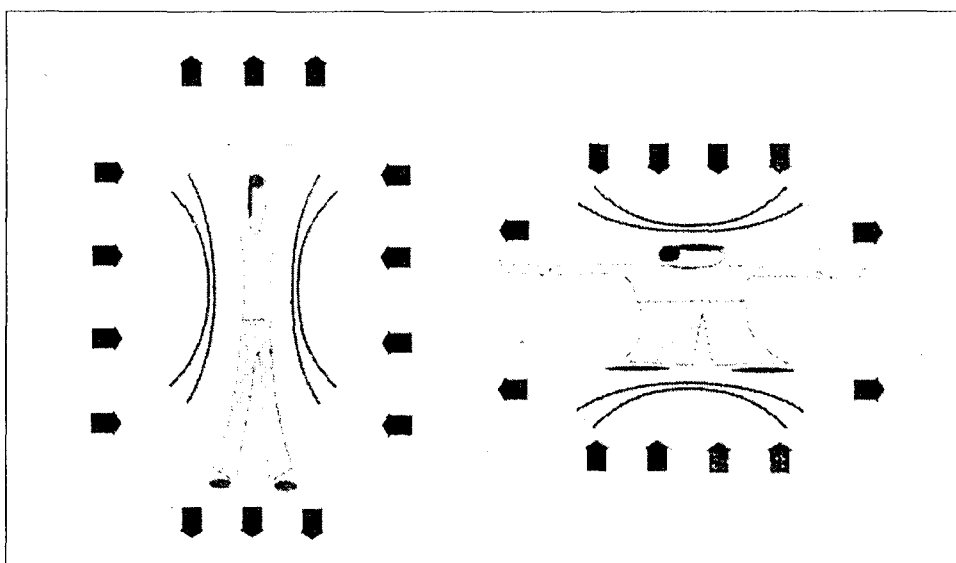


Figure 2.3: Presumed effect of a *very large* polarized gravitational wave on a human being.

2.3 The Doppler effect

We are concerned with the search for waves that are monochromatic in their origin. Moreover, we want to *see* them with a gravitational antenna placed on the Earth's surface. Then, if the wave is emitted by an object which is not at rest with respect to the detector, its characteristic frequency will be modified by the classical Doppler effect.

Let us consider the amplitude of a scalar plane wave at some point \vec{r} of the space,

$$h(t, \vec{r}) = h(\omega_g t - \vec{k} \cdot \vec{r}). \quad (2.65)$$

An object that follows a definite trajectory $\vec{r} = \vec{r}(t)$ measures an instantaneous angular frequency that, in general, is no longer equal to ω_g ,

$$\omega_{obs} = \omega_g - \vec{k} \cdot \dot{\vec{r}}. \quad (2.66)$$

In the case we are interested in, $\vec{r}(t)$ is the position of a ground-based detector in the Solar System barycentric frame of reference⁵. We will assume that this frame is at rest or moving with constant velocity, with respect to the source. This assumption leaves only two main contributions to the time-dependent frequency change⁶, the rotation of the Earth and its orbital motion around the Sun. So, we will split $\vec{r}(t)$ in two new vectors

$$\vec{r}(t) = \vec{r}_S(t) + \vec{r}_E(t) \quad (2.67)$$

in such a way that $\vec{r}_S(t)$ coordinates the position of the centre of the Earth in the barycentric frame, and $\vec{r}_E(t)$ the location of the detector on the surface of the Earth in a comoving, but non-rotating, frame with the origin on its centre.

2.3.1 The rotational term

We shall begin with the study of the contribution due to the rotational motion of the Earth to the Doppler shift of the incoming waves. First of all, we need a system of reference $\{\hat{e}_1, \hat{e}_2, \hat{e}_3\}$, placed in the Earth's centre in order to express \vec{k} and $\vec{r}_E(t)$, and subsequently perform their scalar product.

We will take \hat{e}_3 along the rotational axis, oriented to the North Pole; \hat{e}_1 parallel to the line that joins the astronomical first points of Libra, which marks the autumnal equinox, and Aries, which marks the vernal equinox, and pointing to the latter⁷; and finally $\hat{e}_2 \equiv \hat{e}_3 \times \hat{e}_1$. Whichever the system of reference that

⁵Due to the relative masses of the bodies that constitute the Solar System, the location of the center of masses, origin of barycentric frame, is almost in the very centre of the Sun.

⁶A constant shift in the frequency does not modify the monochromatic character of the wave.

⁷The line is, in fact, defined by the intersection of the equatorial and the ecliptic planes.

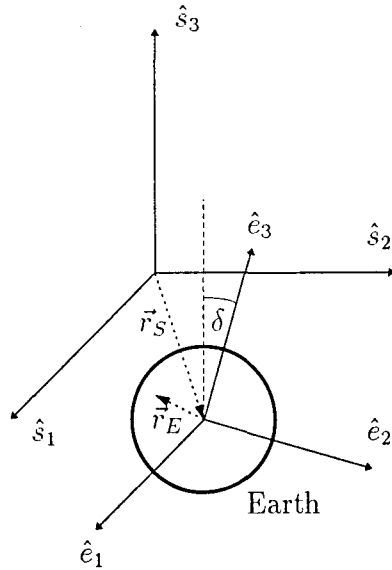


Figure 2.4: Sketch showing how we locate any place on the Earth's surface using \vec{r}_S and \vec{r}_E , and the basis in which we express them. The schematic drawing is intended to stress coincident direction of \hat{e}_1 and \hat{s}_1 , as well as the meaning of the angle δ .

we select, we can always write \vec{k} as follows,

$$\vec{k} = -\frac{\omega_g}{c}(\sin \alpha \cos \beta \hat{e}_1 + \sin \alpha \sin \beta \hat{e}_2 + \cos \alpha \hat{e}_3), \quad (2.68)$$

but in our particular choice, the angular coordinates of the source are just the celestial equatorial coordinates⁸: the codeclination, also known as North Polar distance, α , and the right ascension, β . In addition, in this system of reference the components of \vec{r}_E are also closely related with the common way for locating

⁸We keep, however, the typical ranges in the spherical coordinates for the values of each angle. So, we will have to handle *codeclinations* and *colatitudes*, instead of declinations and latitudes, and convert every angular unit into radians.

a place in a world map,

$$\begin{aligned}\vec{r}_E = & R_E[\sin \theta \cos(\Omega_E(t - t_0^{rot}) + \lambda) \hat{e}_1 \\ & + \sin \theta \sin(\Omega_E(t - t_0^{rot}) + \lambda) \hat{e}_2 + \cos \theta \hat{e}_3],\end{aligned}\quad (2.69)$$

provided that θ and λ are, respectively, the colatitude and the longitude of the detector; R_E is the radius of the Earth, and Ω_E is the angular velocity of the Earth, with respect to the fixed stars. Since we will measure time quantities in Greenwich Universal Time (GUT or, simply, UT), the value of Ω_E , that directly comes from the duration of a sidereal day, is

$$\Omega_E = \frac{2\pi}{23^h 56^m 04^s}, \quad (2.70)$$

and t_0^{rot} must be set equal to the beginning of any of those sidereal days.

The scalar product of the two vectors, \vec{k} and $\vec{r}_E(t)$, now becomes:

$$\vec{k} \cdot \vec{r}_E(t) = -\frac{R_E \omega_g}{c} \sin \theta \sin \alpha \cos \eta - \frac{R_E \omega_g}{c} \cos \theta \cos \alpha, \quad (2.71)$$

where η carries all the temporal dependence,

$$\eta = \Omega_E(t - t_0^{rot}) + \lambda - \beta. \quad (2.72)$$

2.3.2 The orbital term

We shall proceed in a way that will be very similar to that we have already followed in the last section. Moreover, in the construction of the new basis $\{\hat{s}_1, \hat{s}_2, \hat{s}_3\}$ we are going to make use of \hat{e}_1 , because it also lies in the ecliptic plane, just setting

$$\hat{s}_1 = \hat{e}_1; \quad (2.73)$$

this will be useful in the moment we need to refer the new set of vectors in terms of the old basis, and vice versa. On the other hand, the choice of one of the vectors, say \hat{s}_3 , parallel to the normal direction with respect to the ecliptic plane, pointing North, will be helpful when describing the orbital trajectory of our planet. Once we have two elements of the triad, the last one comes from the relation

$$\hat{s}_2 \equiv \hat{s}_3 \times \hat{s}_1. \quad (2.74)$$

In this system of reference, and if we assume that the Earth follows a circular orbit⁹, the expression of \vec{r}_S is as simple as

$$\vec{r}_S = R_S [\cos(\Omega_S(t - t_0^{rev})) \hat{s}_1 + \sin(\Omega_S(t - t_0^{rev})) \hat{s}_2], \quad (2.75)$$

with R_S the Earth-Sun mean distance (one Astronomical Unit), Ω_S , the angular velocity of the Earth in its translational motion, and t_0^{rev} , the date of the autumn equinox.

Only one more step is needed before we can calculate the scalar product of \vec{r}_R and \vec{k} : the transformation rule between the two implied bases. It only depends (Figure 2.4) on one quantity δ , the angle that form the two planes of the equator and the ecliptic, the *inclination* of the Earth's axis,

$$\begin{cases} \hat{s}_1 = \hat{e}_1, \\ \hat{s}_2 = \cos \delta \hat{e}_2 + \sin \delta \hat{e}_3, \\ \hat{s}_3 = -\sin \delta \hat{e}_2 + \cos \delta \hat{e}_3. \end{cases} \quad (2.76)$$

The final result is

$$\begin{aligned} \vec{k} \cdot \vec{r}_S &= -\frac{R_S \omega_g}{c} [\sin \alpha \cos \beta \cos(\Omega_S(t - t_0^{rev})) \\ &\quad + (\cos \delta \sin \alpha \sin \beta + \sin \delta \cos \alpha) \sin(\Omega_S(t - t_0^{rev}))] \end{aligned} \quad (2.77)$$

$$\begin{aligned} &= -\frac{R_S \omega_g}{c} [(\sin \alpha \cos \beta)^2 \\ &\quad + (\cos \delta \sin \alpha \sin \beta + \sin \delta \cos \alpha)^2]^{\frac{1}{2}} \cos(\Omega_S(t - t_0^{rev}) + \phi_S), \end{aligned} \quad (2.78)$$

with ϕ_S equal¹⁰ to

$$\phi_S = \arctan \left[-\frac{\cos \delta \sin \alpha \sin \beta + \sin \delta \cos \alpha}{\sin \alpha \cos \beta} \right]. \quad (2.79)$$

⁹The tiny eccentricity of the elliptic trajectory of our planet (about 1.67×10^{-2}) gives consistency to this approximation, especially if we are going to study at once periods of time no longer than a few days.

¹⁰Since the arctan function is bi-valued (in the 0 to 2π range) ϕ_S must be chosen in such a way that the expression (2.78) is in concordance with expression (2.77).

2.4 The orientation

Let us consider the case of a roughly one-dimensional solid body that interacts with a gravitational wave. In such a case the only relevant deformations induced by the metric perturbation are those that trend to change the length of the object. Therefore we shall consider only the component of the relative acceleration which will eventually appear between any two points of this *bar* that is parallel to the latter:

$$a_{\hat{n}} \equiv \ddot{\ell}_i n^i = \frac{\ell_0}{2} \ddot{h}_{ij} n^i n^j. \quad (2.80)$$

Obviously, the time variations of $a_{\hat{n}}$ may have then their origin not only in the temporal dependence of the gravitational force but also in any external change of the orientation of the bar-like detector with respect to the wave. In the case of ground-based detectors the agent that causes \hat{n} to change is simply the rotation of the Earth. Thus, our goal is to express this vector in the proper basis of the incoming plane wave, in which the only non-vanishing components of h_{ij} are, as we have shown before, h_+ and h_\times .

Let us study closer the case in which \hat{n} lies on the horizontal plane with respect to its location in the planetary surface. A system of reference that is well adapted to the detector is $\{\hat{x}, \hat{y}, \hat{z}\}$ with \hat{x} tangent to the local meridian and pointing to the North, \hat{y} tangent to the local parallel and pointing to the West, and finally \hat{z} following the radial direction, away from the Earth. In that system, see Figure 2.5, \hat{n} takes the form

$$\hat{n} = \cos \Psi \hat{x} + \sin \Psi \hat{y}, \quad (2.81)$$

where Ψ is the *azimuthal* angle. We will find, in a first step, the actual relationship between \hat{x} , \hat{y} and $\{\hat{e}_1, \hat{e}_2, \hat{e}_3\}$

$$\begin{cases} \hat{x} = -\cos \theta [\cos(\Omega_E(t - t_0^{rot}) + \lambda) \hat{e}_1 - \sin(\Omega_E(t - t_0^{rot}) + \lambda) \hat{e}_2] + \sin \theta \hat{e}_3 \\ \hat{y} = \sin(\Omega_E(t - t_0^{rot}) + \lambda) \hat{e}_1 - \cos \theta \cos(\Omega_E(t - t_0^{rot}) + \lambda) \hat{e}_2 \end{cases} \quad (2.82)$$

The reason why we have selected the $\{\hat{e}_i\}$ as the intermediate basis is because, as we have seen, it is very convenient for describing both terrestrial and celestial vectors.

We will construct now a new vector set $\{\hat{w}_1, \hat{w}_2, \hat{w}_3\}$, with two of its elements, \hat{w}_1 and \hat{w}_2 , selected in such a way that they define the polarization plane

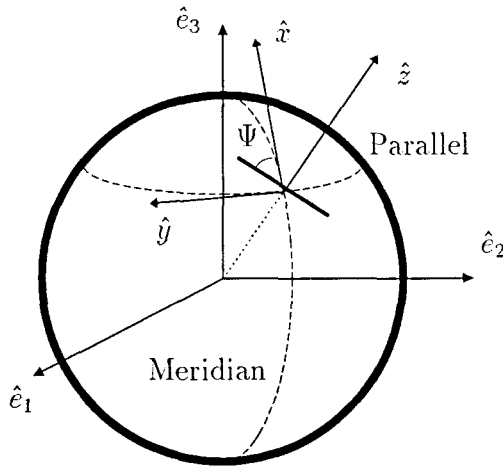


Figure 2.5: Representation of a one-dimensional object lying on a plane tangent to the Earth's surface. We can see here the angular variable Ψ which determines the orientation of the bar in the $\{\hat{x}, \hat{y}, \hat{z}\}$ basis, and the equatorial frame of reference $\{\hat{e}_i\}$.

of the gravity wave; and the third one, \hat{w}_3 , parallel to \vec{k} ,

$$\hat{w}_3 = -\sin \alpha \cos \beta \hat{e}_1 - \sin \alpha \sin \beta \hat{e}_2 - \cos \alpha \hat{e}_3. \quad (2.83)$$

We can force \hat{w}_1 to be on the terrestrial equatorial plane:

$$\hat{w}_1 = \sin \beta \hat{e}_1 - \cos \beta \hat{e}_2, \quad (2.84)$$

and, as usual, $\hat{w}_2 \equiv \hat{w}_3 \times \hat{w}_1$, which leads to

$$\hat{w}_2 = -\cos \alpha \cos \beta \hat{e}_1 - \cos \alpha \sin \beta \hat{e}_2 + \sin \alpha \hat{e}_3, \quad (2.85)$$

as it is depicted in Figure 2.1.

We have thus completed the set of relationships that will allow us to obtain the components of \hat{n} in the $\{w_i\}$ basis

$$n_i = \hat{n} \cdot \hat{w}_i, \quad (2.86)$$

or, explicitly,

$$\begin{cases} n_1 = \cos \Psi \cos \theta \sin \eta + \sin \Psi \cos \eta, \\ n_2 = \cos \alpha \cos \Psi \cos \theta \cos \eta - \cos \alpha \sin \Psi \sin \eta + \sin \alpha \cos \Psi \sin \theta, \\ n_3 = \sin \alpha \cos \Psi \cos \theta \cos \eta - \sin \alpha \sin \Psi \sin \eta - \cos \alpha \cos \Psi \sin \theta. \end{cases} \quad (2.87)$$

In fact, we need only to know the first two components, because we shall work in the **TT** gauge,

$$a_{\hat{n}} = \frac{\ell_0}{2} \left\{ \ddot{h}_+ [n_1^2 - n_2^2] + 2\ddot{h}_x n_1 n_2 \right\} \quad (2.88)$$

$$= \frac{\ell_0}{2} \left\{ \ddot{h}_+ \mathcal{S}_+ + \ddot{h}_x \mathcal{S}_x \right\}, \quad (2.89)$$

where we have introduced the two functions, \mathcal{S}_+ and \mathcal{S}_x ,

$$\begin{aligned} \mathcal{S}_+(t) &\equiv n_1^2 - n_2^2 = \frac{1}{2} [\sin^2 \alpha (1 - 3 \cos^2 \Psi \sin^2 \theta) + \\ &+ (1 + \cos^2 \alpha) (\sin^2 \Psi - \cos^2 \Psi \cos^2 \theta) \cos 2\eta \\ &+ (1 + \cos^2 \alpha) \sin 2\Psi \cos \theta \sin 2\eta \\ &- \sin 2\alpha \cos^2 \Psi \sin 2\theta \cos \eta \\ &+ \sin 2\alpha \sin 2\Psi \sin \theta \sin \eta], \end{aligned} \quad (2.90)$$

$$\begin{aligned} \mathcal{S}_x(t) &\equiv 2n_1 n_2 = \cos \alpha \sin 2\Psi \cos \theta \cos 2\eta \\ &- \cos \alpha (\sin^2 \Psi - \cos^2 \Psi \cos^2 \theta) \sin 2\eta \\ &+ \sin \alpha \sin 2\Psi \sin \theta \cos \eta \\ &+ \sin \alpha \cos^2 \Psi \sin 2\theta \sin \eta, \end{aligned} \quad (2.91)$$

that carry all the information about the directional dependence of the sensitivity of the detector device.

Finally, we devote a few words about why we have defined a new basis for describing the gravitational wave, other than what we introduced in Section 2.2.3. In both cases the criterion we have used to select the third axis is just

the same. This means that \hat{w}_3 is just \hat{k} ; but, as long as we have chosen \hat{i} in such a way it lies in the equatorial plane of the source, we have preferred the equatorial plane of the Earth in the case of \hat{w}_1 . That is to say, unless the two planes are parallel, those vectors will differ. Nevertheless, we can go back and forth between the bases performing a simple rotation of angle Υ , about the \vec{k} axis. The expression of Υ in terms of other angles, with a clearer physical meaning can be found in Appendix A.

Once we have rotated the basis, we must not forget to take the **TT** part of the new result,

$$h_+ = h_0 \left\{ \frac{1 + \cos^2 \iota}{2} \cos 2\Upsilon \cos(\omega_g t + \varphi_g) - \cos \iota \sin 2\Upsilon \sin(\omega_g t + \varphi_g) \right\}, \quad (2.92)$$

$$h_\times = h_0 \left\{ \frac{1 + \cos^2 \iota}{2} \sin 2\Upsilon \cos(\omega_g t + \varphi_g) + \cos \iota \cos 2\Upsilon \sin(\omega_g t + \varphi_g) \right\}. \quad (2.93)$$

We realize that if the wave originally was circularly polarized (i.e. $\cos \iota = \pm 1$), it maintains this property and Υ becomes meaningless.

2.5 The overall waveform

We shall finish this chapter summing up the different contributions to the final functional form of the expected driving force. As stated in equation (2.89) the mutual acceleration that will experience any two points of an extended object, due to the interaction with a plane gravitational wave, can be written in terms of its polarizations, $h_+(t)$ and $h_\times(t)$, and the sensitivity functions, $\mathcal{S}_+(t)$ and $\mathcal{S}_\times(t)$, which we have given in equations (2.90) and (2.91),

$$a_n = \frac{\ell_0}{2} \{ \ddot{h}_+(t) \mathcal{S}_+(t) + \ddot{h}_\times(t) \mathcal{S}_\times(t) \}. \quad (2.94)$$

The two polarizations, in their turn, are *quasi-sinusoidal* functions,

$$h_\pm = h_0 \mathcal{P}_\pm \cos(\omega_g \{t + \delta t\} + \varphi_\pm), \quad (2.95)$$

with

$$\mathcal{P}_+ = \sqrt{\left(\frac{1 + \cos^2 \iota}{2}\right)^2 \cos^2 2\Upsilon + \cos^2 \iota \sin^2 2\Upsilon}, \quad (2.96)$$

$$\mathcal{P}_\times = \sqrt{\left(\frac{1 + \cos^2 \iota}{2}\right)^2 \sin^2 2\Upsilon + \cos^2 \iota \cos^2 2\Upsilon}, \quad (2.97)$$

and

$$\tan(\varphi_\pm - \varphi_g) = \pm \frac{2 \cos \iota}{1 + \cos^2 \iota} (\tan 2\Upsilon)^{\pm 1}; \quad (2.98)$$

because δt is itself a non-linear function of time,

$$\delta t = t_S \cos(\Omega_S t + \varphi_S) + t_E \cos(\Omega_E t + \varphi_E), \quad (2.99)$$

where the values of t_S , t_E , φ_S and φ_E ,

$$t_S = \frac{R_S}{c} \sqrt{(\sin \alpha \cos \beta)^2 + (\cos \delta \sin \alpha \sin \beta + \sin \delta \cos \alpha)^2}, \quad (2.100)$$

$$t_E = \frac{R_E}{c} \sin \theta \sin \alpha, \quad (2.101)$$

$$\varphi_S = \phi_S - \Omega_S t_0^{rev}, \quad (2.102)$$

$$\varphi_E = \lambda - \beta - \Omega_E t_0^{rot}, \quad (2.103)$$

come directly from the expressions (2.78), (2.71) and (2.72). As the observational time increases, the characteristics of the gravitational driving force will differ more and more from the monochromatic ones. This topic, however, will be developed in the next chapter.

Chapter 3

The antenna

The world was to me a secret which I desired to divine.
Curiosity, earnest research to learn the hidden laws of
nature, gladness akin to rapture, as they were unfolded to
me, are among the earliest sensations I can remember.

—Mary Shelley, *Frankenstein, or the Modern Prometheus*

3.1 Introduction

We are going to develop in this chapter the key topics concerning the detector:
the cryogenic resonant antenna *Explorer* [2, 3, 6].

We shall begin with a general outline of the way in which the detector works. We have stated in the previous chapter that when a gravitational wave interacts with extended body it tends to modify the shape of the object, and we have explicitly shown this effect analyzing the layout of a set of non-interacting point-like particles. In the present case, however, the object of our study is a metallic cylinder and the monitored deformations are those that change its length. Thus we shall use the elasticity theory, applied to a one-dimensional finite medium, in order to derive and solve the equations that fulfill the bar ends. Moreover, we will see how the behaviour of the extremes of the elastic cylinder can be described with a harmonic-oscillator model.

Nevertheless, the metallic bar is not the only component of the *Explorer* detector. The vibrations of the cylinder are amplified and translated into voltage variations thanks to a resonant transducer [21, 16] attached there. The electric voltage is then transformed into magnetic flux and fed into a d.c. SQUID, a

superconducting quantum interference device that acts as amplifier of the signal [19], that is finally recorded together with more useful information coming from different sensors, in binary format.

All this process of acquisition of the data must be done trying to keep the level of noise as low as possible, if we really want to detect the presence of the weak disturbances that a gravitational wave causes. To this end the detector is mechanically isolated from the external world by a cascade of consecutive damping systems. Moreover, most of the components of the antenna (the bar, the transducer, the d.c. SQUID...) are cooled down to the temperature of the liquid helium, 2.6 Kelvin degrees. This reduces the disturbances due to the thermal vibrations of those parts of the experimental device.

Following the results corresponding to the cylinder alone, we will model behaviour the whole physical apparatus using a mechanical kit made of springs, dampers and masses. We obtain the solution of the equations derived from the model and then we apply it to the case in which the driving force comes from the interaction of a monochromatic gravitational wave with the bar.

We also spend some time in the study of the unavoidable companion of the signal in any experimental measure: the noise. We will review the major contributions to that disturbing process, and the properties it has, because only with a precise knowledge of the characteristic traits of both signal and noise will we be able to distinguish one from the other.

We will finish the chapter with a detailed description of the contents of the computer files that the data acquisition system of the *Explorer* antenna generates with the multiple information that the detector registers.

3.2 Elastic bars and gravitational waves

We shall present in this section how a weak gravitational wave couples with an elastic body. Since our interest is concerned in the behaviour of the ends of a aluminium cylinder, we shall concentrate our study in a finite one-dimensional elastic bar. Moreover, our final purpose is to show how the extended body can be rightfully described using a harmonic oscillator model, after a suitable redefinition of the parameters. So we have selected a relatively clean system: we have considered neither damping nor coupling with other forces than the driving one.

3.2.1 The elastic model

The equation that fulfills a one-dimensional elastic object is [47, 57]

$$\frac{\partial^2 \mathbf{d}(l, t)}{\partial t^2} = v_s^2 \frac{\partial^2 \mathbf{d}(l, t)}{\partial l^2} + \mathcal{F}(l, t) \quad (3.1)$$

where $\mathbf{d}(l, t)$ is the longitudinal displacement that suffers, at the time t , the point that originally (i.e. before the object was perturbed) was in l , v_s is the velocity of sound in the material the object is made of, and $\mathcal{F}(l, t)$ is the external force (per unit of mass) that in our case, as it is shown in expression (2.94), takes the form

$$\mathcal{F}(l, t) = l \mathcal{G}(t). \quad (3.2)$$

The solution of equation (3.1) have also to fit the boundary conditions which follow from the fact that the bar ends move freely:

$$\left. \frac{\partial \mathbf{d}(l, t)}{\partial l} \right|_{l=-\frac{L_b}{2}} = \left. \frac{\partial \mathbf{d}(l, t)}{\partial l} \right|_{l=\frac{L_b}{2}} = 0 \quad (3.3)$$

where L_b is the length of the object.

The general solution of (3.1), once we have performed a Fourier transform,

$$\frac{\partial^2 \tilde{\mathbf{d}}(l, \omega)}{\partial l^2} + \frac{\omega^2}{v_s^2} \tilde{\mathbf{d}}(l, \omega) = -\frac{l}{v_s^2} \tilde{\mathcal{G}}(\omega) \quad (3.4)$$

is simply

$$\tilde{\mathbf{d}}(l, \omega) = A(\omega) \sin \left(\frac{\omega}{v_s} l + \phi(\omega) \right) - \frac{l}{\omega^2} \tilde{\mathcal{G}}(\omega). \quad (3.5)$$

In order to determine $A(\omega)$ and $\phi(\omega)$ we will use the constrains that impose the boundary conditions (3.3),

$$A(\omega) \frac{\omega}{v_s} \cos \left(\pm \frac{\omega L_b}{2v_s} + \phi(\omega) \right) - \frac{1}{\omega^2} \tilde{\mathcal{G}}(\omega) = 0, \quad (3.6)$$

two expressions which may be suitably convined, yielding in this way

$$A(\omega) \frac{\omega}{v_s} \sin \left(\frac{\omega L_b}{2v_s} \right) \sin \phi(\omega) = 0 \quad (3.7)$$

and

$$A(\omega) \frac{\omega}{v_s} \cos\left(\frac{\omega L_b}{2v_s}\right) \cos \phi(\omega) = \frac{1}{\omega^2} \tilde{\mathcal{G}}(\omega). \quad (3.8)$$

The solution of this system of equations when¹

$$\omega \neq 2n \frac{\pi v_s}{L_b}, \quad (3.9)$$

is

$$\phi(\omega) = n\pi, \quad (3.10)$$

$$A(\omega) = (-1)^n \frac{v_s}{\omega^3} \frac{1}{\cos\left(\frac{\omega L_b}{2v_s}\right)} \tilde{\mathcal{G}}(\omega), \quad (3.11)$$

where n is any integer number. This apparent arbitrariness disappears when we put together both results in equation (3.4). We shall show this fact writing the explicit form of the (Fourier transformed) displacement of the end of the elastic bar,

$$\tilde{x}_b(\omega) \equiv \tilde{\mathbf{d}}(L_b/2, \omega) = \frac{v_s}{\omega^3} \tan\left(\frac{\omega L_b}{2v_s}\right) \tilde{\mathcal{G}}(\omega) - \frac{L_b}{2\omega^2} \tilde{\mathcal{G}}(\omega). \quad (3.12)$$

If no driving force is applied, formulæ (3.7) and (3.8) reduce to

$$\sin\left(\frac{\omega L_b}{2v_s}\right) \sin \phi(\omega) = 0 \quad (3.13)$$

and

$$\cos\left(\frac{\omega L_b}{2v_s}\right) \cos \phi(\omega) = 0, \quad (3.14)$$

a system of equations that can be solved only for certain values of ω ,

$$\omega_{res}^{(n)} \equiv n \frac{\pi v_s}{L_b}. \quad (3.15)$$

which are called the *eigenfrequencies*, because the elastic body vibrates precisely at these frequencies when no external perturbation acts on it. Those *resonant* frequencies also coincide with the spectral components of the driving force which the bar are most sensitive to. Let us show that, exploring the value

¹The meaning of those particular frequency values is discussed below.

of expression (3.12) in the vicinity of the first resonant frequency of the object, i.e. when $n = 1$,

$$\omega_b \equiv \omega_{res}^{(1)} = \frac{\pi v_s}{L_b}. \quad (3.16)$$

We split ω in two terms, just defining $\Delta\omega$,

$$\Delta\omega \equiv \omega - \omega_b, \quad (3.17)$$

and introducing it in equation (3.12):

$$\tilde{x}_b(\omega) = -\frac{L_b}{\pi} \frac{\omega_b}{\omega^3} \cot\left(\frac{\pi\Delta\omega}{2\omega_b}\right) \tilde{\mathcal{G}}(\omega) - \frac{L_b}{2\omega^2} \tilde{\mathcal{G}}(\omega). \quad (3.18)$$

We shall assume afterwards that $\Delta\omega$ is small enough to approximate the cotangent function,

$$\tilde{x}_b(\omega) \approx -\frac{2L_b}{\pi^2} \frac{1}{\omega_b(\omega - \omega_b)} \tilde{\mathcal{G}}(\omega), \quad (3.19)$$

revealing so not only that $\tilde{x}_b(\omega)$ diverges² in the resonance but that the bar shall be more sensitive to perturbations which excite its first longitudinal mode of vibration instead of higher ones, due to the $1/\omega_b$ factor.

To be more precise, we have to point out that expression (3.19) also applies to any other odd resonant frequency, i.e. $\omega_{res}^{(3)}$, $\omega_{res}^{(5)}$, etcetera; but not to the even ones —recall the constraint in expression (3.9). In fact when considered these frequencies in more detail one must conclude that the even modes cause no displacement at all on the bar end:

$$\tilde{x}_b(\omega_{res}^{(2n)}) \equiv 0. \quad (3.20)$$

This means that the amplitude of the vibrations associated to the actual *second* monitored mode are three times smaller than those corresponding to its first fundamental mode, when the bar is perturbed by an external agent with the same spectral weight in both resonant frequencies. This fact compels us to consider only the study and even the storage of the response of the cylinder in the neighbourhood of ω_b .

²When the dissipative terms are take into account the mathematic divergence disappears yielding a possibly sharp but smooth maximum.

3.2.2 The spring-like model

Once we have shown that the most relevant response of an elastic bar to a gravitational-like driving force shall take place in the vicinity of ω_b , we are going to compare it with the behaviour of a forced harmonic oscillator. Let us consider a massless spring attached to a *wall*, a reference point which can not be shifted. Fastened to the free end of the spring —see Figure 3.1— we find a point-like mass m_b . The stiffness of the spring, k_b , have such a value that its related resonant frequency is just the first mode of vibration of the elastic bar we are considering,

$$k_b = m_b \omega_b^2. \quad (3.21)$$

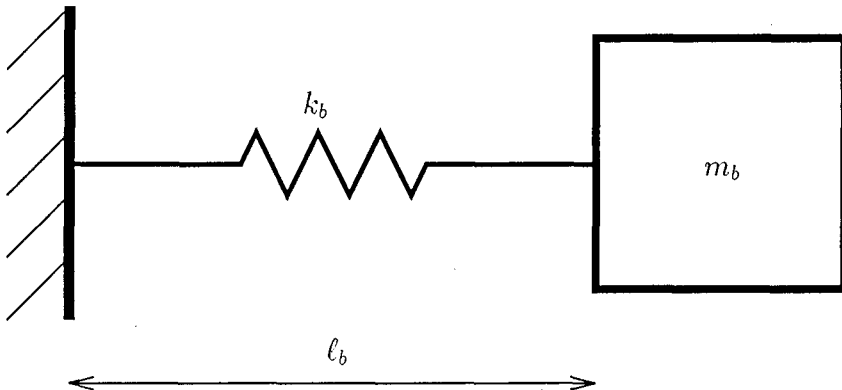


Figure 3.1: Spring-like model for the elastic cylinder.

We shall also assume that the harmonic oscillator we have obtained with the described layout is driven by the same external force of the preceding section. In this case, however, the gravitational coupling only affects the mass m_b and thus it must be evaluated in its unperturbed location ℓ_b . Since no peculiar motion is supposed in absence of external influence, ℓ_b coincides with the length of the unstressed spring. Thus $\mathbf{x}_b(t)$, the small displacement respect the equilibrium point that the mass may experience, fulfills the following equation:

$$\frac{d^2 \mathbf{x}_b}{dt^2} + \omega_b^2 \mathbf{x}_b = \ell_b \mathcal{G}(t). \quad (3.22)$$

Once we have Fourier transformed the formula (3.22), the value of $\tilde{\mathbf{x}}_b(\omega)$ can be found performing only elementary algebra,

$$\tilde{\mathbf{x}}_b(\omega) = -\frac{\ell_b}{\omega^2 - \omega_b^2} \tilde{\mathcal{G}}(\omega). \quad (3.23)$$

an expression that displays the following leading form when $\omega \sim \omega_b$

$$\tilde{\mathbf{x}}_b(\omega) \approx -\frac{\ell_b}{2 \omega_b(\omega - \omega_b)} \tilde{\mathcal{G}}(\omega). \quad (3.24)$$

Comparing formulæ (3.19) and (3.24) we conclude that if we want to model the vibrations of the end of an elastic bar in the vicinity of its first resonant frequency as those of a harmonic oscillator, we have to set

$$\ell_b = \frac{4}{\pi^2} L_b. \quad (3.25)$$

This value of ℓ_b is then the effective length of the cylinder when modeled by a spring with a mass attached to its end. What reminds us that we shall also solve the question of relating the true mass of the bar, say M_b , with the fictitious mass of the harmonic-oscillator model. The value m_b thus becomes, in a similar sense, the effective mass of the cylinder.

Let us consider solution of equation (3.1) when there are no external forces applied: the first normal mode of vibration of the solid. It is easy to check that

$$\mathbf{d}(l, t) = A \sin\left(\pi \frac{l}{L_b}\right) \sin(\omega_b t), \quad (3.26)$$

not only fulfills equation (3.1) but also the boundary conditions shown in (3.3). Let us compute, for instance, the kinetic energy of that mode³,

$$\begin{aligned} E_{kin} &= \frac{M_b A^2 \omega_b^2}{2 L_b} \cos^2(\omega_b t) \int_{-L_b/2}^{L_b/2} \sin^2\left(\pi \frac{l}{L_b}\right) dl \\ &= \frac{A^2 \omega_b^2 M_b}{4} \cos^2(\omega_b t), \end{aligned} \quad (3.27)$$

and we shall compare it with that of a body attached to a spring.

³We will assume that the bar is uniform in density.

The displacement that experiences the end of the bar is just

$$\mathbf{x}_b(t) = A \sin(\omega_b t), \quad (3.28)$$

clearly a solution of (3.22) if $\mathcal{F} = 0$. When dealing with a harmonic oscillator all the mass m_b undergoes the same movement, and the kinetic energy is simply

$$E_{kin} = \frac{A^2 \omega_b^2 m_b}{2} \cos^2(\omega_b t). \quad (3.29)$$

We thus conclude that the effective mass of the bar is:

$$m_b = \frac{M_b}{2}. \quad (3.30)$$

3.3 The experimental device

We have seen in the previous section why an elastic bar is a feasible (and easy to model) candidate to be chosen as a gravitational-wave antenna. Throughout the present section we are going to describe with some detail the *Explorer* detector, the actual experimental device whose output data we will analyze in this essay. As we shall see soon, it is a bit more complex than a simple elastic bar, however. The *Explorer* consists of a cylindrical aluminium bar equipped with a resonant capacitive transducer connected to a d.c. SQUID amplifier, via a superconducting transformer. The whole thing is surrounded with several shells whose intermediate cavities either are filled with cooling agents or act as thermal isolation tanks, due to their induced vacuum, as can be seen in Figure 3.2.

The detector is located at the CERN laboratories, 6.1° East longitude, 46.2° North latitude, and oriented 39.3° eastward, relative to the local North direction.

3.3.1 The resonant bar

The core of the *Explorer* detector is a cylinder made of 2270 kg of Al 5056 (an alloy of aluminum and magnesium), with a diameter of 60 cm and 3 m in length, which is hanging from a titanium cable wrapped around its central section, 2 m long and 5 mm in diameter, all of them inside a vacuum chamber whose

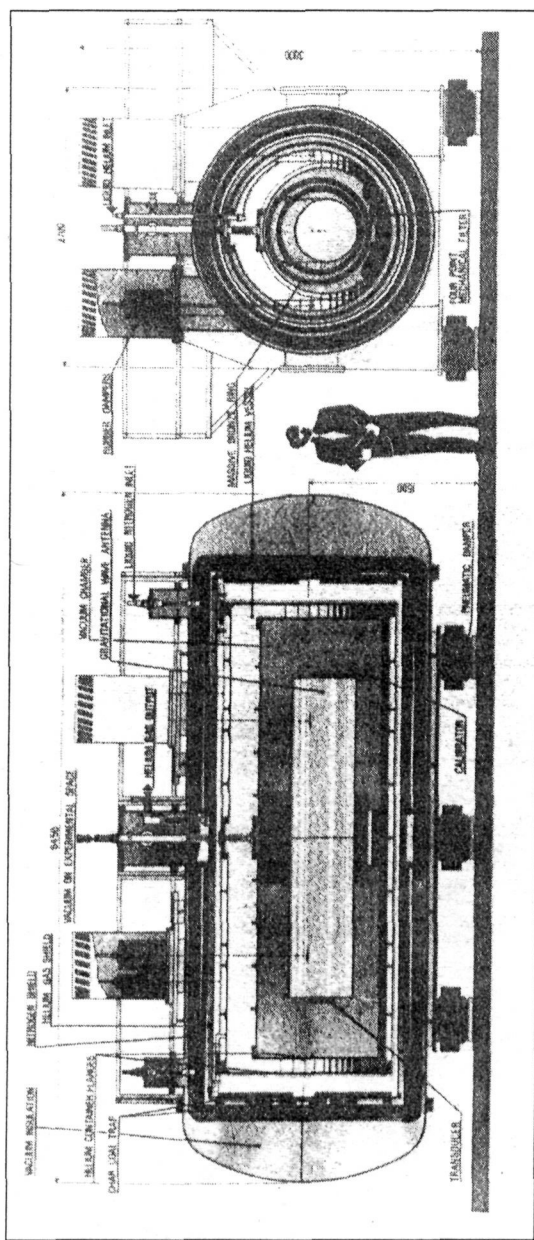


Figure 3.2: Blueprint for the *Explorer* gravitational-wave detector.

temperature was, at the time we are interested in, about 2.6 K. That is the innermost of a set of five concentric chambers, arranged like those Russian dolls and constructed with the purpose of cooling the bar and keeping its temperature stable at that low value. Next to this vacuum chamber is one filled with liquid-helium at 1.8 K. the following with the gas evaporated off that container, with a temperature near 30 K, the next one with liquid nitrogen and, finally another vacuum enclosure linked to a structure resting on dampers, which isolate it from ground vibrations.

In fact, each component of the detector is suspended from the previous one with the aim of isolating the bar from external acoustic and seismic disturbances, specially from those in the spectral range in which the cylinder is more sensitive, in the neighbourhood of f_b . In the case of the *Explorer* detector, the actual value of the (first) resonant frequency is

$$f_b = 915.7 \text{ Hz.} \quad (3.31)$$

The proper mode is not only characterized by its frequency (as we have assume in Section 3.2) but also by its *merit factor*, Q_b , a measure of the energy losses of the bar when it vibrates: larger is its value, more time the oscillation induced by any perturbation will remain. In fact τ_b ,

$$\tau_b = \frac{Q_b}{\pi f_b}, \quad (3.32)$$

is the time that the amplitude of such a vibration takes to drop by a factor of e : the decay time of the mode. Obviously, it is in our interest that the bar, like the rest of components, dissipates the energy that eventually could deposit a gravitational wave at the slowest possible rate in order to increase the chance of detection, and with this purpose is chosen the building material of the cylinder.

3.3.2. The transducer

Fastened to one end of the bar we find the transducer, a mushroom-shaped object, 0.4 kg in weight, that has a double purpose.

First of all, the transducer is designed to couple mechanically with the bar: it has also a main resonant frequency, associated with its flexural vibrations, that falls very close (but is not exactly equal) to the first longitudinal mode of the cylinder [69, 21]. This good tuning makes that the vibrational energy

is resonantly transferred between them, what leads to a magnification of the amplitude of the transducer vibration, when compared to the bar one⁴. This new resonator, however, will also contribute noticeably to the overall energy losses of the system, because its own merit factor, Q_t , is about two orders of magnitude smaller than Q_b .

On the other hand, the disk-like part of the transducer is a constitutive component of a two-plate capacitor of $C_t = 3890 \text{ pF}$. Before the antenna starts to operate a voltage bias of $V_t = 320 \text{ V}$ is applied between its plates, creating an electric field of $E_t = 6.15 \times 10^6 \text{ V/m}$ in the $52 \mu\text{m}$ that separate the two plates. These are connected through a second condenser, as shown in Figure 3.3, in such a way that only when the gap between the plates varies, due to

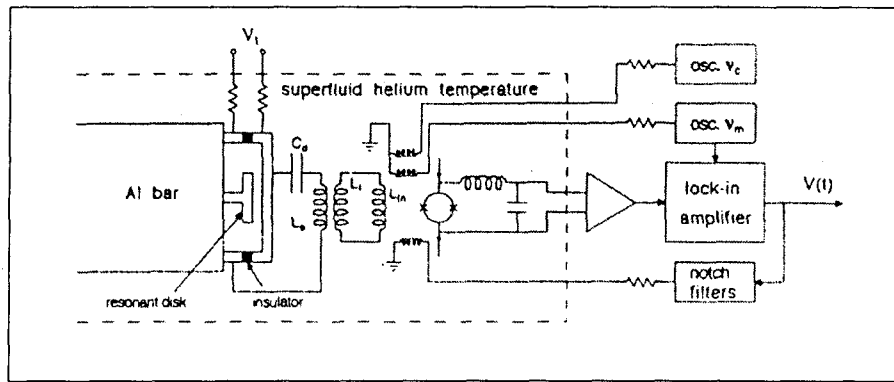


Figure 3.3: Diagram of the amplification system of the antenna.

the relative motion of the transducer and the bar end⁵, an electric current is induced. The capacitance, therefore, turns distances into voltages in such a way that the output is directly the product of three quantities: the change in the separation of the plates itself, $x(t)$, the value of the field E_t and a geometrical factor, $\gamma_t = 0.85$, determined by the mode shape of the transducer vibrations [67].

⁴In Section 3.4 we shall explain with more detail the reason of this amplification effect in the relative amplitudes of the oscillations.

⁵The second plate of the capacitor follows the cylinder vibrations, as also depicted in Figure 3.3.

3.3.3 The amplifier

The primary electric circuit connected to the capacitive transducer consists of a second capacitance, the so-called *decoupling* capacitance ($C_d = 100 \text{ nF}$), that avoids the automatic discharge of the transducer right after the application of the voltage bias, and a *primary* inductance ($L_0 = 2.5 \text{ H}$). There is also a *secondary* inductance ($L_i = 1.6 \mu\text{H}$), and these two components that have a mutual coupling factor of $\kappa_t = 0.77$, form a superconducting transformer whose purpose is to match the high impedance of the transducer with the low inductance ($L_{in} = 1.0 \mu\text{H}$) of the d.c. SQUID input coil.

The impedance of the whole circuit, attending to its layout, is [6]

$$Z(\omega) = \frac{1}{i\omega} \frac{C_t + C_d}{C_t C_d} + i\omega L_0 \left[1 - \kappa_t^2 \frac{L_i}{L_i + L_{in}} \right] + R_t, \quad (3.33)$$

where R_t accounts for the energetic losses of the various elements. This means that, as in the cases of the bar and the transducer, we have a merit factor related to the electrical part of the antenna which we can not neglect, because it turns out to be quite smaller than Q_b and Q_t . In fact, we can go further into the comparison, since the electric circuit behaves also like a damped harmonic oscillator, with its own resonant frequency, ω_{el} . The actual ω_{el} can be easily obtained from the expression of $Z(\omega)$ because

$$\left. \frac{dZ(\omega)}{d\omega} \right|_{\omega=\omega_{el}} = 0. \quad (3.34)$$

In our case, this leads to the following relationship,

$$\omega_{el} = \sqrt{\frac{(C_t + C_d)(L_i + L_{in})}{C_t C_d L_0 [L_i(1 - \kappa_t^2) + L_{in}]}} \quad (3.35)$$

and a numerical value, $f_{el} \sim 2 \times 10^3 \text{ Hz}$, that is far beyond the proper frequencies of the two other oscillators, $f_b \simeq 915.7 \text{ Hz}$ for the bar, as we have mentioned, and $f_t \simeq 910.4 \text{ Hz}$ for the transducer when it is fully operative⁶. This disparity of values has as a direct consequence that this new mode does not practically couple to the previous ones and therefore we will be free to

⁶The precision is justified, because the voltage bias applied to the transducer modifies substantially the value of the resonant frequency of its first flexural mode.

disregard it when we derive the equations that will characterize the behaviour of the detector (a detailed discussion of the problem of solving the system of the three coupled oscillators can be found in reference [86]).

The intensity of the current that passes through the input coil of the d.c. SQUID, $I_{in}(t)$, can now be expressed in terms of the variations of the gap between the plates of the transducer, and all the parameters that determine the electric circuit,

$$\tilde{I}_{in}(\omega) = \kappa_t \frac{\sqrt{L_0 L_i}}{L_i + L_{in}} \frac{\gamma_t E_t}{Z(\omega)} \tilde{\mathbf{x}}(\omega). \quad (3.36)$$

The input coil and the d.c. SQUID, more than just a planar coil, show a mutual inductance of

$$\mathcal{M}_{in} = 10^6 \Phi_0 / A \simeq 2 \text{ nH}, \quad (3.37)$$

where we have introduce the flux quantum, $\Phi_0 \simeq 2.068 \times 10^{-15}$ Wb. At this moment, we are able to translate lengths into fluxes acting on the d.c. SQUID, almost all that we need to know, as we shall see, in order to relate the final output of the antenna with the relative distance changes between the bar and transducer, and subsequently with the amplitude of the gravitational wave that causes them. The d.c. Superconducting QUantum Interference Device [23] is actually the most sensitive detector of magnetic flux, capable of discriminating flux variations of much less than Φ_0 , and transforming them into voltages, afterwards. Nevertheless, the gain of the d.c. SQUID may experience some fluctuations, inherent in the physical principle that governs the operation of the device, and for this reason the quantum amplifier is continuously monitored by means of a calibration a.c. magnetic flux of fixed root-mean-square⁷ (r.m.s. hereafter) amplitude, $\Phi_c = 1.33 \times 10^{-5} \Phi_0$, at a frequency of $f_c = 913$ Hz. This control signal eases the task of finding the conversion factor between fluxes and final voltages, because we can obtain it just from the experimental data, and then forget the amplification rate of the d.c. SQUID and all the following electrical components. That completes the required tools for rewriting the output voltage of the whole detector in terms of the vibrations of the cylinder and its mushroom-shaped companion.

⁷In this case we deal with a deterministic function and the mean has to be understood as a temporal integration over some suitable interval of time, a period for instance.

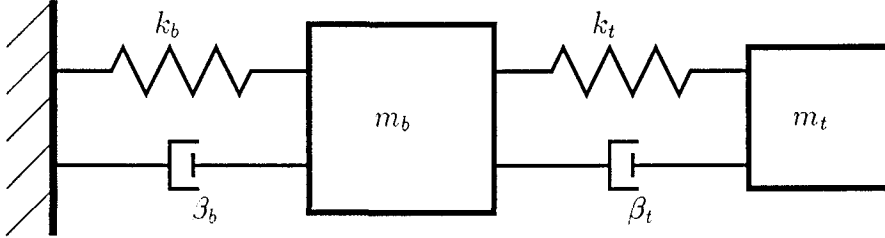


Figure 3.4: Mechanical model for the bar-transducer system.

3.4 The resonator coupling

We shall present here the set of equations, and its solution, which must fulfill the displacements of the bar end and the free transducer plate respectively: \mathbf{x}_b and \mathbf{x}_t . As has been pointed out in Section 3.3.3, the model shall account for the mechanical resonators and not for the electric one. Although we shall not consider any sort of coupling term between the two kind of resonating systems, we will argue that the value of some parameters is in practice settled by the electronic amplifier.

The equations [21, 70] will be derived from the mechanical model shown in Figure 3.4, two coupled harmonic oscillators with damping,

$$\begin{cases} m_b \ddot{\mathbf{x}}_b + 2m_b \beta_b \dot{\mathbf{x}}_b + k_b \mathbf{x}_b + 2m_t \beta_t (\dot{\mathbf{x}}_b - \dot{\mathbf{x}}_t) + k_t (\mathbf{x}_b - \mathbf{x}_t) = F_b, \\ m_t \ddot{\mathbf{x}}_t + 2m_t \beta_t (\dot{\mathbf{x}}_t - \dot{\mathbf{x}}_b) + k_t (\mathbf{x}_t - \mathbf{x}_b) = F_t; \end{cases} \quad (3.38)$$

which are driven by the overall sum of the external forces F_b and F_t , among what we shall find the gravitational-wave induced ones.

Now, we have to relate the parameters of the model (mass, stiffness and dissipation of each oscillator) to the physical constants of the detector. We have already given the relationship between m_b and M_b in equation (3.30), whereas k_b and ω_b are related by the common expression shown in (3.21). A similar relationship applies to k_t ,

$$k_t = m_t \omega_t^2, \quad (3.39)$$

and the link between the true and the effective mass of the transducer is just the same “geometrical factor” that we have introduced in Section 3.3.2,

$$m_t = \gamma_t M_t. \quad (3.40)$$

The parameters that account for the dissipative effects in the two oscillators, β_b and β_t , are simply the inverses of the decay times of the proper modes of the bar and the transducer, a quantities already defined in Section 3.3,

$$\beta_b = \frac{\omega_b}{2Q_b} = \tau_b^{-1}, \quad (3.41)$$

$$\beta_t = \frac{\omega_t}{2Q_t} = \tau_t^{-1}. \quad (3.42)$$

Using some of the previous expressions and defining the forces per unit of (effective) mass \mathcal{F}_b and \mathcal{F}_t , we can rewrite (3.38) in the form:

$$\begin{cases} \ddot{\mathbf{x}}_b + 2\beta_b \dot{\mathbf{x}}_b + \omega_b^2 \mathbf{x}_b + 2\beta_t \mu (\dot{\mathbf{x}}_b - \dot{\mathbf{x}}_t) + \mu \omega_t^2 (\mathbf{x}_b - \mathbf{x}_t) = \mathcal{F}_b, \\ \ddot{\mathbf{x}}_t + 2\beta_t (\dot{\mathbf{x}}_t - \dot{\mathbf{x}}_b) + \omega_t^2 (\mathbf{x}_t - \mathbf{x}_b) = \mathcal{F}_t, \end{cases} \quad (3.43)$$

where we have condensed all the dependence of the problem relative to the involved masses, into the parameter μ ,

$$\mu \equiv \frac{m_t}{m_b} \simeq 3 \times 10^{-4}. \quad (3.44)$$

A common technique used in order to solve systems of coupled ordinary differential equations, like (3.43), is the Fourier transform,

$$\begin{pmatrix} -\omega^2 + \omega_b^2 + \mu \omega_t^2 + i2\omega(\beta_b + \mu \beta_t) & -\mu(\omega_t^2 + i2\omega\beta_t) \\ -(\omega_t^2 + i2\omega\beta_t) & -\omega^2 + \omega_t^2 + i2\omega\beta_t \end{pmatrix} \begin{pmatrix} \tilde{\mathbf{x}}_b \\ \tilde{\mathbf{x}}_t \end{pmatrix} = \begin{pmatrix} \tilde{\mathcal{F}}_b \\ \tilde{\mathcal{F}}_t \end{pmatrix}, \quad (3.45)$$

because it reduces the problem to finding the inverse of a matrix, in our case a rank-two square one,

$$\tilde{\mathbf{x}}_b = \frac{1}{D(\omega)} \left([-\omega^2 + \omega_t^2 + i2\omega\beta_t] \tilde{\mathcal{F}}_b + \mu [\omega_t^2 + i2\omega\beta_t] \tilde{\mathcal{F}}_t \right), \quad (3.46)$$

$$\tilde{\mathbf{x}}_t = \frac{1}{D(\omega)} \left([\omega_t^2 + i2\omega\beta_t] \tilde{\mathcal{F}}_b + [-\omega^2 + \omega_b^2 + \mu \omega_t^2 + i2\omega(\beta_b + \mu \beta_t)] \tilde{\mathcal{F}}_t \right), \quad (3.47)$$

where $D(\omega)$ is just the determinant of the referred matrix,

$$\begin{aligned} D(\omega) \equiv & (-\omega^2 + \omega_t^2 + 2i\omega\beta_t)(-\omega^2 + 2i\omega\beta_b + \omega_b^2 + \mu(\omega_t^2 + 2i\omega\beta_t)) \\ & - \mu(\omega_t^2 + 2i\omega\beta_t)^2, \end{aligned} \quad (3.48)$$

which can be written in the following form,

$$D(\omega) = (\omega - \omega_+ - i\beta_+)(\omega + \omega_+ - i\beta_+)(\omega - \omega_- - i\beta_-)(\omega + \omega_- - i\beta_-), \quad (3.49)$$

with ω_{\pm} , β_{\pm} real and nonnegative. The values of ω_{\pm} , when the involved merit factors are much greater than $\mu^{-\frac{1}{2}}$, can be obtained from the expression,

$$\omega_{\pm}^2 = \frac{\omega_b^2 + \omega_t^2(1 + \mu)}{2} \pm \frac{1}{2}\sqrt{(\omega_b^2 - \omega_t^2)^2 + 2\mu\omega_t^2(\omega_b^2 + \omega_t^2) + \mu^2\omega_t^4}, \quad (3.50)$$

that, in our case yields

$$f_- = 904.7 \text{ Hz}, \quad (3.51)$$

for the *minus* mode, and

$$f_+ = 921.3 \text{ Hz}, \quad (3.52)$$

for the *plus* mode⁸. We could now proceed with the respective expressions of β_+ and β_- involving ω_b , ω_t , β_b and β_t , but it would be useless, because the electric layout that scarcely affects the resonant frequencies of the two modes, determines [6] the values of their merit factors and hence β_{\pm} . Since we have taken in this essay the position of including in the analytical model of the detector only the elastic resonators we are going to quote simply the actual numbers,

$$Q_- = 0.77 \times 10^6 \quad (3.53)$$

and

$$Q_+ = 1.01 \times 10^6, \quad (3.54)$$

and leave aside the problem of their explicit (and a bit cumbersome) calculation.

Once we have identified the parameters of the model we can draw some conclusions. Let us study the response of both, transducer and bar, to a perturbation acting only on the latter —this will be the case of a gravitational wave interacting with the antenna, as we shall argue later. The formulæ (3.47) and (3.47) which describe the coupled system in the vicinity of the new resonant modes, when no external force acts on the transducer, reduce to:

$$\tilde{x}_b(\omega_{\pm}) = \frac{1}{D(\omega_{\pm})} (-\omega_{\pm}^2 + \omega_t^2 + i2\omega_{\pm}\beta_t) \tilde{\mathcal{F}}_b, \quad (3.55)$$

$$\tilde{x}_t(\omega_{\pm}) = \frac{1}{D(\omega_{\pm})} (\omega_t^2 + i2\omega_{\pm}\beta_t) \tilde{\mathcal{F}}_b. \quad (3.56)$$

⁸We can check with this figures the relationship $\omega_b\omega_t = \omega_+\omega_-$, that follows from equation (3.50).

If the frequencies of the two original harmonic oscillators (as it is the case of the *Explorer* detector) are *well tuned*, i.e.,

$$\frac{(\omega_b - \omega_t)^2}{\omega_t^2} \ll 2\mu, \quad (3.57)$$

then the leading term of those expressions are,

$$\tilde{x}_b(\omega_{\pm}) \approx \mp \sqrt{\mu} \frac{\bar{\omega} \omega_t}{D(\omega_{\pm})} \tilde{\mathcal{F}}_b, \quad (3.58)$$

$$\tilde{x}_t(\omega_{\pm}) \approx \frac{\omega_t^2}{D(\omega_{\pm})} \tilde{\mathcal{F}}_b, \quad (3.59)$$

where we have introduced $\bar{\omega}$, a sort of mean frequency,

$$\bar{\omega}^2 \equiv \frac{\omega_t^2 + \omega_b^2}{2}. \quad (3.60)$$

We can see that, just as we have stated in Section 3.3.2, the amplitude of the oscillation in the transducer plate is amplified, exactly by a factor $\mu^{-\frac{1}{2}}$, with respect to the cylinder vibrations [],

$$\tilde{x}_t(\omega_{\pm}) \sim \frac{\tilde{x}_b(\omega_{\pm})}{\sqrt{\mu}}. \quad (3.61)$$

The fact that the actual measured displacement is the change in the relative distance between the end of the bar and the transducer, $\mathbf{x}(t) = \mathbf{x}_t(t) - \mathbf{x}_b(t)$, does not affect at all the magnification effect, because of the small value of the mass ratio μ :

$$\tilde{\mathbf{x}}(\omega_{\pm}) \approx \tilde{x}_t(\omega_{\pm}). \quad (3.62)$$

Moreover, we can obtain the explicit form of $\tilde{\mathbf{x}}(\omega)$ from (3.47) and (3.47),

$$\tilde{\mathbf{x}}(\omega) = \frac{1}{D(\omega)} [(-\omega^2 + \omega_b^2 + i2\omega\beta_b)\tilde{\mathcal{F}}_t + \omega^2\tilde{\mathcal{F}}_b], \quad (3.63)$$

and therefore we will be able to predict the response of the system to any kind of excitation we can express in terms of the two forces per unit mass (that is, accelerations) \mathcal{F}_b and \mathcal{F}_t .

3.5 The antenna response to a gravity wave

Before dealing with gravitational waves we must point out that due to the relative magnitude of the terms preceding \mathcal{F}_b and \mathcal{F}_t in the vicinity of the resonances, we shall disregard any effect of the wave on the transducer or, in other words, we may consider $\mathcal{F}_t = 0$. The appropriate value for the external perturbation acting on the bar, namely \mathcal{F}_b , related to gravitational plane wave, comes directly from the right-hand side of equation (2.94), with the only remarkable particularity that we must substitute ℓ_0 by the effective length of the bar, ℓ_b , related to the true dimensions of the elastic cylinder, L_b , by the equation (3.25).

3.5.1 The exact calculation

We shall go on with the calculation of the Fourier transform of the function \mathcal{F}_b ,

$$\tilde{\mathcal{F}}_b = \frac{\ell_b}{2} (\tilde{\mathcal{C}}_+ + \tilde{\mathcal{C}}_\times) \quad (3.64)$$

where the $\tilde{\mathcal{C}}_\pm$ are the convolution of $\tilde{\mathcal{S}}_\pm$ and \tilde{h}_\pm ,

$$\tilde{\mathcal{C}}_\pm(\omega) = -\frac{1}{2\pi} \int_{-\infty}^{+\infty} d\omega' \omega'^2 \tilde{h}_\pm(\omega') \tilde{\mathcal{S}}_\pm(\omega - \omega'). \quad (3.65)$$

The computation of $\tilde{\mathcal{S}}_+$ and $\tilde{\mathcal{S}}_\times$, according with their temporal dependency, shown in formulæ (2.90) and (2.91), yields a superposition of Delta distributions,

$$\begin{aligned} \tilde{\mathcal{S}}_+ &= \frac{\pi}{2} (1 + \cos^2 \alpha) (\sin \Psi - i \cos \Psi \cos \theta)^2 e^{2i\eta_0} \delta(\omega - 2\Omega_E) \\ &- i\pi \sin 2\alpha \cos \Psi \sin \theta (\sin \Psi - i \cos \Psi \cos \theta) e^{i\eta_0} \delta(\omega - \Omega_E) \\ &+ \pi \sin^2 \alpha (1 - 3 \cos^2 \Psi \sin^2 \theta) \delta(\omega) \\ &+ i\pi \sin 2\alpha \cos \Psi \sin \theta (\sin \Psi + i \cos \Psi \cos \theta) e^{-i\eta_0} \delta(\omega + \Omega_E) \\ &+ \frac{\pi}{2} (1 + \cos^2 \alpha) (\sin \Psi + i \cos \Psi \cos \theta)^2 e^{-2i\eta_0} \delta(\omega + 2\Omega_E), \end{aligned} \quad (3.66)$$

$$\begin{aligned} \tilde{\mathcal{S}}_\times &= i\pi \cos \alpha (\sin \Psi - i \cos \Psi \cos \theta)^2 e^{2i\eta_0} \delta(\omega - 2\Omega_E) \\ &+ 2\pi \sin \alpha \cos \Psi \sin \theta (\sin \Psi - i \cos \Psi \cos \theta) e^{i\eta_0} \delta(\omega - \Omega_E) \end{aligned}$$

$$\begin{aligned}
& + 2\pi \sin \alpha \cos \Psi \sin \theta (\sin \Psi + i \cos \Psi \cos \theta) e^{-i\eta_0} \delta(\omega + \Omega_E) \\
& - i\pi \cos \alpha (\sin \Psi + i \cos \Psi \cos \theta)^2 e^{-2i\eta_0} \delta(\omega + 2\Omega_E),
\end{aligned} \tag{3.67}$$

where η_0 is just

$$\eta_0 = \eta(0). \tag{3.68}$$

The expression of $\tilde{x}(\omega)$ in terms of \tilde{h}_+ and \tilde{h}_x is slightly breath-taking at first glance, but very simple when observed in depth,

$$\begin{aligned}
\tilde{x} = & -\frac{\omega^2 \ell_b}{8D(\omega)} [(1 + \cos^2 \alpha)(\sin \Psi - i \cos \Psi \cos \theta)^2 e^{2i\eta_0} (\omega - 2\Omega_E)^2 \tilde{h}_+(\omega - 2\Omega_E) \\
& - 2i \sin 2\alpha \cos \Psi \sin \theta (\sin \Psi - i \cos \Psi \cos \theta) e^{i\eta_0} (\omega - \Omega_E)^2 \tilde{h}_+(\omega - \Omega_E) \\
& + 2 \sin^2 \alpha (1 - 3 \cos^2 \Psi \sin^2 \theta) \omega^2 \tilde{h}_+(\omega) \\
& + 2i \sin 2\alpha \cos \Psi \sin \theta (\sin \Psi + i \cos \Psi \cos \theta) e^{-i\eta_0} (\omega + \Omega_E)^2 \tilde{h}_+(\omega + \Omega_E) \\
& + (1 + \cos^2 \alpha)(\sin \Psi + i \cos \Psi \cos \theta)^2 e^{-2i\eta_0} (\omega + 2\Omega_E)^2 \tilde{h}_+(\omega + 2\Omega_E) \\
& + 2i \cos \alpha (\sin \Psi - i \cos \Psi \cos \theta)^2 e^{2i\eta_0} (\omega - 2\Omega_E)^2 \tilde{h}_x(\omega - 2\Omega_E) \\
& + 4 \sin \alpha \cos \Psi \sin \theta (\sin \Psi - i \cos \Psi \cos \theta) e^{i\eta_0} (\omega - \Omega_E)^2 \tilde{h}_x(\omega - \Omega_E) \\
& + 4 \sin \alpha \cos \Psi \sin \theta (\sin \Psi + i \cos \Psi \cos \theta) e^{-i\eta_0} (\omega + \Omega_E)^2 \tilde{h}_x(\omega + \Omega_E) \\
& - 2i \cos \alpha (\sin \Psi + i \cos \Psi \cos \theta)^2 e^{-2i\eta_0} (\omega + 2\Omega_E)^2 \tilde{h}_x(\omega + 2\Omega_E)].
\end{aligned} \tag{3.69}$$

The Fourier transform of a function such as $h_{\pm}(t)$,

$$h_{\pm}(t) = h_0 \mathcal{P}_{\pm} \cos(\omega_g \{t + t_S \cos(\Omega_S t + \varphi_S) + t_E \cos(\Omega_E t + \varphi_E)\} + \varphi_{\pm}), \tag{3.70}$$

is a little more complex instead. Its calculation involves a double infinite series,

$$\tilde{h}_{\pm}(\omega) = \frac{h_0 \mathcal{P}_{\pm}}{2} (\tilde{\mathcal{H}}(\omega - \omega_g) e^{i\varphi_{\pm}} + \tilde{\mathcal{H}}^*(-\omega - \omega_g) e^{-i\varphi_{\pm}}), \tag{3.71}$$

$$\tilde{\mathcal{H}}(\omega) = 2\pi \sum_{k=-\infty}^{+\infty} \sum_{q=-\infty}^{+\infty} i^{k+q} J_k(\omega_g t_S) J_q(\omega_g t_E) e^{i(k\varphi_S + q\varphi_E)} \delta(\omega - k\Omega_S - q\Omega_E), \tag{3.72}$$

where each term have not only a Delta distribution, but the product of two Bessel functions, J_k and J_q , of an integer order. The whole thing makes the final result for $\tilde{x}(\omega)$ hard to handle. The situation about $x(t)$ is not better, even though the formal calculations of the inverse Fourier transform of $\tilde{x}(\omega)$ is almost direct, due to the fact that we were not able to find a closed expression for it.

3.5.2 The approximate calculation

One may wonder why we need to perform an approximate calculation once we know the *exact* result of the problem. It may also be argued that, even in the case we want a tentative solution, this could be inferred from the exact one. We have seen, however, that the final expressions were obtained in a rather formal way, and they will not be very useful from the viewpoint of practical applications. On the other hand, all the described procedures assume a perfect knowledge of the signals over an infinite extension of time, or, what is the same, an always-running device. Obviously we would not be able to process such amount of information, even if we had it. In fact, we could be interested in the study of the response of the antenna in a period of appreciably shorter duration, with the scope to minimize the effects that in the incoming wave produce the relative motions of the bar with respect to the proper frame of the gravitational radiation. Let us consider that we start our analysis at some time t_1 and we finish it at t_2 , after a time interval in which the variation in the quantities $S_{\pm}(t)$ are so small that we may change them for $\bar{S}_{\pm} = S_{\pm}(\bar{t})$, the values that each one takes in the middle of the interval,

$$\bar{t} \equiv \frac{t_2 + t_1}{2} = t_1 + \frac{\Delta t}{2}. \quad (3.73)$$

This in practice constrains Δt to be quite shorter than a (sidereal) day,

$$\Delta t \ll \frac{2\pi}{\Omega_E}. \quad (3.74)$$

Furthermore we would also like that the instantaneous frequency,

$$\begin{aligned} \omega_{obs} &= \omega_g - \omega_g t_E \Omega_E \sin(\Omega_E \bar{t} + \varphi_E) - \omega_g t_S \Omega_S \sin(\Omega_S \bar{t} + \varphi_S) \\ &- \omega_g t_E \Omega_E^2 \cos(\Omega_E \hat{t} + \varphi_E)(t - \bar{t}) - \omega_g t_S \Omega_S^2 \cos(\Omega_S \hat{t} + \varphi_S)(t - \bar{t}), \end{aligned} \quad (3.75)$$

(with $\min(t, \bar{t}) \leq \hat{t} \leq \max(t, \bar{t})$)

does not vary noticeably during the observation time. We need then a scale unit in order to compare with $\Delta\omega_{obs}$,

$$\Delta\omega_{obs} = \omega_{obs}(t_2) - \omega_{obs}(t_1), \quad (3.76)$$

and decide if the Doppler effect will distort the monochromatic behaviour of $h_{\pm}(t)$ or not. The frequency resolution naturally associated with a Δt is

$$\omega_{\Delta t} = \frac{2\pi}{\Delta t}, \quad (3.77)$$

and accordingly we shall demand that

$$|\Delta\omega_{obs}| \lesssim \frac{2\pi}{\Delta t}. \quad (3.78)$$

From equations (3.75) and (3.76) we can obtain the next inequality, that links $|\Delta\omega_{obs}|$ with some other physical parameters of the problem,

$$|\Delta\omega_{obs}| \leq \omega_g t_E \Omega_E^2 \Delta t + \omega_g t_S \Omega_S^2 \Delta t, \quad (3.79)$$

including Δt itself. If we set the right-hand of the last expression equal to $2\pi/\Delta t$ we may isolate the maximum value that the time interval should take,

$$\Delta t_{max} = \sqrt{\frac{2\pi}{\omega_g(t_E \Omega_E^2 + t_R \Omega_R^2)}}, \quad (3.80)$$

that clearly depends on the celestial position of the source, and the geographical location of the detector. For the *Explorer* antenna, in the worst case, which roughly corresponds to a source either on the Aries or on the Libra first points, the computation of Δt_{max} yields

$$\Delta t_{max} \simeq 3.4 \times 10^3 \text{ s}, \quad (3.81)$$

for a signal with $f_g \simeq 900 \text{ Hz}$, and its value is mainly dictated by the contribution coming from the rotational motion. In those conditions we shall write

$$h_{\pm}(t) = h_0 \mathcal{P}_{\pm} \cos(\bar{\omega}_{obs} t + \varphi'_{\pm}), \quad (3.82)$$

with

$$\bar{\omega}_{obs} \equiv \omega_g - \omega_g t_E \Omega_E \sin(\Omega_E \bar{t} + \varphi_E) - \omega_g t_S \Omega_S \sin(\Omega_S \bar{t} + \varphi_S), \quad (3.83)$$

and

$$\varphi'_{\pm} = \varphi_{\pm} + \omega_g t_E \cos(\Omega_E \bar{t} + \varphi_E) + \omega_g t_S \cos(\Omega_S \bar{t} + \varphi_S). \quad (3.84)$$

Before we go farther we must notice that although Δt_{max} shall be short enough to prevent $h_{\pm}(t)$ from displaying Doppler-related patterns, is very long when compared with the signal proper time scale,

$$\omega_g^{-1} \simeq 2 \times 10^{-4} \text{ s}, \quad (3.85)$$

which will allow us to perform the Fourier transform of (3.82) as if it was infinite in duration,

$$\tilde{h}_{\pm}(\omega) = \pi h_0 \mathcal{P}_{\pm} \left[e^{i\varphi'_{\pm}} \delta(\omega - \bar{\omega}_{obs}) + e^{-i\varphi'_{\pm}} \delta(\omega + \bar{\omega}_{obs}) \right]. \quad (3.86)$$

Collecting all the information, we will arrive at an expression for $\tilde{x}(\omega)$,

$$\begin{aligned} \tilde{x}(\omega) = & -\frac{\pi \omega^4 \ell_b h_0}{2D(\omega)} \left[(\bar{\mathcal{S}}_+ \mathcal{P}_+ e^{i\varphi'_+} + \bar{\mathcal{S}}_x \mathcal{P}_x e^{i\varphi'_x}) \delta(\omega - \bar{\omega}_{obs}) + \right. \\ & \left. + (\bar{\mathcal{S}}_+ \mathcal{P}_+ e^{-i\varphi'_+} + \bar{\mathcal{S}}_x \mathcal{P}_x e^{-i\varphi'_x}) \delta(\omega + \bar{\omega}_{obs}) \right], \end{aligned} \quad (3.87)$$

from what it is straightforward to obtain the final form for $x(t)$, substantially simpler and handier than that of the previous section:

$$\begin{aligned} x(t) = & -\frac{\bar{\omega}_{obs}^4 \ell_b h_0}{2|D(\bar{\omega}_{obs})|} \left[\bar{\mathcal{S}}_+ \mathcal{P}_+ \cos(\bar{\omega}_{obs} t + \varphi'_+ - \psi) + \right. \\ & \left. + \bar{\mathcal{S}}_x \mathcal{P}_x \cos(\bar{\omega}_{obs} t + \varphi'_x - \psi) \right], \end{aligned} \quad (3.88)$$

where we have set

$$D(\bar{\omega}_{obs}) = |D(\bar{\omega}_{obs})| e^{i\psi}, \quad (3.89)$$

with

$$\tan \psi = \frac{-2\bar{\omega}_{obs}[(\bar{\omega}_{obs}^2 - \beta_-^2 - \omega_-^2)\beta_+ + (\bar{\omega}_{obs}^2 - \beta_+^2 - \omega_+^2)\beta_-]}{(\bar{\omega}_{obs}^2 - \beta_-^2 - \omega_-^2)(\bar{\omega}_{obs}^2 - \beta_+^2 - \omega_+^2) - 4\bar{\omega}_{obs}^2 \beta_+ \beta_-}. \quad (3.90)$$

3.6 The noise

Unfortunately the detector will respond not only to the possible influence of a gravitational signal, but, in different degree, to any external or internal perturbation [35, 70, 6]. That is what we call noise: any random agent acting on the antenna. Due to its intrinsic stochastic nature, noise can not be correctly represented by a deterministic function of time. That does not mean that we know nothing about it. In some cases we can foresee not only its presence but its defining properties. A good instance of that is the unavoidable Brownian noise.

All the bodies, due to the simple fact of having a temperature above the absolute zero, vibrate. The *Explorer* detector, at the time we are planning to

analyze, was cooled down to a temperature of about 2.6 K, just to reduce the amplitude of the thermal perturbations affecting both cylinder and transducer. Since we have modeled them as if they were two one-dimensional oscillators, we shall assign each one, by virtue of the equipartition theorem, a mean energy related to their thermodynamic absolute temperature T,

$$\langle E_{Br} \rangle = \frac{1}{2} K_B T. \quad (3.91)$$

From this it immediately follows that the r.m.s. amplitude of the motions $\mathbf{r}(t)$ induced by the Brownian fluctuations of the transducer,

$$\sqrt{\langle \mathbf{r}_{Br_t}^2 \rangle} = \sqrt{\frac{K_B T}{m_t \omega_t^2}}, \quad (3.92)$$

are much greater than those related to the bar,

$$\sqrt{\langle \mathbf{r}_{Br_b}^2 \rangle} = \sqrt{\frac{K_B T}{m_b \omega_b^2}}, \quad (3.93)$$

as a consequence of the difference on their masses. We can also think about this problem in terms of the *plus* and *minus* modes. So, we shall have a Brownian amplitude associated to each resonant frequency,

$$\sqrt{\langle \mathbf{r}_{Br\pm}^2 \rangle} = \sqrt{\frac{K_B T}{m_\pm \omega_\pm^2}}, \quad (3.94)$$

with the particularity of the introduction of the two effective masses of the modes,

$$m_\pm = \pm \frac{m_b}{\omega_\pm^4} (\omega_\pm^2 - \omega_t^2) (\omega_+^2 - \omega_-^2), \quad (3.95)$$

both positive and related to m_t and m_b through

$$\frac{1}{m_-} + \frac{1}{m_+} = \frac{1}{m_t} + \frac{1}{m_b}. \quad (3.96)$$

The same properties of thermal noise make it behave as an external perturbation, only remembering the stochastic nature and properties of \mathcal{F}_b and \mathcal{F}_t . In particular that for those frequencies in which the detector is more sensitive, in the vicinity of ω_\pm , the amount of Brownian noise will increase, *but* it will

decrease in the frequency range where the antenna amplification is not so good. This means that, in principle, the chance of detecting a gravitational wave with a resonant device should not depend strongly on its frequency [63, 70].

Unfortunately, a second source of noise limits the hopes of having a wide-band resonant antenna: the electric amplifier. The noise that all the electric and magnetic components add to the signal has a white spectrum: it keeps barely the same level in the neighbourhood of the resonances, becoming thus much more important than the thermal noise shortly after one shifts from ω_- or ω_+ . We conclude from the above that it will not prove worthwhile to take into account or even, as we shall see, to store the information concerning frequencies far from the two proper modes of vibration.

The spectral density of this wide-band noise,

$$S_{wb} \simeq 4.5 \times 10^{-12} \Phi_0^2/\text{Hz}, \quad (3.97)$$

is nevertheless about six orders of magnitude smaller than the maxima of the Brownian noise,

$$S_{Br+} = 3.3 \times 10^{-6} \Phi_0^2/\text{Hz}, \quad (3.98)$$

and

$$S_{Br-} = 4.9 \times 10^{-6} \Phi_0^2/\text{Hz}. \quad (3.99)$$

It is also convenient to recall two quantities closely related to the previous, the r.m.s. amplitudes of the magnetic fluxes acting on the d.c. SQUID,

$$\Phi_{Br\pm} = \sqrt{\beta_\pm S_{Br\pm}} \quad (3.100)$$

whose experimental values are,

$$\Phi_{Br+} = 0.97 \times 10^{-6} \Phi_0, \quad (3.101)$$

and

$$\Phi_{Br-} = 1.35 \times 10^{-6} \Phi_0; \quad (3.102)$$

they may help us to find a second derivation of the length-to-flux conversion factor, \mathcal{K} ,

$$\Phi_{Br\pm} = \mathcal{M}_{in} \kappa_t \frac{\sqrt{L_0 L_i}}{L_i + L_{in}} \frac{\gamma_t E_t}{Z(\omega_\pm)} \sqrt{< \mathbf{r}_{Br\pm}^2 >} = \mathcal{K}_\pm \sqrt{< \mathbf{r}_{Br\pm}^2 >}. \quad (3.103)$$

In principle \mathcal{K} is a function that depends on the frequency, because the impedance does; but in the vicinity of the mechanical resonances, and then far away from the electrical one, it can be taken as constant. So we shall have

$$\Phi_{Br\pm} = \mathcal{K} \sqrt{\frac{K_B T}{m_\pm \omega_\pm^2}} = \mathcal{K} \frac{\omega_\pm}{\omega_+^2 - \omega_-^2} \sqrt{\frac{K_B T}{m_b a_\pm}}, \quad (3.104)$$

where we have turned m_\pm into the measurable a_\pm [6]. We have argued that gravitational waves must interact almost exclusively with the bar, whereas the thermal noise mainly arises from the transducer. That means that the same amount of energy will be shared between the modes in a different way, depending on its origin. The two quantities a_+ and a_- are the just the relative ratios, and have to fulfill,

$$a_+ + a_- = 1. \quad (3.105)$$

The actual values for the operating apparatus are

$$a_+ = 0.678, \quad (3.106)$$

and

$$a_- = 0.322. \quad (3.107)$$

From (3.104) it is not difficult to derive the following formula for the conversion factor \mathcal{K} ,

$$\mathcal{K} = (\sqrt{a_+} \Phi_{Br+} + \sqrt{a_-} \Phi_{Br-}) (\omega_+ - \omega_-) \sqrt{\frac{m_b}{K_B T}}. \quad (3.108)$$

Besides the noise that we have just described, we shall have also to face the occasional appearance of multiple sorts of non-stationary noise, maybe in the form of spurious sharp peaks like those in Figure 3.5. We shall have to discriminate them from the true gravitational signals, thanks to their distinctive properties.

3.7 The data acquisition system

It has been pointed out that only in the neighbourhood of the two resonant modes will we have chances of detecting a gravitational wave. So it is useless to keep the information from outside this frequency range. The aim of the procedures we are going to describe next is precisely to remove all the Fourier

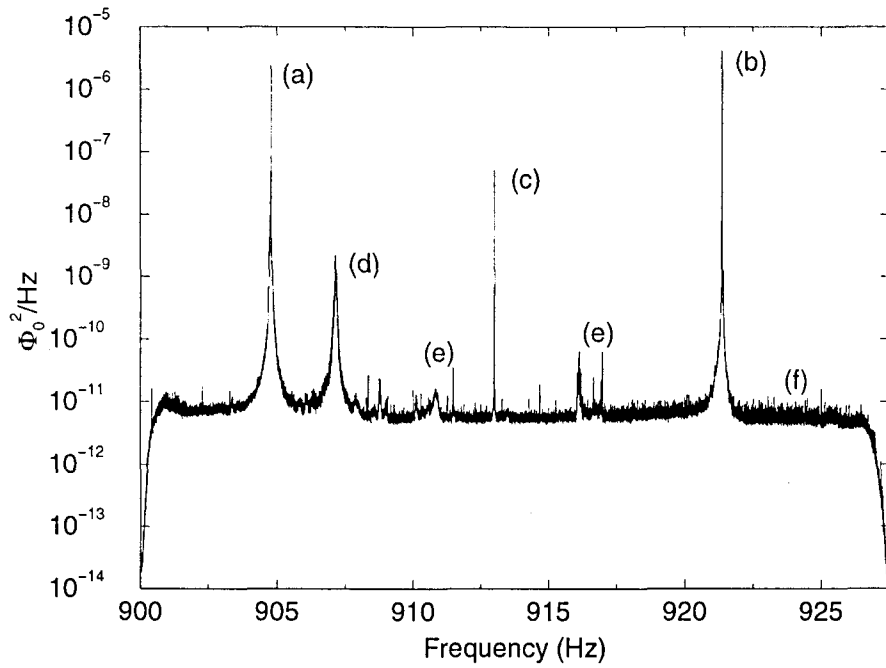


Figure 3.5: Example of power spectral density of the output signal computed with the averaged-periodogram technique. We can easily identify the minus (a) and the plus (b) resonant modes and the calibration flux (c), among a new resonance (d) and several other peaks (e); all of them over the wide-band noise (f).

components of the signal but those approximately comprised between 900 and 927.5 Hz. First of all the output of the antenna is processed in hardware with a bandpass filter with flat response in the range 902-926 Hz. After that, the signal can safely be sampled at 220.07042 Hz, because at this rate the aliasing will not put together the information carried by the spectral interval which remains untouched by the previous filtering. In fact, at this point we keep four times the minimum amount of data needed for encoding a signal whose predominant frequencies are constrained inside a band of about 27.5 Hz. But this reduction, very convenient from the viewpoint of the storage, must be done carefully, in order to avoid, once again, the frequency mixing. The selected strategy, named the **Anti-Aliasing Procedure**, is a software implementation,

applied on a stream of 16384 digital values⁹, which consists in a **Fast Fourier Transform**¹⁰, a subsequent discarding of the points outside the predominant region and finally an inverse **FFT** of the remaining 4096 complex numbers. This means that after the **AAP** the 900 Hz is virtually shifted to zero and the sampling time rises to 18176 μ s. Those processed temporal series will fill just one of the several channels that the acquisition system of the antenna saves using the **R87** data format. The contents of the rest of the channels, sampled all of them sixteen times slower, are as different as four data streams taken after two lock-in filters, one for each resonant mode, a calibration signal for those ones, a direct-acquisition channel, the wide-band noise level measured at 909 Hz, the output of two seismographs, one surveying low frequencies and the other the 900-930 Hz range, an electro-magnetic detector that monitors that same band, a channel with the sum of the ticks of two atomic clocks and the output of the apparatus at low frequencies [6].

There are records that do not contain sampled data but information about the *Explorer* antenna, like most of the numerical values of the parameters which we have shown in this chapter, about the data acquisition system itself and even some technical comments on the detector operation. Each record has also a header which can tell us from the record length to the precise time of acquisition, besides lots of other aspects¹¹ that will be very useful in the digital data analysis that we are going to describe in the next chapter.

⁹Moreover, the time pieces are taken in such a way they overlap, with the purpose of smoothing any border effect the procedure could introduce.

¹⁰We shall describe this computational algorithm with more detail in the next chapter.

¹¹For further specifications on the **R87** data format see Appendix B.

Chapter 4

Data analysis

It is an old maxim of mine that when you have excluded the impossible, whatever remains, however improbable, must be the truth.

—Sir Arthur Conan Doyle, *The Adventure of the Beryl Coronet*, in *The Adventures of Sherlock Holmes*

4.1 Introduction

The aim of the data analysis is to get the maximum quantity of information concerning the signal in spite of the perturbing effect of the noise. In noise, as it was mentioned in the preceding chapter, is condensed the action of uncontrollable or uncontrolled agents that affect therefore in a somewhat unpredictable way the detector. Thus it will not display a deterministic behaviour but a random one. In the present chapter we shall develop several strategies with the aim to discriminate between noise and signal. The algorithms will be designed starting from the well-known technique in data analysis of the matched filter.

The matched filter, the best linear filter under some criteria we widely explain in the text, like any other reliable filtering procedure needs of precise information about both signal and noise. The most relevant assumption we shall make in the case of the latter is that it can be satisfactorily modeled by a Gaussian stochastic process, whereas the target of our searching procedure will be, as we have repeatedly announced, a monochromatic wave, a sinusoidal function with a constant but unknown characteristic frequency. The consequences that the Doppler shift will produce in the waveform if the signal has an astro-

nomical origin will not be fully addressed in the first place, but considered and corrected *a posteriori*. Since the celestial coordinates of any eventual source will be also unknown we shall design an all-sky search procedure.

Two main algorithms are developed in this chapter devoted to the data analysis, depending on one particular trait of the frequency of the wave. A filtering procedure can not check the presence of a signal for *all* the possible values (a continuum) that its frequency may take, even in the case in which the scanned spectral band is limited in extension. So, only a finite set of frequencies can be taken into account, settled by the discrete Fourier transform procedure. The first method assumes that the actual wave frequency is just one of those in the Fourier spectrum of the data [52]. A better performance of the filter with respect the most usual algorithm —averaging Fourier transforms' square moduli— is achieved. We illustrate the good performance of the technique adding a control signal to real data. The agreement between the theoretical predictions and the experimental behaviour of the algorithm is also shown.

Nevertheless, if no frequency in the filter bank exactly matches the proper of the signal, the preceding method becomes useless when analyzing long stretches of data. Therefore, the second procedure is designed with the aim of relaxing the described frequency constraint and giving room to that effect [53, 54]. The price to pay is mainly condensed in the new filter performance which decreases with respect the previous algorithm. The filter properties are again checked before the algorithm is extensively applied to six months of real data recorded by the *Explorer* detector in 1991.

After the massive data processing we shall point out the presence of some outcomes which hardly can be produced by the random nature of noise. The origin of those notorious candidates to be gravitational signals will not be discussed in this essay, we shall limit our conclusions to the very presence of statistically relevant positive results.

Finally, the reader may wish to take a look at Appendix C, where it can be found the source code of the C-language programs we design with the purpose of implementing all these algorithms, among other useful computational tools.

4.2 Data filtering

Any experimental data stream may or may not contain the precise information we are interested in, which we generically call *the signal*, but if it is really

there it will be undoubtedly buried under noise. As we have mentioned in the previous chapter, the presence of this perturbing agent of random behaviour in the detector output is always guaranteed and, considering the foreseeable weakness of any kind of gravitational wave, but especially the monochromatic ones, seriously threatens to completely mask the signal itself.

According to that, the first objective of any filtering procedure shall be to enhance the signal and simultaneously to decrease the level of the noise in the data. The result of this balance, usually measured by the so-called *signal-to-noise ratio*, will determine the chance of detection of that particular sort of signal. In the second place, after the analysis process we should be able to conclude not merely the presence of the signal in the experimental data but the concrete value of the different parameters, in our case the frequency and the amplitude. When more traits of the wave, like its polarization state, can be estimated from the analysis of the filter outcome it will be feasible to compute the celestial location of the radiation source, the first step towards gravitational astronomy.

4.2.1 Linear filters

As it has been said we shall assume that the experimental data stream $\mathbf{u}(t)$ is the sum of two well-different contributions,

$$\mathbf{u}(t) = \mathbf{x}(t) + \mathbf{r}(t), \quad (4.1)$$

the signal we are looking for, $\mathbf{x}(t)$, a deterministic function, and the noise $\mathbf{r}(t)$, which we model as a stochastic process¹. Considering that the random component of the data only affects the signal in this additive way supposes the first of a series of assumptions that we will be forced to undertake. The behaviour of the noise conditions the choice of the filter much as the functional form of $\mathbf{x}(t)$ does, and so we need to impose some constraints concerning the noise properties, whose fulfillment will be tested afterwards.

¹We have deliberately repeated the notation used in Chapter 3, when we spoke about changes in the transducer gap. The amplification (and physical transformation) introduced by all the electro-magnetic devices will be disregarded in the following theoretical development because it can be reduced to the presence or not of a multiplicative constant. This means that before any practical analysis procedure we should properly normalize the true experimental data.

The data processing we are going to present in this section relies in the application of a linear filter, $g(t)$, to the experimental stream $u(t)$,

$$y \equiv \int_{-\infty}^{\infty} g(t)u(t)dt. \quad (4.2)$$

The filter output, y , will help us in our task of deciding whether the signal is actually present or not, and it clearly depends on the particular choice of the filter. Nevertheless, we can not predict the concrete value of this quantity due to the fact that the noise is of stochastic nature and thus y itself is a random variable. Actually, we can split it in two terms,

$$y = y_x + y_r, \quad (4.3)$$

one of them, again, fully deterministic, y_x ,

$$y_x = \int_{-\infty}^{\infty} g(t)x(t)dt, \quad (4.4)$$

and the other y_r of random character.

$$y_x = \int_{-\infty}^{\infty} g(t)r(t)dt. \quad (4.5)$$

Therefore the mean value of y is just,

$$\langle y \rangle = y_x + \langle y_r \rangle, \quad (4.6)$$

and, since we will assume that we deal with a zero-mean noise, that is

$$\langle r(t) \rangle = 0, \quad (4.7)$$

equation (4.8) will reduce to,

$$\langle y \rangle = y_x, \quad (4.8)$$

the result of the action of the filter on the signal we search for.

We realize then that the mean of y can not be a good estimator of the efficiency of the filter, because it tells nothing about the coupling between $g(t)$

and $\mathbf{r}(t)$. We shall move our attention to the moment of the next order, and so compute the mean square value² of \mathbf{y} , $\langle \mathbf{y}^2 \rangle$,

$$\langle \mathbf{y}^2 \rangle = \mathbf{y}_x^2 + \langle \mathbf{y}_r^2 \rangle = \langle \mathbf{y}_r^2 \rangle (1 + \rho), \quad (4.9)$$

where we have introduced ρ , the signal-to-noise ratio (**SNR**),

$$\rho \equiv \frac{\mathbf{y}_x^2}{\langle \mathbf{y}_r^2 \rangle}, \quad (4.10)$$

a parameter that weights the relative strength of the response of both signal and noise in the filtering process. It follows from the same expression (4.9) that the degree of contribution of the filtered noise to the final value of \mathbf{y} depends on the **SNR**, being less important as the value of ρ increases and

$$\langle \mathbf{y}^2 \rangle \xrightarrow{\rho \gg 1} \mathbf{y}_x^2. \quad (4.11)$$

Usually those quantities \mathbf{y}_x^2 and $\langle \mathbf{y}_r^2 \rangle$ are expressed in terms of integrals not in the time domain but in the frequency domain. The first one seems to be a direct translation of (4.4) in which t has been changed to ω , except by a complex-conjugate symbol that, in fact, may be located in either of the two factors,

$$\mathbf{y}_x^2 = \left(\frac{1}{2\pi} \int_{-\infty}^{\infty} \tilde{\mathbf{x}}^*(\omega) \tilde{\mathbf{g}}(\omega) d\omega \right)^2. \quad (4.12)$$

The expression for $\langle \mathbf{y}_r^2 \rangle$,

$$\langle \mathbf{y}_r^2 \rangle = \int_{-\infty}^{\infty} dt \int_{-\infty}^{\infty} dt' \langle \mathbf{r}(t) \mathbf{r}(t') \rangle \mathbf{g}(t) \mathbf{g}(t'), \quad (4.13)$$

is far more interesting, specially when the noise is stationary. In this case, the *autocorrelation*, $R(t, t')$, of the stochastic process $\mathbf{r}(t)$ depends only on absolute time differences,

$$\langle \mathbf{r}(t) \mathbf{r}(t') \rangle \equiv R(t, t') = R(t - t') = R(t' - t), \quad (4.14)$$

and then we can use this property,

$$\langle \mathbf{y}_r^2 \rangle = \int_{-\infty}^{\infty} dt \int_{-\infty}^{\infty} dt' R(t - t') \mathbf{g}(t) \mathbf{g}(t') = \frac{1}{2\pi} \int_{-\infty}^{\infty} S(\omega) |\tilde{\mathbf{g}}(\omega)|^2 d\omega \quad (4.15)$$

²Our final goal is to analyze experimental data coming from the *Explorer* detector, so we will consider only real time functions. However, all the statements and proofs may be easily generalized or adapted to complex time functions.

in order to introduce the Fourier Transform of $R(t)$,

$$S(\omega) \equiv \int_{-\infty}^{\infty} R(t)e^{-i\omega t} dt = 2 \int_0^{\infty} R(t) \cos(\omega t) dt, \quad (4.16)$$

the *power spectral density* of the noise, $S(\omega)$, a real nonnegative³ even function that, as we shall see, condenses all the information that we will eventually need to know about $\mathbf{r}(t)$ when designing the optimum filter.

4.2.2 The matched filter

Once we have present the **SNR** as a useful measure of the filter performance we can now consider the question from the opposite side; we can look for the *linear filter* that maximizes ρ for a given signal and noise. The function $\mathbf{g}(t)$ that fulfills this condition is called the *matched filter* [39, 71].

The simplest approach to the resolution of the stated problem needs Cauchy-Schwarz inequality which reads: *for any* $v(x)$ *and* $w(x)$,

$$\left| \int_a^b v(x)w(x)dx \right|^2 \leq \int_a^b |v(x)|^2 dx \int_a^b |w(x)|^2 dx, \quad (4.17)$$

furthermore, the equality sign holds if and only if

$$w(x) \propto v^*(x), \quad (4.18)$$

(almost) everywhere in the interval of integration. Let us start with a suitable reorganization of \mathbf{y}_x^2 ,

$$\left| \int_{-\infty}^{\infty} \tilde{\mathbf{x}}^*(\omega)\tilde{\mathbf{g}}(\omega)d\omega \right|^2 = \left| \int_{-\infty}^{\infty} \frac{\tilde{\mathbf{x}}^*(\omega)}{\sqrt{S(\omega)}}\tilde{\mathbf{g}}(\omega)\sqrt{S(\omega)}d\omega \right|^2, \quad (4.19)$$

that shall bring $\langle \mathbf{y}_r^2 \rangle$ in the right-hand side of the inequality after we apply the rule (4.17),

$$\left| \int_{-\infty}^{\infty} \tilde{\mathbf{x}}^*(\omega)\tilde{\mathbf{g}}(\omega)d\omega \right|^2 \leq \int_{-\infty}^{\infty} \frac{|\tilde{\mathbf{x}}(\omega)|^2}{S(\omega)} d\omega \int_{-\infty}^{\infty} |\tilde{\mathbf{g}}(\omega)|^2 S(\omega) d\omega, \quad (4.20)$$

³This property of the power spectral density is not obviously inferred from its very definition, but can be followed looking at expression (4.15). On one side the integrand is the product of $S(\omega)$ and a nonnegative function, $|\tilde{\mathbf{g}}(\omega)|^2$, and on the other side the value of the integral, $\langle \mathbf{y}_r^2 \rangle$, must always nonnegative, independently of the actual choice of the filter $\tilde{\mathbf{g}}(\omega)$; both together lead to $S(\omega) \geq 0$.

so we conclude that,

$$\rho \leq \frac{1}{2\pi} \int_{-\infty}^{\infty} \frac{|\tilde{x}(\omega)|^2}{S(\omega)} d\omega, \quad (4.21)$$

and, according to formula (4.18), the maximization of the **SNR** only will take place when

$$\tilde{g}(\omega) \equiv \mathcal{C} \frac{\tilde{x}(\omega)}{S(\omega)}, \quad (4.22)$$

where \mathcal{C} is an arbitrary constant. Then the **SNR** is the sum of the relative spectral contribution of signal and noise for each frequency,

$$\rho = \frac{1}{2\pi} \int_{-\infty}^{\infty} \frac{|\tilde{x}(\omega)|^2}{S(\omega)} d\omega. \quad (4.23)$$

The case in which the signal $x(t)$ corresponds to a monochromatic function,

$$x(t) = \mathcal{A}_0 \cos(\omega_0 t + \varphi_0), \quad (4.24)$$

seems to be specially advantageous, from the perspective of linear filtering, for several reasons. The calculation of $g(t)$, for instance, needs no knowledge about the explicit value of $S(\omega)$, except for ω_0 , and this one can be re-absorbed by the (new) arbitrary constant $\mathcal{B}(\omega_0)$,

$$g(t) = \frac{\mathcal{C}\mathcal{A}_0}{S(\omega_0)} \cos(\omega_0 t + \varphi_0) = \mathcal{B}(\omega_0) \cos(\omega_0 t + \varphi_0), \quad (4.25)$$

and after all we get a filter that is functionally identical to the signal. Moreover, the value of ρ is formally infinite, unless the power spectral density is also unbounded for ω_0 , because all the energy carried by the wave, which in fact is infinite, is confined in a single frequency. In practical situations, however, the signal and the data stream itself shall be time limited and then these divergences will disappear.

4.2.3 Sampled data of finite length

It is notorious that the previous derivation of the matched filter and the filter procedure itself assumes that

- we have a continuous data stream and,

- we know its value at any instant of time.

In turn, as we have pointed out in the preceding chapter, the data-acquisition system of the detector will provide not a continuous function but a series of N discrete values, obviously finite in length, with a time lag equal to T (as we have seen, $18176 \mu s$ in our case), between two consecutive samples. So we will have

$$\mathbf{u}(n) = \mathbf{x}(n) + \mathbf{r}(n) \quad (n = 0, \dots, N - 1). \quad (4.26)$$

The fact that the data are not continuous but discrete will force us to change the integral sign by a finite sum in expression (4.3),

$$\mathbf{y} \equiv \sum_{n=0}^{N-1} \mathbf{g}(n) \mathbf{u}(n), \quad (4.27)$$

and redefine \mathbf{y}_x and \mathbf{y}_r accordingly,

$$\mathbf{y}_x \equiv \sum_{n=0}^{N-1} \mathbf{g}(n) \mathbf{x}(n), \quad (4.28)$$

$$\mathbf{y}_r \equiv \sum_{n=0}^{N-1} \mathbf{g}(n) \mathbf{r}(n). \quad (4.29)$$

The choice of the filter that optimizes the **SNR**, defined just like in (4.10),

$$\rho = \frac{\left(\sum_{n=0}^{N-1} \mathbf{g}(n) \mathbf{x}(n) \right)^2}{\sum_{n=0}^{N-1} \sum_{n'=0}^{N-1} R(n - n') \mathbf{g}(n) \mathbf{g}(n')}, \quad (4.30)$$

reduces now to the common problem of finding the maximum of an N -dimensional function, so we only have to demand that the partial derivative of ρ respect each $\mathbf{g}(n)$ vanishes,

$$\frac{\partial \rho}{\partial \mathbf{g}(n)} = 0, \quad (4.31)$$

what leads us to the following condition,

$$\mathbf{x}(n) = \mathcal{D} \sum_{n'=0}^{N-1} R(n - n') \mathbf{g}(n'). \quad (4.32)$$

Now, if we apply a Discret Foureir Transfom,

$$\tilde{\mathbf{x}}(k) \equiv \sum_{n=0}^{N-1} \mathbf{x}(n) e^{-i2\pi kn/N} \quad (k = 0, \dots, N-1), \quad (4.33)$$

to both sides of that relationship, in order to get an expression isomorphic to that in (4.22),

$$\tilde{\mathbf{x}}(k) = \mathcal{D}\tilde{R}(k)\tilde{\mathbf{g}}(k), \quad (4.34)$$

we realize that it can not be achieved unless $R(n - n')$ fulfills,

$$\sum_{n=0}^{N-1} R(n - n') e^{-i2\pi kn/N} = \tilde{R}(k) e^{-i2\pi kn'/N}. \quad (4.35)$$

Arranging the last condition in the form of a matrix product,

$$\begin{aligned} & \begin{pmatrix} R(0) & R(1) & R(2) & \cdots & R(N-1) \\ R(1) & R(0) & R(1) & \cdots & R(N-2) \\ R(2) & R(1) & R(0) & \cdots & R(N-3) \\ \vdots & \vdots & \vdots & & \vdots \\ R(N-1) & R(N-2) & R(N-3) & \cdots & R(0) \end{pmatrix} \cdot \begin{pmatrix} 1 \\ e^{-i2\pi k/N} \\ e^{-i4\pi k/N} \\ e^{-i6\pi k/N} \\ \vdots \\ e^{-i2\pi k \frac{(N-1)}{N}} \end{pmatrix} \\ & = \tilde{R}(k) \begin{pmatrix} 1 \\ e^{-i2\pi k/N} \\ e^{-i4\pi k/N} \\ e^{-i6\pi k/N} \\ \vdots \\ e^{-i2\pi k \frac{(N-1)}{N}} \end{pmatrix} \end{aligned} \quad (4.36)$$

we clearly observe that the vector we have constructed with the exponential terms must be an eigenvector of the Toeplitz autocorrelation matrix, with eigenvalue $\tilde{R}(k)$ for every k , ranging from 0 to $(N-1)$; which, in general, is not true. This means, in particular, that

$$\mathbf{g}(n) = \mathcal{B}(\omega_0) \cos(\omega_0 n T + \varphi_0), \quad (4.37)$$

is no longer the best filter for a signal like

$$\mathbf{x}(n) = \mathcal{A}_0 \cos(\omega_0 n T + \varphi_0), \quad (4.38)$$

with absolute certainty. Nevertheless, it is still a very good choice for two main reasons: it shall approach to the optimum filter as N increases and it is easy to deal with, not only within the scope of analytical calculations but also in the computational one, as we will explain later.

4.3 Non-leaking signals embedded in noise with known spectrum

4.3.1 A non-leaking pure monochromatic signal

As has been pointed out, throughout this chapter we are going to present several strategies with the aim of detecting the presence of pure monochromatic signals in a given stretch of data. Then we should settle first what we mean by *pure monochromatic signals*: it is a series like that in expression (4.38) with

$$\mathcal{A}_0 \equiv h_0 \frac{\ell \omega_g^4}{2|D(\omega_g)|} \quad (4.39)$$

and

$$\omega_0 \equiv \omega_g - \omega_{ini}. \quad (4.40)$$

The difference between the actual frequency of the gravitational radiation⁴, ω_g , and the frequency of the wave, ω_0 , has its origin, let us recall it, in a procedure that takes place during the data-acquisition stage and introduces a new frequency origin,

$$f_{ini} = 900.0267781\text{Hz}. \quad (4.41)$$

With this particular choice for the parameters, $\mathbf{x}(n)$ may represent, as can be inferred from (3.88), the response of the resonant antenna to a linear-polarized monochromatic gravitational wave when we neglect the effects induced by the proper motions of the Earth, and we understand h_0 not as the maximum amplitude of the emitted wave but as the received one.

As pointed out in the introduction of the present chapter, we want to develop a general method whose operativity does not depend on the existence of

⁴To be more exact we should use in this expressions not ω_g but $\bar{\omega}_{obs}$, the *mean* observed frequency —see Section 3.5.2, equation (3.83). Nevertheless we shall delay all questions concerning the Doppler shift until Section 4.6.3 in this same chapter.

prior information about the source. So, in principle, the value of the frequency f_0 of the signal we can detect must be within the interval

$$0 \leq f_0 < \frac{1}{2T}, \quad (4.42)$$

where $1/T$ is our Nyquist frequency. Obviously no search strategy can afford the endless analysis of all the frequencies in that window, so we shall be forced to select a finite set of frequencies to scan. Nevertheless, the very functional form of the filter shows us that we shall perform **DFTs** in its implementation, and this defines the set of frequencies which will be searched in actual practice:

$$fT = \frac{k}{N} \quad k \in \{0, \dots, N - 1\}. \quad (4.43)$$

Moreover, for practical reasons, all the **DFTs** will be numerically computed using the fast Fourier transform (**FFT**) algorithm [37, 74], a very optimized procedure which naturally computes at once all spectral components, with the only restriction that the number of samples be an exact power of 2.

In this and the following sections, we shall assume that the signal is *well matched* by the spectral template. By this we mean that the frequency of the signal is in fact one of those in equation (4.43), so that all the signal is in one single bin of the **FFT**, with no *leakage* to the neighbouring ones. More precisely, we shall be assuming that

$$f_0 T = \frac{k_0}{N}, \quad (4.44)$$

where k_0 is one of $1, \dots, \frac{N}{2} - 1$, though we do not know which. We shall disregard the study of any k_0 bigger than $N/2$ because it would be redundant since they represent nothing but negative frequencies. The value $k_0 = 0$ is also disregarded since, among other considerations, it represents no wave at all, but a constant signal, and thence it can hardly the behaviour of a signal with the original frequency f_{ini} .

Summing up, the target of the present analysis will be to assess the presence of a signal

$$\mathbf{x}(n) = A_0 \cos(2\pi k_0 n/N + \varphi_0) \quad (4.45)$$

in the experimental data series $\mathbf{u}(n)$, using the filter

$$\mathbf{g}(n; k, \varphi) = \mathcal{B} \cos(2\pi k n/N + \varphi). \quad (4.46)$$

depending on the two unknown parameters, k and φ , which we shall eventually estimate. Besides the advantageous property of the absence of frequency leakage in the filter output of such signals, equation (4.45) shows that $\mathbf{x}(n)$ is a periodic function over the entire processed period, because $\mathbf{x}(N)$ is equal to $\mathbf{x}(0)$. In fact, this relationship holds for any sample,

$$\mathbf{x}(n + N) = \mathbf{x}(n). \quad (4.47)$$

and it will be a crucial aspect for the developments which we shall introduce below.

4.3.2 The filter performance and the role of \mathcal{B}

We had already announced our intention of using the filter shown in expression (4.46) even though it is no the matched one, in the sense that it does not maximizes the **SNR**. Let us compute the two quantities \mathbf{y}_x^2 and $\langle \mathbf{y}_r^2 \rangle$, in order to evaluate the actual goodness of the filter. \mathbf{y}_x^2 is different from zero only if a signal is really present *and* the value of the parameter k matches k_0 , i.e. the filtered signal does not leak across different frequency bins,

$$\mathbf{y}_x^2(k, \varphi) = \left[\frac{A_0 \mathcal{B} N}{2} \right]^2 \cos^2(\varphi - \varphi_0) \delta_{kk_0}. \quad (4.48)$$

For $\langle \mathbf{y}_r^2(k, \varphi) \rangle$ we have the more complex formula,

$$\begin{aligned} \langle \mathbf{y}_r^2(k, \varphi) \rangle &= \frac{\mathcal{B}^2 N}{2} \sum_{n=-N+1}^{N-1} R(n) \left(1 - \frac{|n|}{N} \right) \cos(2\pi kn/N) \\ &\quad - \mathcal{B}^2 \frac{\cos(2\pi k/N - 2\varphi)}{\sin(2\pi k/N)} \sum_{n=0}^{N-1} R(n) \sin(2\pi kn/N). \end{aligned} \quad (4.49)$$

It is worthwhile to stop and closely study the meaning of the two different terms in the last expression. The first one, which seem to be the most predominant of them, due to the presence of the factor N in it, may be easily linked with the power spectral density of the noise. A well-known way of estimating $S(\omega)$ is through the *periodogram*⁵, $s(k; N)$, a computational technique based

⁵An averaged version of this estimator was used in the production of Figure 3.5, as it is mentioned in its own caption.

on the Wiener-Khintchine theorem [45],

$$\mathbf{s}(k; N) = \frac{T}{N} \left| \sum_{n=0}^{N-1} \mathbf{r}(n) e^{-2\pi kn/N} \right|^2, \quad (4.50)$$

and when we compute its expected value we obtain, up to constant factors, the expression that we are looking for⁶.

$$\langle \mathbf{s}(k; N) \rangle = T \sum_{n=-(N-1)}^{N-1} R(n) \left(1 - \frac{|n|}{N}\right) \cos(2\pi kn/N). \quad (4.51)$$

Finding the meaning of the second term in the right-hand side of equation (4.49) is much less straightforward than the previous one. If we check the value of the correlation between the real and the imaginary parts of the DFT of $\mathbf{r}(n)$, we realize that it is not equal to zero, as it should be if we dealt with mean-free continuous functions and Fourier Transforms,

$$\begin{aligned} \langle \Re\{\tilde{\mathbf{r}}(k)\} \Im\{\tilde{\mathbf{r}}(k)\} \rangle &= - \sum_{n=0}^{N-1} \sum_{n'=0}^{N-1} R(n-n') \cos(2\pi kn/N) \sin(2\pi kn'/N) \\ &= - \sum_{n=0}^{N-1} R(n) \sin(2\pi kn/N), \end{aligned} \quad (4.52)$$

and that the final expression is also present in (4.49). Since we plan to extensively use this property of statistical independence between the real and imaginary part of any DFT, we coherently conclude⁷ that

$$\sum_{n=0}^{N-1} R(n) \sin(2\pi kn/N) \sim 0, \quad (4.53)$$

and so,

$$\langle \mathbf{y}_r^2(k, \varphi) \rangle \approx \mathcal{B}^2 \frac{NS(k; N)}{2T}. \quad (4.54)$$

⁶If we compare $\langle \mathbf{s}(k; N) \rangle$ with the definition of $S(\omega)$ given in (4.16) we shall observe, besides the presence of T instead of dt , the introduction of the factor $(1 - |n|/N)$, a weighting function that naturally takes into account that our knowledge of $R(n)$ becomes more and more imprecise when considering larger values for n .

⁷Obviously this argumentative reasoning does not demonstrate that expression (4.53) really holds. Nevertheless, we shall see in Section 4.3.4 that for ensuring the consistency of our filtering procedure we have to assume that $R(n) \sim 0$ when $n \sim N$.

where we have defined $S(k; N)$,

$$S(k; N) \equiv \langle \mathbf{s}(k; N) \rangle = \frac{T}{N} \left\langle \left| \sum_{n=0}^{N-1} \mathbf{r}(n) e^{-i2\pi kn/N} \right|^2 \right\rangle, \quad (4.55)$$

just for simplifying the notation.

Putting together expressions (4.48) and (4.49) we finally get for the **SNR** an expression that closely resembles the result that we shall get from (4.23) if we had considered the case of a continuous monochromatic signal,

$$\rho = \frac{\mathcal{A}_0^2 NT}{2S(k; N)} \cos^2(\varphi - \varphi_0) \delta_{kk_0} \equiv \rho_0 \cos^2(\varphi - \varphi_0) \delta_{kk_0}, \quad (4.56)$$

with ρ_0 ,

$$\rho_0 \equiv \frac{\mathcal{A}_0^2 NT}{2S(k; N)}, \quad (4.57)$$

the maximum value for ρ we may achieve with the present filter.

The **SNR** is obviously independent of the constant B , so we can freely set it at our will in order to provide \mathbf{y} with some advantageous property. Our particular choice is,

$$\mathcal{B}(k) \equiv \sqrt{\frac{2T}{NS(k; N)}}, \quad (4.58)$$

the factor that makes $\langle \mathbf{y}_r^2(k, \varphi) \rangle$ equal to one. The statistical properties of the noise and the linearity of the filter guarantee that \mathbf{y} is still Gaussian. Then its probability distribution will be completely settled once we know its mean $\langle \mathbf{y} \rangle$, and its variance, σ_y^2 which in our case coincides with $\langle \mathbf{y}_r^2 \rangle$,

$$\sigma_y^2 \equiv \langle \mathbf{y}^2 \rangle - \langle \mathbf{y} \rangle^2 = \langle \mathbf{y}_r^2 \rangle = 1. \quad (4.59)$$

So, on the one hand, we have forced σ_y to take the same value regardless of the particular scanned frequency, and on the other hand, the mean of $\mathbf{y}(k, \varphi)$,

$$\langle \mathbf{y}(k, \varphi) \rangle = \sqrt{\rho_0} \cos(\varphi - \varphi_0) \delta_{kk_0}, \quad (4.60)$$

shall be zero when either no signal is present in the data or, if there is a signal⁸, for any value of k other than k_0 . In this way, we have designed a bank of filters whose outputs corresponding to pure noise are statistically equivalent, and consequently *can be directly compared*.

⁸In fact, we will put together both cases, since we shall take the criterion of typifying through $\rho_0 = 0$ any frequency that contains no signal, whether or not there is a signal at some other value of k .

4.3.3 Data splitting and averages

So far, we have implicitly assumed that N represents the total amount of stored information we have access to or, in other words, that we can analyze the whole data series in a single filter pass. This is, in many senses, a rather optimistic assumption. First of all, since we want to process several months of experimental data, it should not be surprising that the available (or even existing) computing facilities could not afford such a calculation. Moreover, the output of any experimental device, like *Explorer*, will not be uniform in quality along all the data-acquisition time, and the stationarity of the noise is not preserved over too long periods of time. Then it could be worse to mix *bad* data (those, for instance, with a high level of noise) with *good* data in a single analysis, than simply to veto the stretch that we find unacceptable. But the gaps that we may introduce in rejecting samples of the experimental set are not the unique discontinuities that we shall find in the time series, because in such a long term operation of a detector it is not unlikely that the system suffers sporadic stops. Also the properties of the physical signal could be not so stable to be satisfactorily fit by our models along extensive periods of time.

We shall thus consider that each series of length N is just one among a set of, say, M consecutive⁹ blocks. The reasons for the choice of the particular values of N and M must not necessarily coincide in general. In particular, it is possible that there exist several of those sequences of $N \times M$ data, eventually disconnected, which must be then processed separately.

So, we shall attach a new label α to each quantity in order to be able to specify which of the M blocks of N data we refer to:

$$\mathbf{y}_\alpha(k, \varphi) = \sqrt{\frac{2T}{NS(k; N)}} \sum_{n=0}^{N-1} \mathbf{u}_\alpha(n) \cos(2\pi kn/N + \varphi) \quad (\alpha = 0, \dots, M-1), \quad (4.61)$$

α is actually a shorthand which simplifies the notation,

$$\mathbf{u}_\alpha(n) \equiv \mathbf{u}(n + \alpha N). \quad (4.62)$$

It is obvious, however, that computing $\mathbf{y}_\alpha(k, \varphi)$ for each α will not change the individual values of ρ , as shown by equation (4.56). Our final goal should

⁹The relaxation of this condition, allowing for the existence of missing whole blocks, introduces minor changes in all the following discussion. So the derived expressions can be easily adapted to this case.

be then to combine them in a suitable way which allows us to make the final **SNR** as high as possible. The definition (4.62) is, in this sense, very revealing because, when combined with (4.45) and (4.47), shows the most important feature of a non-leaking monochromatic wave: the signal \mathbf{x}_α in fact does *not* depend on α ,

$$\mathbf{x}_\alpha(n) = A_0 \cos(2\pi k_0 n / N + \varphi_0) = \mathbf{x}(n). \quad (4.63)$$

We consequently see that, if the signal is present, each of these blocks contains an identical replica of the same stretch of sinusoid in them. This motivates us to define a new random variable $\mathbf{z}(k, \varphi)$,

$$\mathbf{z}(k, \varphi) \equiv \frac{1}{M} \sum_{\alpha=0}^{M-1} \mathbf{y}_\alpha(k, \varphi), \quad (4.64)$$

whose mean value does not differ from that in equation (4.60), but whose variance is reduced as a consequence of this averaging operation. Before we calculate explicitly this quantity and the value of the new associated **SNR**, we are going to focus on the problem of choosing the right value of the phase parameter of the filter, φ .

The conceptually simplest method is to compute $\mathbf{z}(k, \varphi)$ for a lot of different values of that parameter, and select the best, $\bar{\varphi}$, i.e., that which gives a larger output after the filtering procedure.

Nevertheless, we do not need to go into such computationally long process, for the optimum value $\bar{\varphi}$ can be analytically determined as follows. According to its definition, we may write down $\mathbf{z}(k, \varphi)$ as,

$$\mathbf{z}(k, \varphi) = \frac{1}{M} \sqrt{\frac{2T}{NS(k; N)}} \sum_{\alpha=0}^{M-1} [\Re\{\tilde{\mathbf{u}}_\alpha(k)\} \cos \varphi + \Im\{\tilde{\mathbf{u}}_\alpha(k)\} \sin \varphi], \quad (4.65)$$

where

$$\tilde{\mathbf{u}}_\alpha(k) \equiv \sum_{n=0}^{N-1} \mathbf{u}_\alpha(n) e^{-2\pi i kn/N} \quad (4.66)$$

is the **DFT** of $\mathbf{u}_\alpha(n)$. So, we define the $\bar{\varphi}$ imposing a local-maximum condition on $\mathbf{z}(k, \varphi)$:

$$\left. \frac{\partial \mathbf{z}(k, \varphi)}{\partial \varphi} \right|_{\varphi=\bar{\varphi}} = 0; \quad (4.67)$$

we thus find¹⁰

$$\tan(\bar{\varphi}) = \frac{\sum_{\alpha=0}^{M-1} \Im\{\tilde{u}_\alpha(k)\}}{\sum_{\alpha=0}^{M-1} \Re\{\tilde{u}_\alpha(k)\}}. \quad (4.68)$$

Here it is useful to introduce the two random variables, $\mathbb{R}(k)$ and $\mathbb{I}(k)$,

$$\mathbb{R}(k) \equiv \frac{1}{M} \sqrt{\frac{2T}{NS(k; N)}} \sum_{\alpha=0}^{M-1} \Re\{\tilde{u}_\alpha(k)\}, \quad (4.69)$$

$$\mathbb{I}(k) \equiv \frac{1}{M} \sqrt{\frac{2T}{NS(k; N)}} \sum_{\alpha=0}^{M-1} \Im\{\tilde{u}_\alpha(k)\}, \quad (4.70)$$

because they can easily be combined to yield $\mathbf{z}(k, \bar{\varphi})$,

$$\bar{\mathbf{z}}(k) \equiv \mathbf{z}(k, \bar{\varphi}) = \sqrt{[\mathbb{R}(k)]^2 + [\mathbb{I}(k)]^2}, \quad (4.71)$$

where we have defined $\bar{\mathbf{z}}(k)$ as the best output of the filter at a given frequency, extending the notation used with φ .

The statistical properties of the actual filter output $\bar{\mathbf{z}}(k)$ will strongly differ from those of $\mathbf{z}(k, \varphi)$, since the new random variable is the fruit of a *non-linear* filtering process. For instance, its mean is no longer equal to zero, even if there is no signal in the experimental data, as we shall see. This is the reason why we did not undertake a very detailed study of $\mathbf{z}(k, \varphi)$ in the first place.

4.3.4 Probability distribution of $\bar{\mathbf{z}}(k)$

We shall build the probability density¹¹ $p(\bar{\mathbf{z}})$ starting from $p(\mathbb{R})$ and $p(\mathbb{I})$. Those two auxiliary random variables are Gaussian by construction, and are statistically independent, as they are the real and imaginary parts of the Fourier transform of a stationary stochastic process. Then we only have to know the respective means and variances in order to complete the information that will

¹⁰We can ensure that $\bar{\varphi}$ defined in this way leads to a maximum and not a minimum of function $\mathbf{z}(k, \varphi)$ because its second derivative, $\partial_\varphi^2 \mathbf{z}(k, \varphi = \bar{\varphi}) = -\bar{\mathbf{z}}(k)$, is never positive.

¹¹The dependence on k will be sometimes elided with the purpose of ease the reading.

fully settle their probability densities. The mean values of \mathbb{R} and \mathbb{I} can be readily found from their definitions and equation (4.60),

$$\langle \mathbb{R}(k_0) \rangle = \sqrt{\rho_0} \cos \varphi_0, \quad (4.72)$$

$$\langle \mathbb{I}(k_0) \rangle = \sqrt{\rho_0} \sin \varphi_0; \quad (4.73)$$

while for the variances it can be found that both quantities are approximately equal and,

$$\sigma_{\mathbb{R}}^2 \approx \sigma_{\mathbb{I}}^2 \approx \frac{1}{M} \frac{S(kM; NM)}{S(k; N)}. \quad (4.74)$$

The last quotient in the last formula will approach to one only when $R(n) \sim 0$ for values of n near or larger than N . Without that condition, in fact, $S(k; N)$ will be a poor substitute of the exact power spectral density of the noise. So, we shall consider that the correlation time is much shorter¹² than the duration of the individual series, which is in essence equivalent to state that, in spite of their consecutiveness, they are mutually uncorrelated.

The hypotheses we have made lead us to the following expressions for the probability density of \mathbb{R} and \mathbb{I} :

$$p(\mathbb{R}) = \sqrt{\frac{M}{2\pi}} e^{-\frac{M}{2}(\mathbb{R}-\sqrt{\rho_0} \cos \varphi_0)^2} \quad \text{and} \quad (4.75)$$

$$p(\mathbb{I}) = \sqrt{\frac{M}{2\pi}} e^{-\frac{M}{2}(\mathbb{I}-\sqrt{\rho_0} \sin \varphi_0)^2}. \quad (4.76)$$

Hence $p(\bar{z})$ is given, after an integral is evaluated, by

$$p(\bar{z}) = M\bar{z}e^{-\frac{M}{2}(\bar{z}^2+\rho_0)} I_0(M\bar{z}\sqrt{\rho_0}), \quad (4.77)$$

where we have used one of the integral representations of the modified Bessel function of order zero [38], $I_0(y)$,

$$I_0(y) \equiv \frac{1}{2\pi} \int_0^{2\pi} e^{-y \cos x} dx. \quad (4.78)$$

In the absence of signal, i.e., when $\rho_0 = 0$, equation (4.77) reduces to

$$p(\bar{z}) = M\bar{z}e^{-\frac{M}{2}\bar{z}^2}, \quad (4.79)$$

¹²This, in fact, leads to a restriction on the minimal value of N .

an expression which explicitly displays the statistical equivalence of all the frequencies which contain no signal, the property we want to achieve when we set the value of the constant \mathcal{B} . Moreover, in this case, \bar{z} is Rayleigh distributed or, in other words, \bar{z}^2 follows a χ^2 distribution with two degrees of freedom [72].

4.3.5 Mean and variance of $p(\bar{z})$. A new SNR.

We are now interested in the mean and variance of \bar{z} . These correspond to the first two moments of the probability distribution $p(\bar{z})$. It appears that a closed analytic expression can be found for the moments of any order, so we consider it here for completeness.

The m -th moment is defined by

$$\langle \bar{z}^m \rangle \equiv \int_0^\infty M \bar{z}^{m+1} e^{-\frac{M}{2}(\bar{z}^2 + \rho_0)} I_0(M \bar{z} \sqrt{\rho_0}), \quad (4.80)$$

a calculation that becomes straightforward if one uses the relationship [36],

$$L_y(-z) = \frac{1}{\Gamma(y+1)} \int_0^\infty x^y e^{-(x+z)} I_0(2\sqrt{xz}) dx, \quad (4.81)$$

where $L_y(z)$ is the Laguerre function of order y , assuming the normalization condition,

$$L_y(0) = 1, \quad (4.82)$$

and $\Gamma(y)$ is Euler's *gamma* function. The expectation value of the m -th power of \bar{z} is then,

$$\langle \bar{z}^m \rangle = \left(\frac{2}{M}\right)^{\frac{m}{2}} \Gamma\left(\frac{m}{2} + 1\right) L_{\frac{m}{2}}\left(-\frac{M}{2}\rho_0\right). \quad (4.83)$$

The most relevant moments for our purpose are, as has been said, the first and the second. The mean,

$$\langle \bar{z} \rangle = \sqrt{\frac{\pi}{2M}} L_{\frac{1}{2}}\left(-\frac{M}{2}\rho_0\right) \quad (4.84)$$

as we announced, will be different from zero even when ρ_0 vanishes, due to the property (4.82) of Laguerre functions,

$$\langle \bar{z} \rangle|_{\rho_0=0} = \sqrt{\frac{\pi}{2M}}. \quad (4.85)$$

Nevertheless, the asymptotic behaviour of the Laguerre function

$$L_y(-x) \xrightarrow{x \gg 1} \frac{1}{\Gamma(y+1)} x^y; \quad (4.86)$$

also shows that $\langle \bar{z} \rangle$, when a signal is present, approaches the maximum mean value which according to (4.60) the random variables $y_\alpha(k, \varphi)$ can possibly reach.

$$\langle \bar{z} \rangle \approx \sqrt{\rho_0}. \quad (4.87)$$

It is worth noting that the formula (4.86) ensures that the last expression holds not only when $\rho_0 \gg 1$ but when $\bar{\rho} \gg 1$, where we have introduced

$$\bar{\rho} = \frac{M}{2} \rho_0, \quad (4.88)$$

a quantity that plays the role of the new **SNR**. The same conclusion can be obtained after the study of the explicit expressions for \bar{z}_x^2

$$\bar{z}_x^2 = \rho_0 \quad (4.89)$$

and $\langle \bar{z}_r^2 \rangle$,

$$\langle \bar{z}_r^2 \rangle = \frac{2}{M}. \quad (4.90)$$

It is relevant to point that, in this case, the **SNR** linearly increases with the total number of filtered samples, $N \times M$,

$$\bar{\rho} = \frac{A_0^2 N M T}{4 S(k; N)}, \quad (4.91)$$

whereas the classical procedure of averaging the square of the moduli of the **DFTs** leads to

$$\bar{\rho}_0 = \frac{\sqrt{M}}{2} \rho_0 = \frac{A_0^2 N \sqrt{M} T}{4 S(k; N)}, \quad (4.92)$$

what means that with our strategy for signals whose frequency is one of the **FFT** samples, we enhance by a factor \sqrt{M} the value of $\bar{\rho}$.

4.4 Non-leaking signals embedded in noise of unknown spectrum

4.4.1 Replacing $S(k; N)$

It is almost redundant to say that the operative method we have just developed requires knowledge of the power spectral density of the noise. The aim of this section is the effective substitution of $S(k; N)$ in the definition of the constant \mathcal{B} by a suitable estimate of this quantity obtained from the same data series.

Let us begin with a rearrangement of expression (4.55),

$$S(k; N) = \frac{T}{N} \langle [(\Re\{\tilde{u}_\alpha(k)\} - \Re\{\tilde{x}(k)\})^2 + (\Im\{\tilde{u}_\alpha(k)\} - \Im\{\tilde{x}(k)\})^2] \rangle. \quad (4.93)$$

There is one procedure in this formula that is certainly beyond our reach: we can not perform the statistical average. Our particular choice will be the substitution of that operation by a sum over the entire rank of values of α , because $S(k; N)$, in spite of the formal aspect of (4.93), is *independent of the block label*. The same applies upon replacement of $\tilde{x}(k)$ (obviously also an unknown quantity) since $\tilde{x}(k) = \langle \tilde{u}(k)_\alpha \rangle$,

$$\tilde{x}(k) \rightarrow \frac{1}{M} \sum_{\alpha=0}^{M-1} \tilde{u}_\alpha(k). \quad (4.94)$$

Summing up, the random variable we shall use in order to estimate $S(k; N)$ is $\mathbb{S}(k; N)$,

$$\begin{aligned} \mathbb{S}(k; N) &\equiv \frac{T}{N} \frac{1}{M-1} \sum_{\alpha=0}^{M-1} \left[\left(\Re\{\tilde{u}_\alpha(k)\} - \frac{1}{M} \sum_{\alpha'=0}^{M-1} \Re\{\tilde{u}_{\alpha'}(k)\} \right)^2 \right. \\ &\quad \left. + \left(\Im\{\tilde{u}_\alpha(k)\} - \frac{1}{M} \sum_{\alpha'=0}^{M-1} \Im\{\tilde{u}_{\alpha'}(k)\} \right)^2 \right] \end{aligned} \quad (4.95)$$

where we have divided by $M-1$ and not by M because in this way we will get an unbiased estimator, i.e.

$$\langle \mathbb{S}(k; N) \rangle = S(k; N). \quad (4.96)$$

Now, we can replace the unknown spectral density by $\mathbb{S}(k; N)$ in any preceding expression, thus obtaining a new filter output $\mathbb{Z}(k)$ which, unlike $\bar{z}(k)$, we are

able to compute directly from the raw experimental data $\mathbf{u}_\alpha(n)$. With an analogous procedure to the already exposed we obtain $p(\mathbb{Z})$ and all its related quantities, including the corresponding **SNR**. Instead of starting anew from scratch, we shall calculate the probability density of \mathbb{Z} in two steps, using previous results.

Let us introduce the auxiliary random variable $\mathbb{W}(k)$

$$\mathbb{W}(k) \equiv \frac{\mathbb{S}(k; N)}{S(k; N)}, \quad (4.97)$$

which allows us to define $\mathbb{Z}(k)$ in a simple way,

$$\mathbb{Z} \equiv \frac{\bar{\mathbf{z}}}{\sqrt{\mathbb{W}}}, \quad (4.98)$$

thanks to the fact that all the terms containing $S(k; N)$ in both random variables *mutually* cancel out. Since \mathbb{W} and $\bar{\mathbf{z}}$ are statistically independent, and $p(\bar{\mathbf{z}})$ was given in the last section, we have thus reduced the problem to obtaining $p(\mathbb{W})$ and performing a final integration.

The probability density of \mathbb{W} can be found in most reference books on Probability [72], because it is the arithmetic mean of the squares of $2M - 2$ zero-mean independent Gaussian variables with unit variances. So $(2M - 2)\mathbb{W}$ follows a χ^2 distribution with precisely $2M - 2$ degrees of freedom,

$$p(\mathbb{W}) = \frac{(M-1)^{M-1}}{\Gamma(M-1)} \mathbb{W}^{M-2} e^{-(M-1)\mathbb{W}}. \quad (4.99)$$

4.4.2 The actual filter output \mathbb{Z} and its distribution

The ratio in (4.98) which we have used for defining \mathbb{Z} is a familiar one in elementary statistics, and follows a Student's t -distribution if $\bar{\mathbf{z}}$ is a zero-mean Gaussian variable. Nevertheless, the expression for $p(\bar{\mathbf{z}})$ is far from a normal density function, as we have shown in (4.77), what compels us to perform an explicit calculation, leading to the result

$$p(\mathbb{Z}) = \frac{M\mathbb{Z}}{\left[1 + \frac{M}{2M-2}\mathbb{Z}^2\right]^M} \exp\left(-\frac{M\rho_0}{2 + \frac{M}{M-1}\mathbb{Z}^2}\right) L_{M-1}\left(-\frac{M^2\mathbb{Z}^2\rho_0}{4M-4+2M\mathbb{Z}^2}\right), \quad (4.100)$$

where once again we have made use of the formula (4.81). When no signal is present in the data at one particular frequency, expression (4.100) reduces to

$$p(\mathbb{Z}) = \frac{M\mathbb{Z}}{\left[1 + \frac{M}{2M-2}\mathbb{Z}^2\right]^M}. \quad (4.101)$$

As a matter of fact, \mathbb{Z}^2 in this case follows a Fisher's F -distribution with 2 and $2M - 2$ degrees of freedom, because it is the ratio of two χ^2 random variables with those degrees of freedom, respectively.

In order to compute the moments of the density function of \mathbb{Z} , the simplest approach is not to use the final expression of $p(\mathbb{Z})$ but an intermediate formula

$$p(\mathbb{Z}) = M\mathbb{Z} \frac{(M-1)^{M-1}}{\Gamma(M-1)} e^{-\frac{M}{2}\rho_0} \int_0^\infty \mathbb{W}^{M-1} e^{-\mathbb{W}[M-1+\frac{M}{2}\mathbb{Z}^2]} I_0(M\mathbb{Z}\sqrt{\rho_0\mathbb{W}}) d\mathbb{W}, \quad (4.102)$$

that will avoid the problem of the integration of Laguerre functions with negative arguments. We thus find

$$\langle \mathbb{Z}^m \rangle = \left[(M-1)^{\frac{m}{2}+1} \frac{\Gamma\left(M-1-\frac{m}{2}\right)}{\Gamma(M)} \right] \left(\frac{2}{M}\right)^{\frac{m}{2}} \Gamma\left(\frac{m}{2}+1\right) L_{\frac{m}{2}}\left(-\frac{M}{2}\rho_0\right), \quad (4.103)$$

where we have chosen a layout that emphasizes the resemblance with the result corresponding to $\langle \bar{z}^m \rangle$. The term inside the square brackets approaches unity when $M \gg m$, and then we recover the formula (4.83). It is especially interesting to note that, in particular, the newly defined **SNR** remains unchanged. Let us split the second order moment of $p(\mathbb{Z})$,

$$\langle \mathbb{Z}^2 \rangle = \frac{M-1}{M-2} \frac{2}{M} \left(1 + \frac{M}{2}\rho_0\right), \quad (4.104)$$

in two terms, namely $\langle \mathbb{Z}_r^2 \rangle$ and $\langle \mathbb{Z}_x^2 \rangle$,

$$\langle \mathbb{Z}^2 \rangle = \langle \mathbb{Z}_r^2 \rangle + \langle \mathbb{Z}_x^2 \rangle. \quad (4.105)$$

When no signal is present, $\rho_0 = 0$, the value of $\langle \mathbb{Z}^2 \rangle$ is merely due to the response of the filtering procedure to the noise,

$$\langle \mathbb{Z}_r^2 \rangle = \frac{M-1}{M-2} \frac{2}{M}, \quad (4.106)$$

so we will accordingly assign to the signal the rest of the outcome,

$$\langle \mathbb{Z}_x^2 \rangle = \frac{M-1}{M-2} \rho_0, \quad (4.107)$$

and therefore,

$$\bar{\rho} = \frac{\langle \mathbb{Z}_x^2 \rangle}{\langle \mathbb{Z}_r^2 \rangle} = \frac{M}{2} \rho_0. \quad (4.108)$$

4.4.3 A practical example

This section is devoted to show the result of such procedure when applied on a small stretch of data taken by the *Explorer* in August 13rd of 1991, and successive days. The starting date was randomly selected since the final purpose of the present analysis is not extracting conclusions on the presence of gravitational waves but on the practical performance of the method itself. We have thus externally introduced a sinusoidal signal with the required absence of frequency leakage in order to check the ability of the method for revealing it. The signal, corresponding to a gravitational wave with an amplitude of $h_0 = 10^{-22}$, was placed at about 904.5 Hz with the purpose of achieving $\rho_0 \sim 1$ when the number of filtered samples was $N = 131072$, a little less than forty minutes. This particular value may seem arbitrary in this context, but it has a physical reason which we shall explain later. Once we set N we can pin down the precise frequency bin that will hide the control signal: $k_0 = 10656$. We use the term *hide* because a **SNR** close to one does not ensure an easy identification. Let us see what happens when we process six hours of data ($M = 9$). Even though the **SNR** of the whole procedure, $\bar{\rho}$, is greater than one –see (4.88)–, looking at Figure 4.1.a it is hard to decide whether the signal is really present or not. Nevertheless, the problem can be solved increasing the value of M , thereby processing a longer stretch of data: half a day (Figure 4.1.b), a day (Figure 4.1.c) and two days (Figure 4.1.d).

With the output of the filtering process for the values of k other than k_0 we can compute¹³ the distribution of \mathbb{Z} , because when no signal is present it does not depend on k . The case $M = 9$ is again very interesting because it offers us the possibility of comparing the experimental distribution with $p(\tilde{\mathbf{z}})$ and $p(\mathbb{Z})$, checking in this way (see Figure 4.2.a) that \mathbb{Z} really follows the second and

¹³In fact, we do not need to remove k_0 (or any other presumed signal) necessarily before we compute the output distribution, because at most it is only a point among 2^{16} .

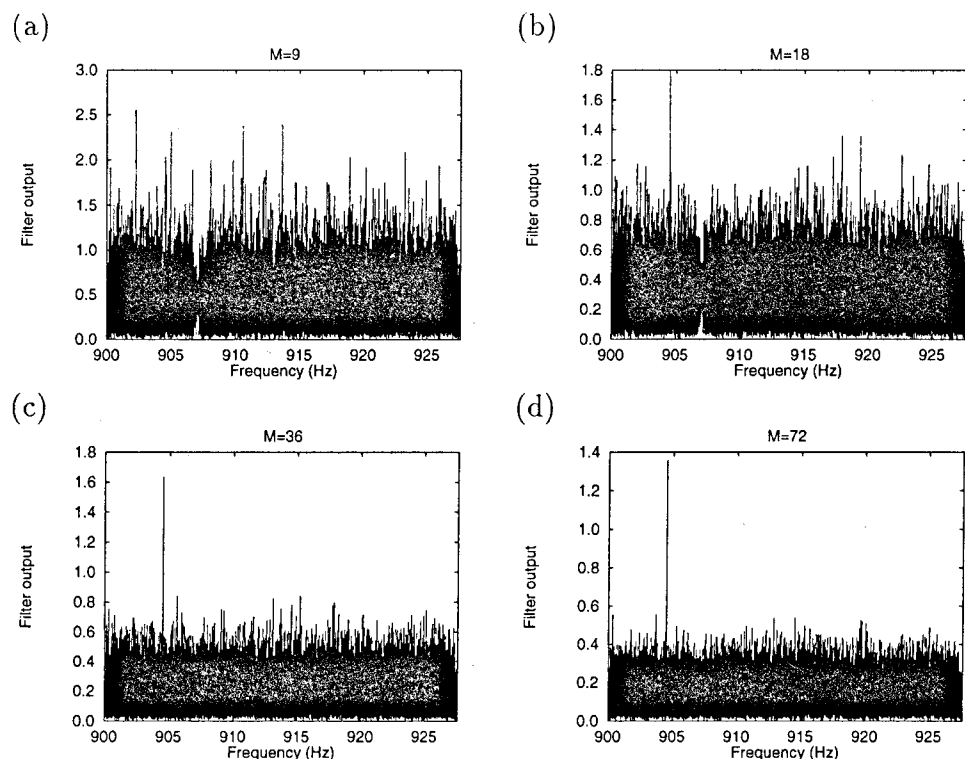


Figure 4.1: Output of the analysis procedure when the filtered stretch barely extends: (a) six hours, (b) twelve hours, (c) a day and (d) two days. Every time series begins at the same instant of August 13rd of 1991.

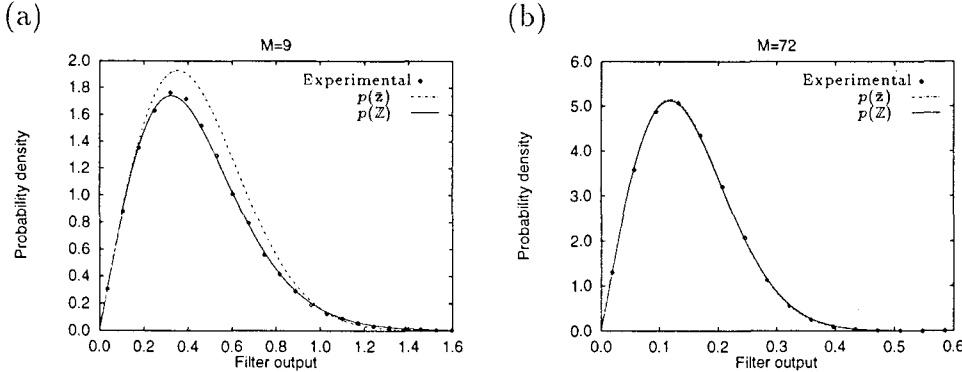


Figure 4.2: Comparison of the experimental output distribution of \mathbb{Z} with $p(\bar{z})$ and $p(Z)$, both in absence of signal, when (a) $M = 9$ and (b) $M = 72$.

not the first. For higher values of M the two probability densities converge and become almost indistinguishable from the one another (Figure 4.2.b). In both instances, however, the coincidence between theoretical and experimental distribution is remarkable.

Moreover, the explicit form of $p(Z)$ is very useful, not only in order to compare it with the experimental one, but to fix a threshold λ_0 , which shall help us in the task of deciding whether there is a signal hidden in the data or not. We will calculate the *error of the first kind*, or false-alarm probability, \mathcal{Q}_0 , as a function of λ_0 ,

$$\mathcal{Q}_0 \equiv \int_{\lambda_0}^{\infty} p(Z) dZ = \frac{1}{\left[1 + \frac{M}{2M-2}\lambda^2\right]^{\frac{M-1}{2}}}. \quad (4.109)$$

and then we shall set the upper bound depending on the number of *false alarms* (i.e. mistakes) we can afford, the well-known Neyman-Pearson criterion [39]:

$$\lambda_0 = \sqrt{\frac{2M-2}{M} \left(\frac{1}{\mathcal{Q}_0^{\frac{1}{M-1}}} - 1 \right)}. \quad (4.110)$$

Table 4.1 shows how λ_0 varies both with respect to the value of \mathcal{Q}_0 and the number of processed data blocks, M . Comparing the numbers in the table with the four graphs in Figure 4.1 some conclusions can be drawn:

- $\mathcal{Q}_0 = 10^{-3}$: A false alarm probability much higher than the inverse of the number of scanned frequencies leads to the presence of a considerable amount of filter outputs which surpass the threshold, and therefore no reliable assessment can be given.
- $\mathcal{Q}_0 = 10^{-5}$: When $\mathcal{Q}_0 \sim N^{-1}$ we expect that $\mathbb{Z}(k)$ exceeds λ_0 only in a few cases. In such a way, for $M = 9$ and $M = 18$ just two and three frequencies respectively give a positive result, including in the second case our control signal. This one is the only relevant outcome in the case of $M = 36$ and $M = 72$.
- $\mathcal{Q}_0 = 10^{-7}$: Lower levels of false alarm tolerance must be settled in order to differentiate the external signal from the noise-induced outputs. This particular value, for instance, implies that if we cut the six moth of data we want to analyze in pieces of one day long ($M = 36$), and then perform the described procedure with each one of them, the most likely is that only one, among the entire set of results, surpasses the threshold. A positive result shall be then considered as a reliable candidate to be a true signal.

\mathcal{Q}_0	λ_0			
	$M = 9$	$M = 18$	$M = 36$	$M = 72$
10^{-3}	1.56	0.97	0.65	0.45
10^{-5}	2.39	1.35	0.87	0.59
10^{-7}	3.40	1.73	1.07	0.71

Table 4.1: Value of the threshold λ_0 corresponding to different choices of \mathcal{Q}_0 for each of the considered block number M .

4.5 Leaking signals embedded in known spectrum noise

4.5.1 A leaking signal

We are going to start this section considering the effects that the presence of a general-frequency signal in the data may produce in the results we have exposed in the preceding sections. In particular, we shall study the new statistical properties of the random variables $y_\alpha(k, \varphi)$, that determine the characteristics of \mathbb{R} and \mathbb{I} , and consequently of \bar{z} .

So, in the following we shall relax the condition (4.44),

$$f_0 T = \frac{k_0 + \epsilon_0}{N} \quad (4.111)$$

by introducing the real parameter ϵ_0 ,

$$-\frac{1}{2} \leq \epsilon_0 < \frac{1}{2}, \quad (4.112)$$

whose effective consequence is that $x_\alpha(n)$ is no longer independent of α , which appears in the form of an accumulative phase shift whenever ϵ_0 is different from zero,

$$x_\alpha(n) = A_0 \cos(2\pi[k_0 + \epsilon_0]n/N + 2\pi\alpha\epsilon_0 + \varphi_0). \quad (4.113)$$

It is true that the frequency remainder also lowers the maximum filter output, due to the spectral leakage of the signal,

$$\langle y_\alpha(k_0, \varphi) \rangle = \sqrt{\rho_0} \frac{\sin(\pi\epsilon_0)}{N \sin(\pi\epsilon_0/N)} \cos\left(\pi\epsilon_0 \left[1 - \frac{1}{N}\right] + \varphi_0 - \varphi + 2\pi\alpha\epsilon_0\right); \quad (4.114)$$

nevertheless it is the block dependence that damages the filtering procedure, because it is responsible of the sinc-like behaviour of the mean values of $\mathbb{R}(k_0)$ and $\mathbb{I}(k_0)$, when considered as functions of M ,

$$\langle \mathbb{R}(k_0) \rangle = \sqrt{\rho_0} \frac{\sin(\pi\epsilon_0 M)}{NM \sin(\pi\epsilon_0/N)} \cos\left(\pi\epsilon_0 \left[M - \frac{1}{N}\right] + \varphi_0\right), \quad (4.115)$$

$$\langle \mathbb{I}(k_0) \rangle = \sqrt{\rho_0} \frac{\sin(\pi\epsilon_0 M)}{NM \sin(\pi\epsilon_0/N)} \sin\left(\pi\epsilon_0 \left[M - \frac{1}{N}\right] + \varphi_0\right). \quad (4.116)$$

This fact turns the search strategy not so robust as desired, in the sense that for a given ϵ_0 there always exists a value M_0 ($\sim 1/\epsilon_0$) for M , above which the **SNR** decreases noticeably. The frequency band where the analysis method works efficiently thus decreases with the number of averaged blocks, a very undesirable feature. We now investigate how this problem can be addressed.

4.5.2 Phase-varying filter

As already stated, since the origin of the problem is a carried over phase, we shall solve it introducing a new block-dependent filter with one more parameter, ϵ :

$$g_\alpha(n; k, \varphi, \epsilon) = \sqrt{\frac{2T}{NS(k; N)}} \cos(2\pi kn/N + \varphi + 2\pi\alpha\epsilon). \quad (4.117)$$

with the purpose to compensate the phase shift. Starting from this new $g_\alpha(n; k, \varphi, \epsilon)$, we can calculate the value of each $y_\alpha(k, \varphi, \epsilon)$,

$$y_\alpha(k, \varphi, \epsilon) = \sqrt{\frac{2T}{NS(k; N)}} |\tilde{u}_\alpha(k)| \cos(\Phi_\alpha(k) - \varphi - 2\pi\alpha\epsilon), \quad (4.118)$$

where the following notation has been used:

$$\tilde{u}_\alpha(k) = |\tilde{u}_\alpha(k)| e^{i\Phi_\alpha(k)}. \quad (4.119)$$

Through a definition formally identical to (4.64), we shall establish $z(k, \varphi, \epsilon)$. Once again it is possible to obtain $\bar{\varphi}$ using a local-maximum condition, like that in (4.67),

$$\left. \frac{\partial z(k, \varphi, \epsilon)}{\partial \varphi} \right|_{\varphi=\bar{\varphi}} = 0, \implies \tan(\bar{\varphi}) = \frac{\sum_{\alpha=0}^{M-1} |\tilde{u}_\alpha(k)| \sin(\Phi_\alpha(k) - 2\pi\alpha\epsilon)}{\sum_{\alpha=0}^{M-1} |\tilde{u}_\alpha(k)| \cos(\Phi_\alpha(k) - 2\pi\alpha\epsilon)}. \quad (4.120)$$

The value of $\bar{\varphi}$ leads now to the following expression for $z(k, \bar{\varphi}, \epsilon)$,

$$z(k, \bar{\varphi}, \epsilon) = \frac{1}{M} \sqrt{\frac{2T}{NS(k; N)}} |\tilde{\tilde{u}}(k; \epsilon)|, \quad (4.121)$$

a relationship that involves a new quantity, $\tilde{\mathbf{u}}(k; \epsilon)$, which formally is also a DFT,

$$\tilde{\mathbf{u}}(k; \epsilon) \equiv \sum_{\alpha=0}^{M-1} \tilde{\mathbf{u}}_\alpha(k) e^{-2\pi i \alpha \epsilon}. \quad (4.122)$$

The template for ϵ , just like in the case of the frequency grid, will be dictated by the convenience of the use of the FFT algorithm in the computation of $\tilde{\mathbf{u}}(k; \epsilon)$. We shall therefore estimate ϵ_0 within the following discrete rank of values¹⁴ of ϵ :

$$\epsilon = \frac{q}{M'} \quad q \in \{0, \dots, M' - 1\}, \quad (4.123)$$

where, in principle, M' , by the way an exact power of 2, must not necessarily coincide with M . M' has to be greater than M if we do not want to waste available information, but on the other hand, it seems that larger and larger values of M' should produce an endless increment of precision in the estimation of ϵ_0 . Nevertheless, as we will show in the next section, M' should be kept as low as possible.

4.5.3 Statistical properties of \bar{z}

The mechanism for finding \bar{q} is then very simple. We must compute all the $\mathbf{z}(k, \varphi, q/M')$ and select that q which gives the largest output, just defining $\bar{z}(k) = \mathbf{z}(k, \varphi, \bar{q}/M')$, i.e.,

$$\bar{z}(k) = \max_{q \in \{0, \dots, M'-1\}} \{\mathbf{z}(k, \varphi, q/M')\}. \quad (4.124)$$

When no signal is present at some frequency, it can be proved that again,

$$p(\mathbf{z}) = M \mathbf{z} e^{-\frac{M}{2} \mathbf{z}^2}, \quad (4.125)$$

no matter the choices for k and q . So, in that case, the probability density of $\bar{z}(k)$, since it is the maximum of M' equally distributed random variables [72], is given by

$$p(\bar{z}) = M M' \bar{z} e^{-\frac{M}{2} \bar{z}^2} \left[1 - e^{-\frac{M}{2} \bar{z}^2}\right]^{M'-1}. \quad (4.126)$$

We have not been able to compute $\langle \bar{z} \rangle$ other than in the form of an alternating finite series, which is almost useless for obtaining generic conclusions

¹⁴As usual, any value for q equal or bigger than $M'/2$ is related to a negative ϵ .

about it. Instead of the mean value of \bar{z} we shall compute its most probable value. The function $p(\bar{z})$ reaches its maximum (when $M' \gg \sqrt{e}$) for

$$\bar{z} \approx \sqrt{\frac{2}{M} \ln M'}, \quad (4.127)$$

a quantity that decreases as M increases, and when M' decreases. This shows the convenience of setting M' as the first exact power of 2 greater than M . With the second-order moment of the distribution we have in principle a similar problem, although in this case the alternating series can be transformed into a non alternating one,

$$\langle \bar{z}^2 \rangle = \frac{2}{M} \sum_{l=1}^{M'} \binom{M'}{l} \frac{(-1)^{l+1}}{l} = \frac{2}{M} \sum_{l=1}^{M'} \frac{1}{l}. \quad (4.128)$$

For large values of M' we can approximate the result using the definition of the Euler's γ constant,

$$\langle \bar{z}^2 \rangle \approx \frac{2}{M} (\ln M' + \gamma). \quad (4.129)$$

Since the output of the procedure in absence of noise is

$$\bar{z}_x = \sqrt{\rho_0} \frac{\sin(\pi\epsilon_0)}{N \sin(\pi\epsilon_0/N)}, \quad (4.130)$$

the new **SNR** shall be (if $M' \gg 1$)

$$\bar{\rho} = \rho_0 \left(\frac{\sin(\pi\epsilon_0)}{N \sin(\pi\epsilon_0/N)} \right)^2 \frac{M}{2(\ln M' + \gamma)}. \quad (4.131)$$

The standard procedure of averaging the square of the moduli of the **DFTs** gives for a general leaking signal the following **SNR**:

$$\bar{\rho}_0 = \rho_0 \left(\frac{\sin(\pi\epsilon_0)}{N \sin(\pi\epsilon_0/N)} \right)^2 \frac{\sqrt{M}}{2}, \quad (4.132)$$

what represents an improvement with the present method of

$$\frac{\bar{\rho}}{\bar{\rho}_0} = \frac{\sqrt{M}}{\ln M' + \gamma}, \quad (4.133)$$

a ratio larger than one, when (4.129) holds, that increases with the number of blocks.

4.6 Leaking signals embedded in noise of unknown spectrum

4.6.1 A spectral estimator

The task of replacing $S(k; M)$ in the filter definition is much more complex than in the non-leaking case. The natural starting point is the value of $\tilde{\mathbf{u}}(k; q/M')$ for q other than \bar{q} , but this presents two main problems. First of all, the fact that we are only able to choose \bar{q} out of a discrete set leaves open the unpleasant possibility that the value of the signal frequency lies just in the middle of a bin. This means that we shall ignore the precise way in which the signal energy will be distributed among the different q 's, and thus the relative magnitude of $\tilde{\mathbf{u}}(k; \bar{q}/M')$ when compared with the rest of outputs. The scenario can be even worse, because we have no guarantees that \bar{q}/M' corresponds to the best approach to the actual ϵ_0 : the noise can mislead us into an inaccurate value of the signal frequency, leaving thus the *true* $\tilde{\mathbf{u}}(k; \epsilon_0)$ among the discarded ones.

Instead of constructing an estimator for $S(k; M)$ in the hope that none of the previously stated possibilities really takes place, what could lead us again to a filtering procedure too sensitive to the signal's peculiar properties, we are going to choose a *democratic* estimate $\mathbb{S}(k; N)$: perhaps it will not be so accurate as it could, but it will not show appreciable differences in its performance depending on the actual frequency of the wave.

We define $\mathbb{S}(k; N)$ through an expression that closely resembles that in equation (4.95),

$$\begin{aligned} \mathbb{S}(k; N) &\equiv \frac{T}{NM} \frac{1}{M' - 2} \sum_{q \neq \bar{q}} \left[\left(\Re\{\tilde{\mathbf{u}}(k; q/M')\} - \frac{1}{M} \sum_{q' \neq \bar{q}} \Re\{\tilde{\mathbf{u}}(k; q'/M')\} \right)^2 \right. \\ &\quad \left. + \left(\Im\{\tilde{\mathbf{u}}(k; q/M')\} - \frac{1}{M} \sum_{q' \neq \bar{q}} \Im\{\tilde{\mathbf{u}}(k; q'/M')\} \right)^2 \right], \end{aligned} \quad (4.134)$$

where the $\tilde{\mathbf{u}}_\alpha(k)$ have been substituted by $\tilde{\mathbf{u}}(k; q/M')$, and the sums do not contain the term where the signal is supposed to be located, $\tilde{\mathbf{u}}(k; \bar{q}/M')$.

Once more we replace $S(k; N)$ by $\mathbb{S}(k; N)$ in the definition of \bar{z} , in order to get a new random variable Z which we can compute using only experimental

data. This quantity inherits two characteristic traits from the way we estimate the spectral density of the noise.

On the one hand, if the signal is large enough the filter output may have a saturation limit, which will depend on the particular values of some parameters, such as M or M' . This means that \mathbb{Z} will not surpass a certain threshold, even if the amplitude of the signal increases indefinitely. The reason for that behaviour can be found in the fact that when the signal is much more intense than the noise, what is really difficult to estimate is not the presence of the former but the properties of the latter. So in these cases $\mathbb{S}(k; N)$ will overestimate $S(k; N)$. It must however be stressed that the whole effect results in an change in the value of ρ_0 , and thus does not actually set an upper bound in the **SNR** $\bar{\rho}$. On the other hand, when no signal is present at a particular frequency, $\mathbb{S}(k; N)$ will underestimate $S(k; N)$, since we do not use \bar{q} when computing it, and $\tilde{\mathbf{u}}(k; \bar{q}/M')$ has the biggest modulus among all the $\tilde{\mathbf{u}}(k; q/M')$.

Since we are able to compute the overall probability density of $\mathbb{Z}(k)$ neither in a single step, even if no signal is present, nor in two step as in Section 4.6, because the auxiliary random variable $\mathbb{W}(k)$ defined like in (4.97) is no longer independent of $\bar{\mathbf{z}}(k)$; we shall obtain it by some non-algebraic mean. We will introduce a *tentative* $p(\mathbb{Z})$ inspired by the limiting probability density $p(\bar{\mathbf{z}})$, because when M is large enough both must coincide:

$$p(\mathbb{Z}) = MM'w\mathbb{Z}e^{-\frac{M}{2}w\mathbb{Z}^2} \left[1 - e^{-\frac{M}{2}w\mathbb{Z}^2}\right]^{M'-1}. \quad (4.135)$$

The new parameter w , which condenses all the differences between $p(\bar{\mathbf{z}})$ and $p(\mathbb{Z})$, measures in some suitable sense the bias of the spectral estimator $\mathbb{S}(k; N)$, i.e.,

$$w \sim \frac{\langle \mathbb{S}(k; N) \rangle}{S(k; N)}. \quad (4.136)$$

This point of view is somewhat vain since we are not in a position to compute $\langle \mathbb{S}(k; N) \rangle$ theoretically, as it has been stated. The value of w , however, can be estimated from the filter output itself, using for instance the relationship (4.128), replacing $\bar{\mathbf{z}}$ by $\sqrt{w}\mathbb{Z}$, and the statistical mean by an average over the filter output:

$$w = \frac{N \sum_{l=1}^{M'} l^{-1}}{M \sum_{k=0}^{N/2-1} \mathbb{Z}^2(k)}. \quad (4.137)$$

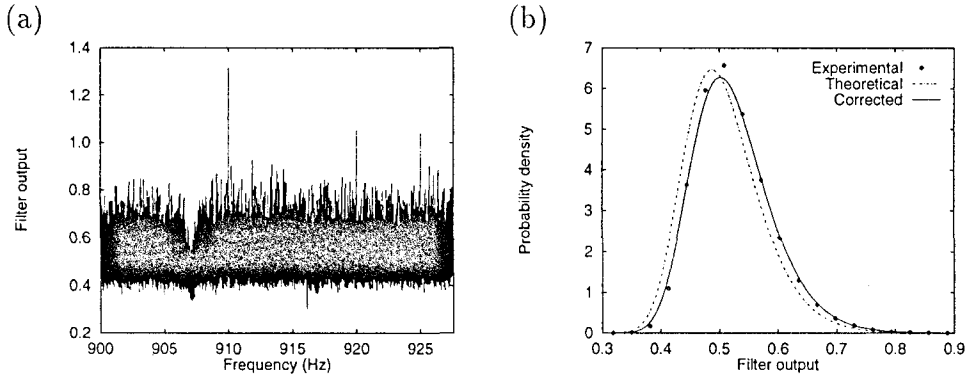


Figure 4.3: Here we find (a) the output of the filtering procedure, $\mathbb{Z}(k)$, for $N = 131072$, $M = 36$ and $M' = 64$, what represents about one day of data, and (b) its experimental distribution compared with the theoretically expected, $p(\bar{\mathbf{z}})$, and corrected one, $p(\mathbb{Z})$.

The procedure we shall use to compute (4.137) also remind us that, regardless of its probability density, $\mathbb{Z}(k)$ can be obtained from the experimental time series. We set the value of the w quantity *a posteriori*, once the filtering process has finished. In fact, the functional form of $p(\mathbb{Z})$ has its very origin in the comparative study of the actual distribution $\mathbb{Z}(k)$ and the probability density of reference, $p(\bar{\mathbf{z}})$, for different values for the free parameters. Much like we will do in the next section.

4.6.2 A single filtering process

Let us begin analyzing a stream of about one day of the *Explorer* data with the layout used in Section 4.4.3, i.e. $N = 131072$ and $M = 36$ ($M' = 64$). In fact, we will choose exactly the same time series, starting on August 13rd of 1991, in order to be able to compare the non-leaking and the leaking methods. So we get the results shown in Figure 4.3.a, which differ from the corresponding Figure 4.1.c in a fundamental aspect: we have added no signal to $\mathbf{u}_\alpha(n)$. The filter output for all frequencies, including the prominent peak placed at about 910 Hz, is due exclusively to the experimental information, i.e., it was not artificially added to the data.

A plot of the distribution of $\mathbb{Z}(k)$ can be found in Figure 4.3.b, where it is contrasted with $p(\bar{\mathbf{z}})$ in (4.126), the *theoretical* probability density, and with

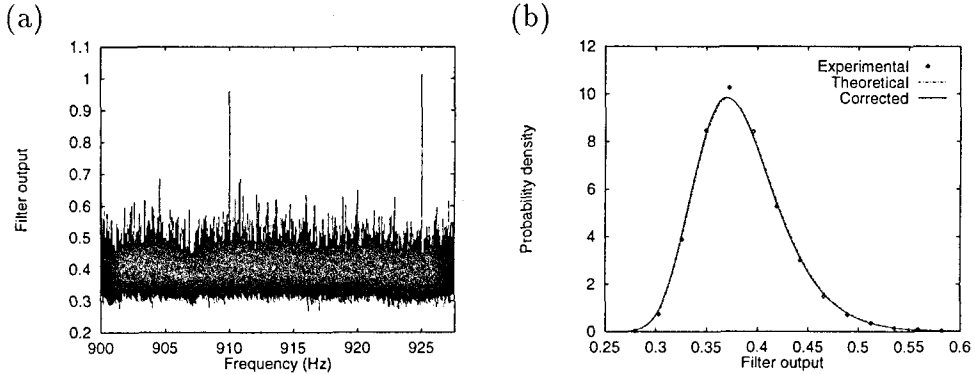


Figure 4.4: Here we find (a) the output of the filtering procedure, $\mathbb{Z}(k)$, for $N = 131072$, $M = 72$ and $M' = 128$, what represents about two days of data, and (b) its experimental distribution compared with $p(\bar{z})$ and $p(\mathbb{Z})$: in this case it is hard to distinguish one from the other.

$p(\mathbb{Z})$ once w was computed following the prescription shown in (4.137), the *corrected* one. The agreement of the latter with the experimental probability density is again remarkable.

It is convenient to point out that when the number of processed blocks increases, the value of w rapidly approaches one, thus becoming an irrelevant parameter. As a matter of fact, Figure 4.4, where we present the same procedure with the same data, but extending the processed time to two days, shows that $p(\bar{z})$ is then a sufficiently accurate expression for the probability density of the filter output.

Once we have checked the goodness of our tentative probability density we can analyze the statistical relevance of the outcome corresponding to 910 Hz, computing again \mathcal{Q}_0 in terms of λ_0 . Equation (4.135) leads to the following expression for the error of the first kind, in

$$\mathcal{Q}_0 = 1 - \left[1 - e^{-\frac{M}{2}w\lambda_0^2} \right]^{M'}, \quad (4.138)$$

and hence,

$$\lambda_0 = \sqrt{-\frac{2}{Mw} \ln \left(1 - [1 - \mathcal{Q}_0]^{\frac{1}{M'}} \right)}. \quad (4.139)$$

Following the criteria we have illustrated in Section 4.4.3, we set $\mathcal{Q}_0 = 10^{-7}$. The related values of λ_0 are: $\lambda_0 = 1.09$ for $M = 36$ ($M' = 64$), and $\lambda_0 = 0.76$

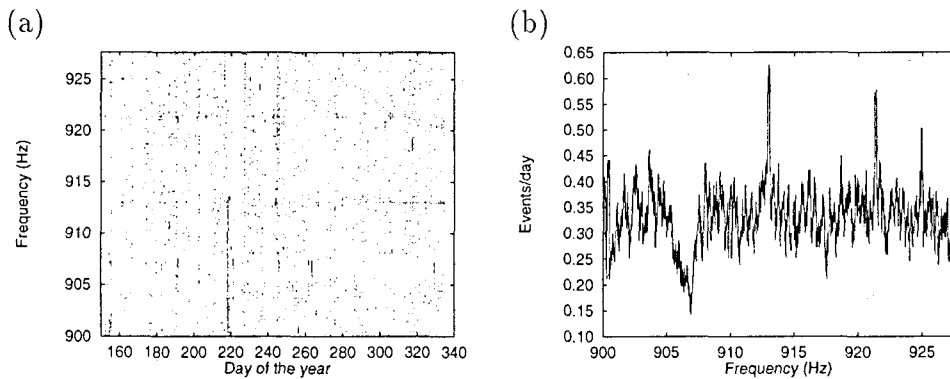


Figure 4.5: Set of frequencies (a) whose value of \bar{z} exceeds the threshold that corresponds to $N = 131072$, $M = 36$, $M' = 64$ and $Q_0 = 10^{-3}$; and (b) their coincidences along the six month period (June — November, 1991).

for $M = 72$ ($M' = 128$). Looking at Figure 4.3.a it is obvious that, besides the peak placed at about 910 Hz, two more outcomes exceed the given threshold. Moreover, two of these three outstanding outputs are also present in the two-day analysis (see Figure 4.4.a).

4.6.3 Massive data processing

These relevant threshold-crossing results impel us to consider the convenience of performing a wider analysis on the experimental data set. Since we have explicitly shown that the filtered output of a one day stretch displays interesting features we shall split the six months of data in pieces of $N \times M$ samples, with $N = 131072$ and $M = 36$. Choosing larger values for M and N will trivially lead to better SNRs, but it can bring about some undesired problems. First, the assumption we have made about the stationarity of the noise can be hardly maintained over periods of time longer than a few days. Obviously this argument is only qualitative and does not provide us with a fixed value for the maximum length of the processed series. The same statement applies to the following argument.

Up to this moment we have not explicitly mentioned the question of the Doppler effect, even though in fact it has determined, from the very beginning, the value of one parameter of the filtering procedure: the number of scanned frequencies, N , besides of being a exact power of 2 in order to allow the use

of the **FFT** algorithm in the search procedure, is the biggest value, given our sampling time, which does not exceed the condition shown in formula (3.81). We recall that this limiting value was obtained when we constrained the observed frequency of the gravitational wave to be within a single spectral bin, in spite of the disturbing effect of the Doppler shift. This guarantees the monochromatic nature of the signal when performing *single DFTs*, but not over the entire filtered series. This is the second reason that compels us to restrict to one day the stretch of data we filter in a single pass. Since when considering small time scales the most important frequency shift is related to the rotational motion of the Earth, processing one day series of data shall ensure, at least, a democratic misapplication of our search procedure because it will be affected in a similar way by the daily Doppler.

Having in mind all these restrictions we have performed a systematic filtering procedure whose outcome is a set of 145 output files¹⁵ like that displayed in Figure 4.3.a. Once the entire operation was completed, we scanned the filtered data, looking for relevant peaks. In this way Figure 4.5.a shows the frequencies corresponding to different days whose respective values of \mathbb{Z} have exceeded the level established by $Q_0 = 10^{-3}$. The corresponding threshold λ_0 has been chosen so low deliberately, because in this way we can try to find primary recurrence patterns along the six months we analyze. However, we do not compare single frequencies from different days, but rather a window of about 0.2 Hz in width around each of them, because when considering such a period of time the consequences of the orbital Doppler effect can not be neglected.

The orbital term sets the value of the spectral band we must survey in 0.2 Hz, because this is just twice the maximum frequency shift that a monochromatic signal, reaching the *Explorer* from an arbitrary celestial location, may undergo. So, for each value of k we count the number of days in which there is at least a filter output within the referred window that surpasses the given threshold. Then we divide this quantity by the number of days that contains more than one of those *sticking out* outputs, and finally plot the result of this scanning procedure in Figure 4.5.b.

The presence of the most prominent peak, placed at about the 913 Hz, is due

¹⁵Notoriously this number of days represents less than six months. Nevertheless, we must recall that the detector was not continuously operating during this half a year. The data acquisition process thus suffered sporadic stops and, since we only kept the one day long output files, some temporal stretches were discarded.

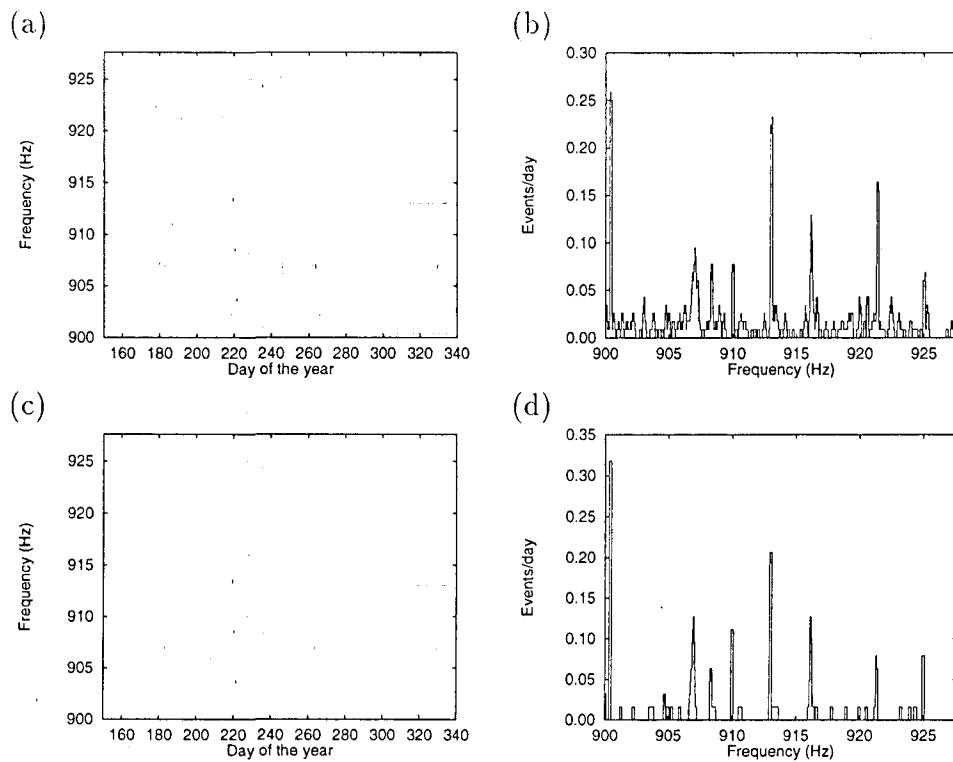


Figure 4.6: Results of the match procedure for higher cut-off levels: (a)—(b) $Q_0 = 10^{-5}$ and (c)—(d) $Q_0 = 10^{-7}$. We can see how some frequency peaks stand.

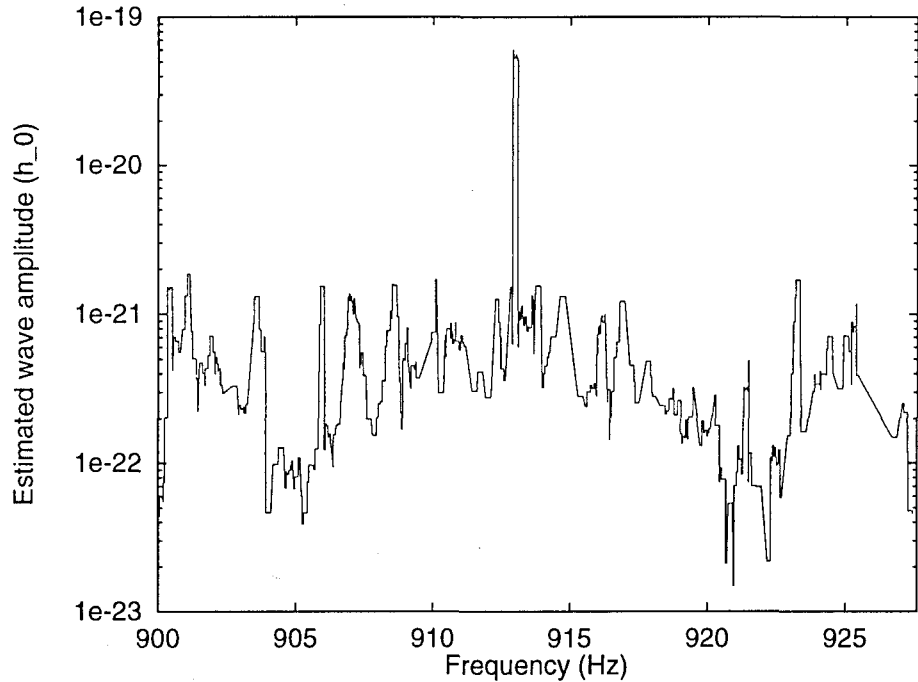


Figure 4.7: Estimated value for h_0 computed from the outcomes depicted in Figure 4.6.a

to a detector calibration signal. This signal, introduced by the antenna amplification system *before* the data were sampled, is absolutely indistinguishable from a pure monochromatic gravitational wave. Its unveiling by our method represents a solid proof of its efficiency. Nevertheless, there are a few other relevant peaks with unknown origin (at 900, 907, 910 and 916 Hz, for instance) whose presence becomes even more apparent when we raise λ_0 —as we can see in Figure 4.6.

A deeper analysis is needed, possibly studying case by case, before we can reject or accept these candidates to be a gravity-induced monochromatic signal. Nevertheless, we would like to finish this chapter plotting in Figure 4.7 the mean amplitudes that should correspond to the outcomes shown in Figure 4.6.a, in the case that all of them had been produced by the interaction of a monochromatic gravitational wave with the cryogenic detector *Explorer*.

Conclusions

We close this work with a general outlook of the developed topics and the main results we have achieved.

This essay, as reveals the title itself, is devoted to the search for monochromatic gravitational-wave signals in the data of the cryogenic detector *Explorer*. With this aim several filtering procedures have been designed and applied. Nevertheless, since a detailed knowledge of the response of the detector to the incoming wave is needed for the development of those algorithms, we have begun our exposition with a detailed study of both, signal and antenna. In fact, our final purpose was to write a self-consistent text, covering most of the aspects of the complex stated problem. We hope that the reader will find this objective has been accomplished.

We present in this final chapter a list that summarizes our activity and where we have *emphasized* our major contributions.

- We have reviewed the linear approximation of General Relativity and also used the standard quadrupole formula to obtain the waveform of the outgoing gravitational radiation corresponding to a spinning solid body. We have then computed the received waveform in the case in which the source is an astronomic object (like an isolated pulsar) and the detector is planted on the Earth surface, taking into account:
 - the frequency shift caused in the monochromatic wave by the Doppler effect, related to the orbital and rotational motions of our planet, and
 - the time-dependent variations in the amplitude of the gravitational wave due to the change in the orientation of our directional detector, consequence again of the rotational motion of Earth.

The results have been expressed in terms of *geographical* (longitudes, latitudes...) and *astronomical* (declinations, right ascensions...) common parameters, and thus can be *directly* computed using the information collected in any table of ephemeris.

- We have outlined the way in which a metric perturbation couples with a resonant cylinder, using the theory of elasticity. We have also described the rest of components of the cryogenic antenna *Explorer* and derived the equations that determine the behaviour of the detector. We have solved these equations in the case in which the system is driven by a monochromatic gravitational wave coming from an astronomical source. The response of the detector was first obtained in a rather formal way and then recomputed using an approximate development. These *explicit results* were not found in the consulted literature.
- We have designed *two new filtering algorithms* for detecting monochromatic signals *which exhibit a better performance* than the most common technique—averaging square moduli of the Fourier transforms of the experimental data series. In fact, our main strategy is based in the estimation of both modulus *and phase* of the signal. The first of these methods must be applied when the frequency of the signal is well matched by our spectral template, whereas the second fits the more general case of a signal with arbitrary, but fixed, frequency. Since in the latter scenario we impose *no restriction* on the wave parameters, the signal-to-noise ratio achieved by the associated filtering procedure is slightly lower than in the first case, where we reach the *same result* that we would obtain analyzing all the data in a *single filter pass*.
- The two filtering strategies were developed assuming in the first place that the spectral density of the noise was a known quantity. A generalization of both algorithms with a *built-in spectral estimator* was implemented, thus allowing its direct application when this information is not available by other means. In all cases a *wide probabilistic study* of the search procedures was performed in order to *evaluate and assess the significance* of the outcomes they produce.
- The general-frequency algorithm for noise with unknown spectrum, was extensively used when performing a *massive* filtering upon the data record-

ded by the *Explorer* detector between June and November of 1991. The output of that systematic processing was analyzed taking into account the possible effects eventually caused in the signal by the *Doppler spectral shift*, and applying *probabilistic reasonings* based on the well-known Neyman-Pearson criterion. As a result of this search several *statistically relevant* outcomes were found. Unveiling the origin of those positive results is a matter of further (and deeper) research.

Appendix A

A.1 Overview

In Chapter 2 we have stated that we must expect that the h_+ and h_\times components of a gravitational wave coming from a rotating object, like a pulsar, take, in general, the form displayed in (2.92) and (2.93), rather than that in (2.49) and (2.50). The latter expressions could lead us to the conclusion that we only have to look for signals that are elliptically polarized, but this will not be enough, unless we know in advance the identity of the source; otherwise we will ignore the exact orientation of the main axes of polarization. This is what is behind the angle Υ , and we shall link its value with other angles with a more familiar meaning, such those that the rotation axis of the object forms with the propagation direction of the wave or with the Earth's axis.

A.2 The angle Υ

The problem of finding the value of the angle Υ , attending to its definition, is equivalent to the calculation of the scalar product of \hat{i} and \hat{w}_1 (see Figure 2.1 in Chapter 2),

$$\cos \Upsilon = \hat{i} \cdot \hat{w}_1, \quad (\text{A.1})$$

and it would be a straightforward computation if we had the expression of each tensor in a common basis, which we do not.

We shall solve the resolution of the stated problem just introducing the components of a third vector, \hat{p}_3 , in the $\{\hat{e}_i\}$ basis,

$$\hat{p}_3 = \sin \sigma \cos \zeta \hat{e}_1 + \sin \sigma \sin \zeta \hat{e}_2 + \cos \sigma \hat{e}_3. \quad (\text{A.2})$$

The two new angular quantities, σ and ζ , are not, nevertheless, fully unknown for us. The first is simply the angle that form the two equatorial planes of the source and the Earth, and, on the other hand, the second can be easily related to ι (see again Figure 2.1),

$$\cos \iota = \hat{p}_3 \cdot \hat{k} = -\sin \alpha \sin \sigma \cos(\zeta - \beta) - \cos \alpha \cos \sigma, \quad (\text{A.3})$$

an expression that will be helpful soon.

Once we have \hat{p}_3 we can *construct* again \hat{p}_1 , from the vectorial product of the first and \hat{k} ,

$$\begin{aligned} \hat{p}_3 \times \hat{k} &= [\sin \alpha \cos \sigma \sin \beta - \cos \alpha \sin \sigma \sin \zeta] \hat{e}_1 \\ &+ [\cos \alpha \sin \sigma \cos \zeta - \sin \alpha \cos \sigma \cos \beta] \hat{e}_2 \\ &+ [\sin \alpha \sin \sigma \sin(\zeta - \beta)] \hat{e}_3, \end{aligned} \quad (\text{A.4})$$

because

$$\hat{p}_1 = \frac{\hat{p}_3 \times \hat{k}}{\sin \iota}. \quad (\text{A.5})$$

One more step is needed before we can obtain the value of Υ : we must recall that $\hat{i} \equiv \hat{p}_1$ and complete the scalar product of (A.1),

$$\cos \Upsilon = \frac{\sin \alpha \cos \sigma - \cos \alpha \sin \sigma \cos(\zeta - \beta)}{\sin \iota}, \quad (\text{A.6})$$

or, using (A.3),

$$\cos \Upsilon = \frac{\cos \sigma + \cos \alpha \cos \iota}{\sin \alpha \sin \iota}; \quad (\text{A.7})$$

a relationship that involves quantities, as we have mentioned, with an easier physical interpretation.

Appendix B

B.1 Overview

We present here the **R87** data format specifications, with minor modifications with respect to what one could find, at the time that this essay was being written, in '<http://www.roma1.infn.it/rog/datanalysis/r87.html>'.

B.2 The R87 data format.

The archived sampled data are collected in direct access files on disk. The files are composed of records, all of the same length. There are different types of records. The types are:

1. Sampled data.
2. Physical parameters.
3. Experimenters comments.
4. DAGA system setup.

All records have a header of at least 90 integer*2 words. The general structure of the records of the first type is

Header
First Data Field
Second Data Field (optional)
Third Data Field (optional)

Each data field has a particular sampling time. Each data field contains the samples of a certain number of channels, so the samples are, in the case of n channels,

CH1 sample 1

CH2 sample 1

.....

CHn sample 1

CH1 sample 2

.....

The first sample of each channel of each field has the same time, and is in the header.

There are different methods of representing the samples, using one or two bytes. In the case of the data of the *Explorer* which we have analyzed, the samples are INTEGER*2 numbers either with the sampling delta equal to 0.004883 V, or with an offset of 2048 and a sampling delta of 0.005 V; depending on the value of header word H_ADC.

A complete list of the header words, including a short description of their respective roles, can be found in Table B.1. In the case of the data of Explorer 1990—91, some of the header values were equal or similar to those in Table B.2, and some other header variables were not defined at that time.

In our files, there were 12 channels in field 1 and 1 in field 2, as it is shown in Table B.3. The last channel constitutes indeed what we have call along this essay *the experimental data series*.

1	H_LREC	rec. length (in words)	2	H_LHEA	total header length (in w.)
3	H_KREC	record number	4	H_ANTG	gravitational antenna
5	H_KRUN	run number	6	H_TIPR	record type
7	H_LCO1	length of data field 1 (total number of samples)	8	H_NCA1	field 1 channels number
9	H_LCO2	length of data field 2	10	H_NCA2	field 2 channels number
11	H_LCO3	length of data field 3	12	H_NCA3	field 3 channels number
13	H_ANNO	year	14	H_DOY	day of the year
15	H_ORE	hour	16	H_MIN	minutes
17	H_SEC	seconds	18	H_MSEC	milliseconds
19		sampl. ms for field 1	20		sampling microsec. field 1
21	H_OPTIM	time offset (ms)	22	H_ADC	A/D code (tab.)
23	H_LHE1	header field 1 length	24	H_LHE2	header field 2 length
25	H_OPFL	operation flag	26		
27	H_NSIN	number of sintet.	28		Freq. sint. 1 (Hz)
29		Freq. sint. 1 (10^{-4} Hz)	30		Freq. sint. 2 (Hz)
31		Freq. sint. 2 (10^{-4} Hz)	32		Freq. sint. 3 (Hz)
33		Freq. sint. 3 (10^{-4} Hz)	34		Freq. sint. 4 (Hz)
35		Freq. sint. 4 (10^{-4} Hz)	36	H_AMP	electr. ampl. [F16(1000)]
37	H_CDIR	coeff. $V^2 \rightarrow K$ direct acquisit. [in RHEADER(19)]			
39	H_CRI\$1	coeff. $V^2 \rightarrow K$ resonance nu_minus [in RHEADER(20)]			
41	H_CRI\$2	coeff. $V^2 \rightarrow K$ resonance nu_plus [in RHEADER(21)]			
43	V_0	transducer voltage (V)	44	V_1	
45	V_2		46	V_3	
47	V_4		48	V_5	
49	V_6		50	MUX_IND	
51	KFFT_K	n. of AAP FFT	52	KFFT_L	length of FFT
53	KFFT_NP	number of AAP pieces	54	KFFT_J1	beginning of piece 1
55	KFFT_L1	length of piece 1	56	KFFT_J2	beginning of piece 2
57	KFFT_L2	length of piece 2	58	KFFT_J3	beginning of piece 3
59	KFFT_L3	length of piece 3	60	KFFT_NN	n. of FFT in this rec. (1 or 2)
61	H_TAU1	tau nu(-)[F16(.01 s)]	62	H_TAU2	tau nu(+)[F16(.01 s)]
63	H_SIG1	sigma nu(-) [F16(.0001 V)]	64	H_SIG2	sigma nu(+)[F16(.0001 V)]
65	H_SO	sqr. den. r. elec.[F16(1E-6)]	66	H_VART	total var. [F16(.0001 V ²)]
67	H_TEQR	T_eq.rison [F16(1E-5 K)]	68	H_TEQWB	T_eq.wide_band [F16(1E-5 K)]
69	H_TEF1	T_eff nu(-)[F16(1E-6 K)]	70	H_TEF2	T_eff nu(+)[F16(1E-6 K)]
71	H_TEFMF	T_eff M. F. [F16(1E-6 K)]	72	H_KSPET	spectrum number of the run
73	H_CAL	calibration value by lock-in [in RHEADER(37)]			
75	H_CALSPET	calibration value by spectrum [in RHEADER(38)]			
77	H_TAUIMP_1	imposed tau_1 [F16(.01 s)]	78	H_TAUIMP_2	imposed tau_2 [F16(.01 s)]
79	H_FBIMP	imposed F. B. [F16(.000001 V/sqr(Hz))]	80		
81	H_CL1_CORR	(dms)	82	H_CL2_CORR	(dms)
83	H_D2TIM_CORR	(dms)	84		
85			86		
87			88		
89			90		
91			92		
93			94		
95			96		
97			98		
99			100		

Table B.1: Call-names, with a brief explanation about the information they contain, of the header words. Any record in R87 data files includes such a header.

Header	Value
H_LREC	3000
H_LLHEA	200
H_LCO1	1200
H_NCA1	12
H_LCO2	1600
H_NCA2	1
H_LCO3	0
H_NCA3	1
N_MIS1	100
N_MIS2	1600
N_MIS3	0
H_KRUN	192 (example)
H_KREC	1 "
H_TIPR	2 "
H_ANNO	1991 "
H_DOY	206 "
H_ORE	10 "
H_MIN	4 "
H_SEC	31 "
H_MSEC	850 "
H_TSA1	290816
H_TSA2	18176
H_TSA3	0
H_ADC	0

Table B.2: True or typical values the most relevant header registers.

Field 1 [sampling time 290816 μ s]

1	_X-	X nu -
2	_Y-	Y nu -
3	_X+	X nu +
4	_Y+	Y nu +
5	CAL	Calibration
6	DIR	Direct Acquisition
7	ROB	Noise out reson.
8	SLB	Seism low freq.
9	SRF	Seism. resonance
10	EMM	Electro-magn. mon.
11	CLK	Top second
12	ALF	Antenna low freq. or Jolly

Field 2 [sampling time 18176 μ s]

- 1 AAP Direct Acquisition after Anti-Aliasing Procedure

Table B.3: Structure of the fields in the processed files.

Appendix C

C.1 Overview

This appendix gathers the most relevant source code we developed in order to implement the data analysis algorithms we have presented in this essay. We selected the C programming language because of its power, its versatility and its close relationship with the UNIX operating system. Nevertheless, it was within our scope to write platform-independent programs, and thence we decided to follow the ANSI C standards [46, 77]. This solid aim led us to define proper functions which surely can be found in most of the compiler releases or in common scientific libraries, like SNAG.

We shall begin with a description of our external library `Explorer.c`, a set of auxiliary routines used by the data analysis programs. The function specifications are included in the header file `Explorer.h`, besides a list with the values of some physical constants and parameters of the detector. After that we shall present the program that performs the search for non-leaking signals. The case of arbitrary signals and the massive data analysis is the purpose of the three programs we will find in the next section of this appendix. We shall end it with two general-purpose routines which have consistently helped us in our work.

Finally, we want to point out that the computational facilities we have used for running those programs is within the reach of (almost) any research group. All the results that we have included in this essay were obtained using a *Pentium-200* with a *Linux 2.0.1* operating system. The C compiler was also a GNU-project developer's tool: *gcc version 2.7.0*.

C.2 The auxiliary functions

In this section we will introduce the user-defined functions we have designed for the data processing programs. Instead of using built-in routines we have composed an external library with its own header file, where as usual can be found the function declarations. In this file `Explorer.h`, we have also included most of the constant quantities used by the different search algorithms and two user-defined data types:

- `typedef struct {double x, y;} tcomp;`

The `tcomp` data type is surely redundant for almost all compiler distributions, because it simply implements a complex variable. Nevertheless we have explicitly defined it for ensuring the portability of the source code and, especially, the double precision of both members of the structure.

- `typedef struct {int run, l2N, M;} tfilename;`

The `filename` data type was designed to easily carry in one block the information we add to the output filenames generated by `leaking.c`. It contains `run`, the run number, $l2N = \log_2 N$, and $M = M$. We shall widely discuss about this data type later in this section.

```
/* Header file Explorer.h */

#ifndef __Explorer__
#define __Explorer__

/* Common headers */

#include <stdio.h>
#include <stdlib.h>
#include <math.h>
#include <string.h>

/* Useful constants */

#define f_ini 900.0267781 /* Hz */
```

```
#define a_m 0.322841781
#define a_p 0.677876848
#define PHI_m 0.833696125e-4 /* x PHI_0, T = 1 K */
#define PHI_p 0.600385955e-4 /* x PHI_0, T = 1 K */
#define PHI_CAL 1.33e-5 /* x PHI_0 */
#define f_m 904.7885 /* Hz */
#define f_p 921.37327 /* Hz */
#define Q_m 0.710604379e6
#define Q_p 0.104203668e7
#define m_b 1138 /* Kg */
#define long_b 2.97 /* m */
#define K_B 1.380658e-23 /* Boltzmann's constant */
#define f_cal 913 /* Hz */
#define b_cal 0.4 /* Hz */
#define DPI 3.14159265358979323846 /* Double-precision PI */
#define MAX_DOP 0.0924

/* User-defined data type */

typedef struct {double x, y;} tcomp;
typedef struct {int run,l2N,M;} tfilename;

/* User-defined functions */

int another_file(char *IFILE);
int b_r(int nn,int br);
void cosin(int n,tcomp *wn);
void fft(tcomp *ts,int n,int nn,tcomp *wn,int *br,int sign);
void inv(char *by,int ni,int nf,int sw);
void itoa(int num, char *s, int base);
int log_2(int n);
tfilename read_file_name(char *IFILE);
int atoi(char *IFILE,char digits);

#endif
```

The specific purpose of each routine in `Explorer.h` is the following:

- `int another_file(char *IFILE);`

This routine accepts one argument, a pointer to a string which must contain a filename with a special structure: it must include a single point character, preceded by two ASCII characters corresponding to digits, e.g. ``g9108v08.alb''. The routine checks the presence in the actual directory of the *next* file in the series, i.e. ``g9108v09.alb''. It returns 1 if the file exists and 0 otherwise.

- `int b_r(int nn,int br);`

This routine computes the bit-reversed companion of `br`, taking into account `nn` binary digits. Thence `b_r(4,5)` returns 10.

- `void cosin(int n,tcomp *wn);`

This routine fills the complex array `wn` with n^{th} roots of 1. Since the function that needs this array only uses the roots with positive imaginary component, only $n/2$ memory locations are assigned.

- `void fft(tcomp *ts,int n,int nn,tcomp *wn,int *br,int sign);`

The function `fft()` performs the Fast Fourier transform of the data placed in the complex array `ts`, and leaves the result also in `ts`. The array is `n` or equivalently 2^{nn} points in length. The routine uses the information contained in arrays `wn` and `br`, filled thanks to functions `b_t()` and `cosin()`. In this way the main routine needs not compute these quantities each time the function `fft()` is called, avoiding so an important growing of the program running time. This feature is very relevant when performing massive data analysis.

Finally, the function `fft()` provides us with direct or inverse (up to a constant factor) DFTs, depending on the value, ± 1 , of `sign`.

- `void inv(char *by,int ni,int nf,int sw);`

This routine was introduced in order to solve a problem which may appear depending on the actual architecture of the selected computational facility. The way in which a two byte integer is internally stored in a

computer is manufacturer dependent. It can assign first the least significant byte and then the more significant byte, or just the opposite. In the first case the value of `sw` must be equal to 0, whereas in the second case we have to set `sw` equal to 1. Only in the latter scenario the routine performs any work. It swaps two by two the contents of array `by`, starting with the `ni+1` pair, and finishing with the `nf` one.

- `void itoa(int num, char *s, int base);`

This function can be found in most compilers. It converts the integer `num` into its equivalent string, and places the result in the memory location pointed by `s`. The result is computed in base `base`.

- `int log_2(int n);`

This function computes the integer part of the logarithm to the base 2 of the integer `n`. It was designed to avoid any problem produced by an erroneous round off.

- `tfilename read_file_name(char *IFILE);`

This function extracts information *encrypted* in the names of the files generated by the `leaking.c` program. The structure of these filenames is the following: ``genericidentifier.run.12N.M.outputnumber'', e.g. ``leak.193.17.36.1''. The routine obtains the values `run`, `12N` and `M` from string `IFILE` and returns them in `tfilename` format.

- `int strttoi(char *IFILE, char digits);`

This function is almost the *inverse* of `itoa()`: it takes a string `IFILE` containing `digits` figures (decimal base is assumed) and returns its numerical value.

The source code of all the functions we have described is in file `Explorer.c` we present next.

```
/* Source code of Explorer.c */

#include "Explorer.h"
```

```
int another_file(char *IFILE)
{
    int i,p;
    FILE *rf;

    for(i=0;IFILE[i]!='.';i++);
    p=i-1;

    if(IFILE[p]=='9'){
        IFILE[p]='0';
        IFILE[p-1]++;
    }
    else IFILE[p]++;

    if((rf=fopen(IFILE,"rb"))==NULL){
        fclose(rf);
        return 0;
    }
    else {
        fclose(rf);
        return 1;
    }
}

int b_r(int nn,int br)
{
    register int j;
    int pos;

    pos=0;
    for(j=0;j<nn;j++){
        pos=pos<<1;
        pos|=br&1;
        br=br>>1;
    }
    return pos;
}
```

```
void cosin(int n,tcomp *wn)
{
    int i;
    int MAX;

    /* The algorithm uses only k=0,...,n/2 -1 for the com. exp. */

    MAX=n>>1;

    for (i=0;i<MAX;i++){
        wn[i].x=cos(2*DPI*i/n);
        wn[i].y=sin(2*DPI*i/n);
    }
}

void fft(tcomp *ts,int n,int nn,tcomp *wn,int *br,int sign)
{
    int i,j,k,n1,l,i1,i2=1,n2;
    double cs,sn;
    tcomp temp;

    n2=n;

    /* FFT algorithm */

    for (i=0;i<(nn-1);i++){
        n1=n2; n2=n2>>1; i1=0;
        for (j=0; j<n2;j++){
            cs=wn[i1].x; sn=wn[i1].y;
            i1+=i2;
            for (k=j;k<n;k+=n1){
                l=k+n2;
                temp.x=ts[k].x-ts[l].x;
                ts[k].x=ts[k].x+ts[l].x;
                temp.y=ts[k].y-ts[l].y ;
                ts[k].y=ts[k].y+ts[l].y;
            }
        }
    }
}
```

```

        ts[1].x=cs*temp.x+sign*sn*temp.y;
        ts[1].y=cs*temp.y-sign*sn*temp.x;
    }
}
i2=i2<<1;
}

for (k=0;k<n;k+=2){
    l=k+1;
    temp.x=ts[k].x-ts[1].x;
    ts[k].x+=ts[l].x;
    temp.y=ts[k].y-ts[1].y ;
    ts[k].y+=ts[l].y;
    ts[1].x=temp.x;
    ts[1].y=temp.y;
}

/* bit-reversion using array br */

for (i=0;i<n;i++){
    j=br[i];

    if(i<j){
        temp=ts[j];
        ts[j]=ts[i];
        ts[i]=temp;
    }
}
return;
}

void inv(char *by,int ni,int nf,int sw)
{
    char w;
    int i;
}

```

```
if(sw==0) return;
else{
    for(i=ni;i<nf;i++){
        w=by[2*i];
        by[2*i]=by[2*i+1];
        by[2*i+1]=w;
    }
}
}

void itoa(int num, char *s, int base)
{
    int i,lnum,dig;

    lnum=(int)floor(log((double)num)/log((double)base));

    for(i=lnum;i>=0;i--){
        dig=num%base;
        s[i]=48+dig;
        num=num/base;
    }
    s[lnum+1]=0;
    return;
}

int log_2(int n)
{
    int i=-1;
    while(n!=0){
        n=n>>1;
        i++;
    }
    return i;
}

tfilename read_file_name(char *IFILE)
{
```

```

char i,j,pos[4];
tfilename file;

i=0;
for(j=0;j<4;j++){
    for(;IFILE[i]!='.';i++);
    pos[j]=i++;
}
file.run=strtoi(IFILE+pos[0]+1,pos[1]-pos[0]-1);
file.l2N=strtoi(IFILE+pos[1]+1,pos[2]-pos[1]-1);
file.M=strtoi(IFILE+pos[2]+1,pos[3]-pos[2]-1);

return(file);
}

int atoi(char *IFILE,char digits)
{
    int res=0;
    char i;

    for(i=0;i<digits;i++)
        res+=((int)IFILE[i]-48)*pow(10,(double)(digits-i-1));
    return(res);
}

```

C.3 The “non-leaking” data processor

The file `nleaking.c` contains the source code that implements the “non-leaking” algorithm presented in Section 4.4. Like most of the programs we will describe in this appendix, `nleaking.c` is designed as an autonomous routine: it needs no on-line information and thus can be directly sent to any computer queue. All the external parameters and run-time options are fed into the program by means of the parameter file `nleaking.par`. This file allow us to choose the

input and the output filenames, to introduce the key parameters of the external control signal, to establish the extension of the processed stretch of data, setting the value of N and M , and to select the output frequency window we want to finally preserve. The contents of `nleaking.par` are indeed a self-explanatory summary on the capabilities of the filtering program.

```
/* Source code of nleaking.c */

#include "Explorer.h"
#define SYS 0

main()
{
    int i,j,k,nu,LOWCAL,UPCAL,LOW,UP,DIFF,MAX,BLK,LEV,J,K,D,k_o;
    int M,M_MAX,*br,N,N2,NEXT_FILE;
    char caux[4],*cdd,IFILE[60],OFILE[60];
    short int *idd,*iaux,L,H,LF[3],NC[3];
    tcomp *data, *cs,*value,zero={0,0},sum,*sim;
    double f_win,b_win,*med,*var,*phi,T[3],NORM,V;
    double alpha_B,BAR,tau_m,tau_p,ell,h_o,f_o,phi_o;
    FILE *pf,*rf,*wf;

    /* Reading of the actual run parameters */

    pf=fopen("nleaking.par","r");

    fscanf(pf,"%*s%s",IFILE);
    fscanf(pf,"%*s%s",OFILE);
    fscanf(pf,"%*s%lf",&h_o);
    fscanf(pf,"%*s%lf",&f_o);
    fscanf(pf,"%*s%lf",&phi_o);
    fscanf(pf,"%*s%d",&N);
    fscanf(pf,"%*s%d",&M_MAX);
    fscanf(pf,"%*s%lf",&f_win);
    fscanf(pf,"%*s%lf",&b_win);
```

```
fclose(pf);

N2=N/2;
nu=log_2(N);

/* Amplification factor of transducer and SQUID */

alpha_B=2*DPI*(sqrt(a_p)*PHI_p
                +sqrt(a_m)*PHI_m)*(f_p-f_m)*sqrt(m_b/K_B);

/* Detector's parameters */

ell=4*long_b/(DPI*DPI);
tau_m=2*Q_m/f_m;
tau_p=2*Q_p/f_p;
BAR=(pow(f_o*f_o-f_m*f_m+1/(tau_m*tau_m),2)
      +4*pow(f_m/tau_m,2))*(pow(f_o*f_o-f_p*f_p+1/(tau_p*tau_p),2)
      +4*pow(f_p/tau_p,2));
BAR=ell*pow(f_o,4)/(2*sqrt(BAR));

/* h_o in PHI_0 units */

h_o=(alpha_B*BAR);

rf=fopen(IFILE,"rb");

/* Obtaining the length of the record, L, and the header, H */

fread(caux,sizeof(char),4,rf);
inv(caux,0,2,SYS);
rewind(rf);
iaux=(int *)caux;
L=iaux[0];
H=iaux[1];

/* Reading the header */
```

```
if((cdd=malloc(sizeof(char)*2*L))==NULL){
    printf("Memory error.\n");
    exit(1);
}
idd=(int *)cdd;
fread(cdd,sizeof(char),2*H,rf);
inv(cdd,0,H,SYS);
rewind(rf);
for(i=0;i<3;i++){
    LF[i]=idd[6+2*i];
    NC[i]=idd[7+2*i];
    if(LF[i]!=0)
        T[i]=(idd[18]+(double)idd[19]/1000)
            *LF[0]*NC[i]/(1000*(double)LF[i]*NC[0]);
}
LOWCAL=(f_cal-f_ini-b_cal/2)*N*T[1];
UPCAL=(f_cal-f_ini+b_cal/2)*N*T[1];

LOW=(f_win-f_ini-b_win/2)*N*T[1];
if(LOW<0) LOW=0;
UP=(f_win-f_ini+b_win/2)*N*T[1];
if(UP>N2) UP=N2;
if(LOW>UP) exit(1);
DIFF=UP-LOW;

if(idd[21]==0){
    V=0.005;
    LEV=2048;
}
else{
    if(idd[21]==201){
        V=0.004883;
        LEV=0;
    }
    else{
```

```
    printf("Unexpected format.\n");
    exit(1);
}
}

BLK=N/LF[1]+1;
MAX=(BLK+1)*LF[1];

/* Allocating memory */

if((data=malloc(sizeof(tcomp)*MAX))==NULL){
    printf("Memory error.\n");
    exit(1);
}
if((sim=malloc(sizeof(tcomp)*MAX))==NULL){
    printf("Memory error.\n");
    exit(1);
}
if((value=malloc(sizeof(tcomp)*(DIFF*M_MAX)))==NULL){
    printf("Memory error.\n");
    exit(1);
}
if((phi=malloc(sizeof(double)*DIFF))==NULL){
    printf("Memory error.\n");
    exit(1);
}
if((med=malloc(sizeof(double)*DIFF))==NULL){
    printf("Memory error.\n");
    exit(1);
}
if((var=malloc(sizeof(double)*DIFF))==NULL){
    printf("Memory error.\n");
    exit(1);
}
if((br=malloc(sizeof(int)*N))==NULL){
    printf("Memory error.\n");
    exit(1);
}
```

```
}

if((cs=malloc(sizeof(tcomp)*N2))==NULL){
    printf("Memory error.\n");
    exit(1);
}

/* Loading bit-reversion array */

for(i=0;i<N;i++) br[i]=b_r(nu,i);
for(i=0;i<DIFF;i++) var[i]=0;

/* Loading complex-exponential array */

cosin(N,cs);

/* Computing k_o */

k_o=(f_o-f_ini)*T[1]*N;

K=H+LF[0];
J=0;
D=0;
M=0;

do{
    for(i=0;i<(BLK-D);){

        /* Loading data */

        fread(cdd,sizeof(char),2*L,rf);
        inv(cdd,0,L,SYS);

        if(feof(rf)){
            NEXT_FILE=another_file(IFILE);
            if(NEXT_FILE){
                fclose(rf);
                rf=fopen(IFILE,"rb");
            }
        }
    }
}
```

```

        continue;
    }
    else break;
}
if(idd[5]!=1) continue;
i++;
for(j=0;j<LF[1];j++){
    data[J+j].x=(idd[K+j]-LEV)*V; /* V is superfluous */
    data[J+j].y=0;
}
J=J+LF[1];
}
if(feof(rf)) break;
for(j=0;j<N;j++) sim[j]=data[j];

fft(data,N,nu,cs,br,1);
NORM=0;

/* Normalizing data */

for(j=LOWCAL;j<UPCAL;j++)
    NORM+=2*(data[j].x*data[j].x
              +data[j].y*data[j].y);

NORM=sqrt(NORM)/(N*PHI_CAL);
for(j=0;j<N;j++)
    sim[j].x=sim[j].x/NORM;

/* Adding control signal */

for(j=0;j<N;j++)
    sim[j].x+=h_o*cos(2*DPI*((double)k_o*j/N+phi_o));

fft(sim,N,nu,cs,br,1);

/* Only data WITH control signal are kept */

```

```
for(j=LOW;j<UP;j++)
    value[M*DIFF+j-LOW]=sim[j];

for(j=N;j<J;j++)
    data[j-N]=data[j];

J=J-N;
if(J>=LF[1]) D=1;
else D=0;
M++;
}while(M!=M_MAX);

free(data);
free(sim);
free(cdd);
free(br);
free(cs);

fclose(rf);

/* Analysis algorithm */

for(i=0;i<DIFF;i++){
    sum=zero;
    for(j=0;j<M;j++){
        sum.x+=value[j*DIFF+i].x;
        sum.y+=value[j*DIFF+i].y;
    }
    phi[i]=atan2(sum.y,sum.x);
    med[i]=sum.x*sum.x+sum.y*sum.y;
    for(j=0;j<M;j++)
        var[i]+=(value[j*DIFF+i].x*value[j*DIFF+i].x
                  +value[j*DIFF+i].y*value[j*DIFF+i].y);
}
free(value);

wf=fopen(OFILE,"w");
```

```

for(i=0;i<DIFF;i++){
    fprintf(wf,"%le",f_ini+(double)(i+LOW)/(N*T[1]));
    fprintf(wf," %le %le",phi[i],
            sqrt(2*(M-1)*med[i]/(var[i]*M*M-med[i]*M)));
    fprintf(wf,"\n");
    fflush(wf);
}

fclose(wf);

free(phi);
free(med);
free(var);

exit(0);

}

```

We illustrate the file `nleaking.par` with the following *authentic* example: the parameter file used when performing the data filtering whose output is shown in Figure 4.1.a of Chapter 4.

```

IFILE /cdrom/g9108v08.alb
OFILE Z.9
H_0 1.0e-22
F_0 904.49965
PHI_0 0.3
N 131072
M_MAX 9
F_WINDOW 914
BAND_WINDOW 28.0

```

C.4 The massive data processor

This section is devoted to the programs we have developed with the scope of performing the massive data analysis described in Section 4.6.3 of Chapter 4. The main routine is in the file `leaking.c`, whereas `cutter.c` and `coin.c` were designed with the purpose of finding recurrent positive outcomes along the six months we processed. It is not accidental fact that the body of `leaking.c` is very similar to the structure of `nleaking.c`, because we coded the new program starting from the old one. Nevertheless, they display several relevant differences besides the trivial one: `leaking.c` is intended to detect a general (“leaking”) monochromatic signal, no matter whether or not the filter template matches its actual frequency.

The `leaking.c` routine can be programmed to perform more than one filtering procedure using successive stretches of $N \times M$ data. The number of output files we want to get after each program run is settled in the corresponding parameter file `leaking.par`. The input value of `NUM_RUN` determines how many filtering cycles shall be completed before the program ends. Nevertheless, the execution of the routine will be automatically aborted if the required *consecutive R87* data files are not available to the program. We check that the experimental stream have no time gap in it just looking at the contents of the header `H_KRUN`, the run number —see Appendix B. When the data-acquisition process in the *Explorer* detector suffers any kind of temporal stop, the value of `H_KRUN` recorded in the header increases by one unit.

In fact, if we set `NUM_RUN` equal to zero, the program shall operate until all the data corresponding to the same run number was finally processed. Therefore, the output filenames will specify not only the actual values of `12N` and `M`, but the `run` and an order number, as explained before.

Finally, the information we include in these files is the actual frequency of the outcome taking into account the estimated value of ϵ_0 , the frequency shift computed from the latter, the output of the filtering procedure $Z(k_0)$ and the amplitude of the related gravitational perturbation h_0 .

```
/* Source code of leaking.c */

#include "Explorer.h"
```

```

#define SYS 0

main()
{
    int i,j,nu,nuMM,LOWCAL,UPCAL,LOW,UP,DIFF,MAX,BLK,LEV,J,K,D;
    int M,MM,MM2,M_MAX,*br,N,N2,NUM_OUT,num_out,NEXT_FILE,RUN_NUM;
    char caux[4],*cdd,IFILE[60],OFILE[30],END[10],WFILE[50];
    short int *idd,*iaux,L,H,LF[3],NC[3];
    tcomp *data,*cs,*value,zero={0,0},*valuefft;
    double f_win,b_win,med,var,e,val_e,mu;
    double T[3],NORM,V;
    double alpha_B,BAR,tau_m,tau_p,ell,h_o,f_o,aux,sinc;
    FILE *pf,*rf,*wf;

    /* Reading of the actual run parameters */

    pf=fopen("leaking.par","r");

    fscanf(pf,"%*s%s",IFILE);
    fscanf(pf,"%*s%s",OFILE);
    fscanf(pf,"%*s%d",&N);
    fscanf(pf,"%*s%d",&M_MAX);
    fscanf(pf,"%*s%lf",&f_win);
    fscanf(pf,"%*s%lf",&b_win);
    fscanf(pf,"%*s%d",&NUM_OUT);

    fclose(pf);

    N2=N/2;
    nu=log_2(N);

    strcat(OFILE,".");

    /* Amplification factor of transducer and SQUID */

    alpha_B=2*DPI*(sqrt(a_p)*PHI_p
                  +sqrt(a_m)*PHI_m)*(f_p-f_m)*sqrt(m_b/K_B);

```

```
/* Detector's parameters */

ell=4*long_b/(DPI*DPI);
tau_m=2*Q_m/f_m;
tau_p=2*Q_p/f_p;

rf=fopen(IFILE,"rb");

/* Obtaining the length of the record, L, and the header, H */

fread(caux,sizeof(char),4,rf);
inv(caux,0,2,SYS);
rewind(rf);
iaux=(int *)caux;
L=iaux[0];
H=iaux[1];

/* Reading the header */

if((cdd=malloc(sizeof(char)*2*L))==NULL){
    printf("Memory error.\n");
    exit(1);
}
idd=(int *)cdd;
fread(cdd,sizeof(char),2*H,rf);
inv(cdd,0,H,SYS);
rewind(rf);
for(i=0;i<3;i++){
    LF[i]=idd[6+2*i];
    NC[i]=idd[7+2*i];
    if(LF[i]!=0)
        T[i]=(idd[18]+(double)idd[19]/1000)
            *LF[0]*NC[i]/(1000*(double)LF[i]*NC[0]);
}
/* Storing the actual run number */
```

```
RUN_NUM=idd[4];

/* Beginning of all the output filenames */

itoa(RUN_NUM,END,10);
strcat(OFILE,END);
strcat(OFILE,".");
itoa(nu,END,10);
strcat(OFILE,END);
strcat(OFILE,".");

LOWCAL=(f_cal-f_ini-b_cal/2)*N*T[1];
UPCAL=(f_cal-f_ini+b_cal/2)*N*T[1];

LOW=(f_win-f_ini-b_win/2)*N*T[1];
if(LOW<0) LOW=0;
UP=(f_win-f_ini+b_win/2)*N*T[1];
if(UP>N2) UP=N2;
if(LOW>UP) exit(1);
DIFF=UP-LOW;

if(idd[21]==0){
    V=0.005;
    LEV=2048;
}
else{
    if(idd[21]==201){
        V=0.004883;
        LEV=0;
    }
    else{
        printf("Unexpected format.\n");
        exit(1);
    }
}
```

```
BLK=N/LF[1]+1;
MAX=(BLK+1)*LF[1];

/* Allocating memory */

if((data=malloc(sizeof(tcomp)*MAX))==NULL){
    printf("Memory error.\n");
    exit(1);
}
if((value=malloc(sizeof(tcomp)*(DIFF*M_MAX)))==NULL){
    printf("Memory error.\n");
    exit(1);
}

K=H+LF[0];
J=0;
D=0;
num_out=0;

/* Starting the massive analysis */

do{
    num_out++;

    /* Allocating memory */

    if((br=malloc(sizeof(int)*N))==NULL){
        printf("Memory error.\n");
        exit(1);
    }
    if((cs=malloc(sizeof(tcomp)*N2))==NULL){
        printf("Memory error.\n");
        exit(1);
    }

    /* Loading bit-reversion array */
```

```

for(i=0;i<N;i++) br[i]=b_r(nu,i);

/* Loading complex-exponential array */

cosin(N,cs);

M=0;

/* Performing the N X M filtering process */

do{
    for(i=0;i<(BLK-D);){

        /* Loading data */

        fread(cdd,sizeof(char),2*L,rf);
        inv(cdd,0,L,SYS);
        if(feof(rf)){
            NEXT_FILE=another_file(IFILE);

            if(NEXT_FILE){
                fclose(rf);
                rf=fopen(IFILE,"rb");
                continue;
            }
            else break;
        }
        if(idd[5]!=1) continue;
        if(idd[4]!=RUN_NUM) break;
        i++;
        for(j=0;j<LF[1];j++){
            data[J+j].x=(idd[K+j]-LEV)*V; /* V is superfluous */
            data[J+j].y=0;
        }
        J=J+LF[1];
    }
    if(idd[4]!=RUN_NUM){

```

```

printf("New run number!\n");
NUM_OUT=num_out;
break;
}
if(feof(rf)) break;

fft(data,N,nu,cs,br,1);
NORM=0;

/* Normalizing data */

for(j=LOWCAL;j<UPCAL;j++)
NORM+=2*(data[j].x*data[j].x
+data[j].y*data[j].y);

NORM=sqrt(NORM)/(N*PHI_CAL);
for(j=0;j<N;j++){
  data[j].x=data[j].x/NORM;
  data[j].y=data[j].y/NORM;
}
for(j=LOW;j<UP;j++)
value[M*DIFF+j-LOW]=data[j];

for(j=N;j<J;j++)
data[j-N]=data[j];

J=J-N;
if(J>=LF[1]) D=1;
else D=0;
M++;
}
while(M!=M_MAX);

free(br);
free(cs);

/* Computing MM (=M') */

```

```
nuMM=log_2(M);
MM=1<<nuMM;
if(MM<M){
    nuMM++;
    MM<<=1;
}
MM2=MM>>1;

/* Allocating memory */

if((valuefft=malloc(sizeof(tcomp)*MM))==NULL){
    printf("Memory error.\n");
    exit(1);
}
if((br=malloc(sizeof(int)*MM))==NULL){
    printf("Memory error.\n");
    exit(1);
}
if((cs=malloc(sizeof(tcomp)*MM2))==NULL){
    printf("Memory error.\n");
    exit(1);
}

/* Loading bit-reversion array */

for(i=0;i<MM;i++) br[i]=b_r(nuMM,i);

/* Loading complex-exponential array */

cosin(MM,cs);

/* Completing output filename */

strcpy(WFILE,OFILE);
itoa(M,END,10);
```

```
strcat(WFILE,END);
strcat(WFILE,".");
itoa(num_out,END,10);
strcat(WFILE,END);

wf=fopen(WFILE,"w");

/* Selecting the best value for epsilon_o */

for(i=0;i<DIFF;i++){
    for(j=0;j<M;j++){
        valuefft[j].x=value[j*DIFF+i].x;
        valuefft[j].y=value[j*DIFF+i].y;
    }
    for(j=M;j<MM;j++) valuefft[j]=zero;
    fft(valuefft,MM,nuMM,cs,br,1);
    e=0;
    val_e=0;
    for(j=0;j<MM;j++){
        aux=pow(valuefft[j].x,2)+pow(valuefft[j].y,2);
        if(val_e<aux){
            val_e=aux;
            e=j;
        }
    }
}

/* Obtaining the spectrum of the noise */

mu=0;
var=0;
for(j=0;j<MM;j++)
    if(j!=e) mu+=valuefft[j].x;
mu/=(MM-1);
for(j=0;j<MM;j++)
    if(j!=e) var+=pow(valuefft[j].x-mu,2);
aux=var;
```

```

mu=0;
var=0;
for(j=0;j<MM;j++)
    if(j!=e) mu+=valuefft[j].y;
mu/=(MM-1);
for(j=0;j<MM;j++)
    if(j!=e) var+=pow(valuefft[j].y-mu,2);
aux+=var;
aux/=(2*M*(MM-2));

/* Best value for epsilon_o (=e) */

e/=MM;
if(e>0.5) e=e-1;
if(e==0) sinc=1.0/N;
else sinc=sin(DPI*e/N)/sin(DPI*e);
e/=(N*T[1]);

med=sqrt(val_e/aux)/M;

f_o=f_ini+((double)i+LOW)/(N*T[1])+e;

/* Related h_o */

BAR=(pow(f_o*f_o-f_m*f_m+1/(tau_m*tau_m),2)
    +4*pow(f_m/tau_m,2))*(pow(f_o*f_o
    -f_p*f_p+1/(tau_p*tau_p),2)
    +4*pow(f_p/tau_p,2));
BAR=ell*pow(f_o,4)/(2*sqrt(BAR));

h_o=2*sqrt(val_e)*sinc/(M*alpha_B*BAR);

/* Writing results */

fprintf(wf,"%le %le %le %le\n",f_o,e,med,h_o);
fflush(wf);
}

```

```
fclose(wf);

free(valuefft);
free(br);
free(cs);

}while(num_out!=NUM_OUT);

free(value);
free(data);
free(cdd);
fclose(rf);

exit(0);
}
```

We complete the description of `leaking.c` quoting the contents of a possible example for its parameter file `leaking.par`.

```
IFILE /cdrom/g9108v08.alb
OFILE leak
N 131072
M_MAX 36
F_WINDOW 914
BAND_WINDOW 28.0
NUM_OUT 0
```

Once we have a reservoir with the files coming from the `leaking.c` procedure, the next operation is performed by `cutter.c`. This program scans the output files listed in the auxiliary file `LFILE` and keeps the outcomes that exceed the level given by the value `Q1` of the false-alarm probability. The program

creates the file WFILE with the date in which the threshold crossing has taken place, among other distinctive parameters of the relevant frequency output: k_0 , $Z(k_0)$ and h_0 .

```
/* Source code of cutter.c */

#include "Explorer.h"

main()
{
    int i,N2,m,MM;
    char LFILE[256],WFILE[256],IFILE[256];
    double level,*value,*h,date,Q1,s,aux,T;
    tfilename actual;
    FILE *pf,*rf,*wf;

    /* Reading parameter file */

    pf=fopen("cutter.par","r");

    fscanf(pf,"%*s%s",LFILE);
    fscanf(pf,"%*s%s",WFILE);
    fscanf(pf,"%*s%lf",&Q1);
    fscanf(pf,"%*s%lf",&T);

    fclose(pf);

    pf=fopen(LFILE,"r");
    wf=fopen(WFILE,"w");

    do{

        /* Obtaining input filename */

        fscanf(pf,"%s%lf",IFILE,&date);
```

```
if(feof(pf)) continue;
if((rf=fopen(IFILE,"r"))==NULL) continue;

/* Progress indicator */

printf("%s\n",IFILE);
fflush(stdout);

/* Extracting information from filename */

actual=read_file_name(IFILE);
N2=1<<(actual.l2N-1);
m=log_2(actual.M);
MM=1<<m;
if(MM<actual.M) MM<<=1;

/* Allocating memory */

if((value=malloc(sizeof(double)*N2))==NULL){
    printf("Memory error.\n");
    exit(1);
}
if((h=malloc(sizeof(double)*N2))==NULL){
    printf("Memory error.\n");
    exit(1);
}

s=0;
aux=0;
for(i=0;i<N2;i++){
    fscanf(rf,"%*lf%*lf%*lf",value+i,h+i);
    s+=value[i]*value[i];
}
for(i=1;i<=MM;i++) aux+=1.0/i;

/* Computing lambda_o */
```

```

level=sqrt(-s*log(1-pow(1-Q1,1./MM))/(N2*aux));

/* Selecting events */

for(i=0;i<N2;i++){
    if(value[i]>level){
        fprintf(wf,"%lg %d %le %le %le\n",
                date,i,f_ini+(double)i/(2*N2*T),value[i],h[i]);
        fflush(wf);
    }
}
free(value);
free(h);
fclose(rf);

}while(!feof(pf));

fclose(wf);
fclose(pf);

exit(0);
}

```

The following example for `cutter.par` informs `cutter.c` about the auxiliary file `cutter.in` containing the roll of files to be scanned, the output filename `cutter.out`, the selected value for the error of the first kind, `Q1`, and the sampling time `T`.

```

LIST_OF_FILES cutter.in
OUTPUT_FILE cutter.out
Q1 0.00001
T 0.018176

```

The output of the preceding routine is directly the input to the last program shown in this section, `coin.c`. The task of `coin.c` reduces to look for a recurrent pattern in the `cutter.out` file. As we have explained in Chapter 4, we scan a window of about 0.2 Hz in width, centred in all and sundry possible values for k_0 , and register how many times a threshold-crossing frequency is at least present within these spectral band. The routine saves the number of positive events per day which have been found, and the mean value of the amplitude of those candidates to be a gravitational signal.

```
/* Source code of coin.c */

#include "Explorer.h"

main()
{
    int i,N2,LOW,UP,d,freq,*table,GAP;
    char ok,IFILE[256],OFILE[256];
    double day,oldday,Z,h,*maxh,*medh,T;
    FILE *pf,*rf,*wf;

    /* Reading parameter file */

    pf=fopen("coin.par","r");

    fscanf(pf,"%*s%s",IFILE);
    fscanf(pf,"%*s%s",OFILE);
    fscanf(pf,"%*s%d",&N2);
    fscanf(pf,"%*s%lf",&T);

    fclose(pf);

    GAP=2*N2*T*MAX_DOP;

    /* Allocating memory */
```

```
if((table=malloc(sizeof(int)*N2))==NULL){
    printf("Memory error.\n");
    exit(1);
}
if((maxh=malloc(sizeof(double)*N2))==NULL){
    printf("Memory error.\n");
    exit(1);
}
if((medh=malloc(sizeof(double)*N2))==NULL){
    printf("Memory error.\n");
    exit(1);
}

/* Setting array values equal to zero */

for(i=0;i<N2;i++){
    table[i]=0;
    maxh[i]=0;
    medh[i]=0;
}

rf=fopen(IFILE,"r");

/* Counting events */

fscanf(rf,"%lf%d%*lf%lf%lf",&day,&freq,&Z,&h);
if(feof(rf)) exit(1);
oldday=day;
d=1;

do{
    if(day!=oldday){
        for(i=0;i<N2;i++){
            if(maxh[i]!=0){
                table[i]++;
                medh[i]+=maxh[i];
            }
        }
    }
}
```

```
        }
    }
    d++;
    for(i=0;i<N2;i++) maxh[i]=0;
    oldday=day;
}
LOW=freq-GAP;
if(LOW<0) LOW=0;
UP=freq+GAP+1;
if(UP>N2) UP=N2;
for(i=LOW;i<UP;i++){
    if(h>maxh[i]) maxh[i]=h;
}
fscanf(rf,"%lf%d%*lf%lf%lf",&day,&freq,&Z,&h);
}while(!feof(rf));

fclose(rf);

for(i=0;i<N2;i++){
    if(maxh[i]!=0){
        table[i]++;
        medh[i]+=maxh[i];
    }
}

/* Writing results */

wf=fopen(OFILE,"w");
for(i=0;i<N2;i++){
    if(table[i]!=0){
        fprintf(wf,"%le %d %le %le\n",
            f_ini+(double)i/(2*N2*T),i,(double)table[i]/d,
            medh[i]/table[i]);
    }
}
fclose(wf);
free(table);
```

```

    free(maxh);
    free(medh);

    exit(0);
}

```

The last file we have included in this section is again a parameter one. The contents of `coin.par` are in accordance with the previous examples, `leaking.par` and `cutter.par`.

```

IFILE cutter.out
OFILE coin.out
N2 65536
T 0.018176

```

C.5 The auxiliary programs

Finally we are going to present two auxiliary programs of very different nature. The first one, `histo.c` is a simple tool designed to compute histograms from a tabular ASCII file. The program determines the number of columns that configure the input file, using the function `sret()`. Then it asks for the precise column to be processed and for the number of desired subdivisions. After that the routine determines the actual range of values of the input variable and performs the operation, writing the result to a text file. For instance, the “Experimental” points plotted in Figure 4.2 were generated with the `histo.c` program.

```
/* Source code of histo.c */
```

```
#include <stdio.h>

int sret(FILE *);

main()
{
    int i,j,c,nc,div,nr=0,*histo,pos;
    double aux,maxval,minval,band;
    char INFILE[60],OUTFILE[60];
    FILE *rf,*wf;

    /* ASCII input file */

    do{
        printf("INPUT file: ");
        scanf("%s",INFILE);
    }while((rf=fopen(INFILE,"r"))==NULL);

    /* Desired column */

    nc=sret(rf);
    do{
        printf("The file has %d column(s).\nChoose column: ",nc);
        scanf("%d",&c);
    }while((c<1)|| (c>nc));

    /* Establishing maximum and minimum values in file */

    for(i=1;i<c;i++) fscanf(rf,"%*lf");
    fscanf(rf,"%lf",&aux);
    for(i=c+1;i<=nc;i++) fscanf(rf,"%*lf");
    maxval=minval=aux;
    while(!feof(rf)){
        nr++;
        if(aux>maxval) maxval=aux;
        else if(aux<minval) minval=aux;
        for(i=1;i<c;i++) fscanf(rf,"%*lf");
```

```
fscanf(rf,"%lf",&aux);
for(i=c+1;i<=nc;i++) fscanf(rf,"%*lf");
}

rewind(rf);
printf("Number of rows: %d\n",nr);

/* Number of divisions */

do{
    printf("Divisions: ");
    scanf("%d",&div);
}while(div<1);
if((histo=malloc(div*sizeof(int)))==NULL) exit(1);
for(i=0;i<div;i++) histo[i]=0;
band=(maxval-minval)/div;

/* Performing the histogram */

for(j=0;j<nr;j++){
    for(i=1;i<c;i++) fscanf(rf,"%*lf");
    fscanf(rf,"%lf",&aux);
    for(i=c+1;i<=nc;i++) fscanf(rf,"%*lf");
    pos=(aux-minval)/band;
    if(pos==div) pos--;
    histo[pos]++;
}
fclose(rf);

/* Naming output file */

printf("OUTPUT file: ");
scanf("%s",OUTFILE);

/* Writing histogram file */

wf=fopen(OUTFILE,"w");
```

```

for(i=0;i<div;i++)
    fprintf(wf,"%le %le\n",
            minval+(i+0.5)*band,(double)histo[i]/(band*nr));
fclose(wf);

exit(0);
}

int sret(FILE *ip)
{
    int cont=0, a=0, ok=1;
    char caracter;
    while(!a && !feof(ip)){
        caracter=fgetc(ip);
        if((caracter=='\t')||(caracter=='\x20')) ok=1;
        else{
            if(caracter=='\n') a=1;
            else if(ok==1) {
                ok=0;
                cont++;
            }
        }
    }
    rewind(ip);
    return(cont);
}

```

The last program in this appendix, `lector.c`, is curiously the first application we developed. It is a general-purpose program that embodies the most basic features in order to extract information from the **R87** files. In this way, running this program we can transfer any data channel into an ASCII file, obtain the header values of a given record or view the contents of the non-data records, for instance. So, `lector.c` provided us with the minimum required tools when we started to handle the experimental files, and it is the foundations of the data-analysis routines we have previously introduced.

```
/* Source code of lector.c */

#include "Explorer.h"
#define SYS 0

void nodata(char *);
void wf(double *,short int,short int,double,int);

main()
{
    char caux[4],w,*cdd,rfile[60],sfile[60],opt;
    short int *idd,*iaux,L,H,LF[3],NC[3],h;
    double *dd[3],T[3],V;
    int i,j,k,ok,nr,fr,t(nr=0,nr=0,n[3]={0,0,0},f,LEV,
FILE *rf,*sf;

/* Main title */

for(i=0;i<24;i++) printf("\n");
printf("Welcome to lector.\n\n");

/* Obtaining valid input file name */

ok=0;
do{
    printf("INPUT file: ");
    scanf("%s",rfile);
    if((rf=fopen(rfile,"rb"))==NULL)
        printf("Unable to open '%s'.\n",rfile);
    else ok=1;
}while(!ok);

/* Obtaining the length of the record, L, and the header, H */
```

```
    fread(caux,sizeof(char),4,rf);
    rewind(rf);
    iaux=caux;
    inv(caux,0,4,SYS);
    L=iaux[0];
    H=iaux[1];

    /* Reading the header */

    if((cdd=malloc(sizeof(char)*2*L))==NULL){
        printf("Memory error.\n");
        exit(1);
    }
    idd=cdd;
    fread(cdd,sizeof(char),2*H,rf);
    rewind(rf);
    inv(cdd,0,H,SYS);
    for(i=0;i<3;i++){
        LF[i]=idd[6+2*i];
        NC[i]=idd[7+2*i];
        if(LF[i]!=0)
            T[i]=(idd[18]/1e3
                  +idd[19]/1e6)*LF[0]*NC[i]/((double)LF[i]*NC[0]);
    }

    if(idd[21]==0){
        V=0.005;
        LEV=2048;
    }
    else{
        if(idd[21]==201){
            V=0.004883;
            LEV=0;
        }
        else{
            printf("Unexpected format.\n");
            exit(1);
        }
    }
}
```

```
    }

}

/* Starting point and total amount of records */

do{
    printf("Number of records I must read: ");
    scanf("%i",&nr);
}while(nr<0);

do{
    printf("First record I must read: ");
    scanf("%i",&fr);
}while(fr<1);

/* Allocating memory */

for(i=0;i<3;i++){
    if(((dd[i]=malloc(sizeof(double)*LF[i]*nr))==NULL)
        &&(LF[i]!=0)){
        printf("Memory error in field %i.\n",i+1);
        exit(1);
    }
}

/* Reading file */

for(i=0;i<(fr-1);i++){
    fread(cdd,sizeof(char),2*L,rf);
    if(feof(rf)){
        printf("The file %s has only %i records.\n",rfile,i);
        exit(1);
    }
}
for(i=0;i<nr;i++){
    fread(cdd,sizeof(char),2*L,rf);
    if(feof(rf)){
```

```
    printf("The file %s has only %i records.",rfile,fr+i-1);
    break;
}
tnr++;
inv(cdd,0,H,SYS);

/* Looking for a non-data record */
if(idd[5]!=1){
    nodata(cdd);
    continue;
}
nrf++;
inv(cdd,H,L,SYS);
h=H;
for(j=0;j<3;j++){
    for(k=0;k<LF[j];k++){
        dd[j][n[j]]=(idd[h+k]-LEV)*V;
        n[j]++;
    }
    h+=LF[j];
}
}

/* List of available options */

printf("\n\nI have read %i records of first type.\n\n",nrf);
do{
    printf("\n\n      Options:\n\n");
    printf("1. Write channels of field 1 into a text file.\n");
    printf("2. Write channels of field 2 into a text file.\n");
    printf("3. Write channels of field 3 into a text file.\n");
    printf("4. Write the header of record %i into a text file.\n"
          ,fr+tnr-1);
    printf("5. Exit.\n");
    do
    {
        printf("=> ");
        if(idd[5]==1)
            break;
    }
    while(1);
}
```

```

        scanf("\n%c",&opt);
    }while((opt<'1'||(opt>'5'));
f=atoi(&opt)-1;
switch(opt){
    default: wf(dd[f],LF[f],NC[f],T[f],nrf);
              break; /* Options 1-3 */
    case '4': printf("\nOutput file: ");
                scanf("%s",sfile);
                if((sf=fopen(sfile,"wt"))==NULL){
                    printf("Unable to open '%s'.\n",sfile);
                    break;
                }
                fprintf(sf,"Header    Value\n\n");
                for(i=0;i<H;i++)
                    fprintf(sf,"%6i    %i\n",i+1,idd[i]);
                break;
    case '5': break;
}
}while(opt!='5');
printf("\n");
}

void nodata(char *by)
{
    char sfile[30],opt;
    short int *iby;
    int i,nret;
    FILE *sf;

    iby=by;

/* Options related to a non-data record */

    printf("\n\nI have read a record of type %i.\n\n",iby[5]);
    printf("    Options:\n\n");
    printf("1. Write record into a text file.\n");
    printf("2. View record.\n");
}

```

```
printf("3. Skip record.\n");
do{
    printf("=> ");
    scanf("\n%c",&opt);
}while((opt<'1'||opt>'3'));
switch(opt)
{
    case '1': printf("Output file: ");
                scanf("%s",sfile);
                if((sf=fopen(sfile,"wt"))==NULL){
                    printf("Unable to open '%s'.");
                    return;
                }
                for(i=iby[1]*2;i<iby[0]*2;i++){
                    if(by[i]=='\n'){
                        fprintf(sf,"\n");
                        i++;
                    }
                    else fprintf(sf,"%c",by[i]);
                }
                break;
    case '2': nret=0;
                getchar();
                for(i=iby[1]*2;i<iby[0]*2;i++){
                    printf("%c",by[i]);
                    if(by[i]=='\n') nret++;
                    if(nret==23){
                        nret=0;
                        printf(" *** Press ENTER to continue ***");
                        fflush(stdin);
                        getchar();
                    }
                }
                printf("\n");
                printf(" *** Press ENTER to continue ***");
                fflush(stdin);
                getchar();
}
```

```
        for(i=0;i<=23;i++) printf("\n");
        break;
    case '3': break;
}
return;
}

void wf(double *dd,short int LF,short int NC,double T,int nrf)
{
    char sfile[30],time;
    short int nc,*ch;
    int i,j,k,row;
    FILE *sf;

    if((NC==0)|| (LF==0)){
        printf("Data field not available.\n\n");
        return;
    }
    row=(LF*nrf)/NC;
    printf("\nOutput file: ");
    scanf("%s",sfile);
    if((sf=fopen(sfile,"wt"))==NULL){
        printf("Unable to open the file.\n\n");
        return;
    }
    do{
        printf("Number of channels to be preserved (0-%hi): ",NC);
        scanf("%hi",&nc);
    }while((nc<0)|| (nc>NC));
    if((ch=malloc(sizeof(short int)*nc))==NULL){
        printf("Memory error.\n");
        return;
    }
    printf("Choose channels.\n");
    for(i=0;i<nc;i++){
        do{
            printf("Channel n.%hi: ",i+1);
```

```
    scanf("%hi",&ch[i]);
}while((ch[i]<1)|| (ch[i]>NC));
}
printf("\nDo you want a time column (y/n)? ");
fflush(stdin);
scanf("\n%c",&time);
time=tolower(time);
for(i=0;i<row;i++){
    if(time=='y') fprintf(sf,"%lE",i*T);
    for(j=0;j<nc;j++) fprintf(sf," %lE",dd[NC*i+ch[j]-1]);
    fprintf(sf,"\n");
}
return;
}
```

Resum

R.1 Introducció

R.1.1 Rerefons històric

El primer treball sobre ones gravitacionals, és a dir, l'existència de solucions radiatives, dins el marc de la Relativitat General [28], és gairebé tant antic com la teoria mateixa, i és també degut a A. Einstein [29].

Tot i això, a diferència d'altres prediccions de la teoria de la gravetat d'Einstein, com ara el desviament dels raigs de llum, el corriment cap al vermell dels espectres d'emissió o l'explicació completa de la precessió, prèviament observada, en el periheli de Mercuri, la confirmació experimental de la presència d'ones gravitatoris a la Natura ha estat un repte durant molts anys. La raó per aquest comportament esquívola es troba a la conjunció de dos fets. Per una banda, la radiació gravitacional no és el mecanisme predominant d'emissió d'energia¹, també en el cas de les fonts més intenses, aquelles relacionades amb esdeveniments còsmics de caire catastròfic [84, 78]. Tot i això, el valor precís de les proporcions que determinen la importància relativa dels diferents efectes (radiació gravitacional, radiació electromagnètica o l'expulsió de massa, per exemple) que contribueixen a l'emissió d'energia pel sistema continua avui dia com una qüestió oberta al camp de la Astrofísica. Per altra banda, aquestes fonts són elles mateixes objectes astronòmics distants, que per tant, no afecten intensament qualsevol detector d'escala humana, amb independència del principi en què fonamentin el seu funcionament.

¹Aquesta simple afirmació, tot assumint que les ones gravitacionals porten energia va ser, de fet, discutit durant dècades. La idea començà a ésser àmpliament acceptada després del treball de H. Bondi [13].

D'acord amb això, no és sorprenent que la comunitat científica hagués d'esperar més de cinquanta anys fins que el primer resultat afirmant l'*evidència del descobriment de radiació gravitacional* fos anunciat. Va ser J. Weber qui, explotant la seva idea original d'enregistrar les vibracions que una ona gravitacional havia de causar en un objecte elàstic massiu [90], practicà diverses proves [91] emprant cilindres metàl·lics —des d'aleshores, genèricament coneguts com a barres de Weber, en honor seu. Dos d'aquests detectors a temperatura ambient van ser emplaçats a llocs distants (un al Argonne National Laboratory de Chicago, i l'altre a la Universitat de Maryland) per cercar coincidències en les seves respostes, dintre del retard màxim en els respectius temps d'arribada dels esdeveniments [92]. El temps de retard enregistrat també informava de la possible localització de la font, i fins i tot de la polarització de la radiació [93].

Els resultats positius publicats per Weber van impulsar altres grups de recerca a intentar reproduir l'experiment per mitjans independents. Desafortunadament, els nous resultats no només no confirmaren les conclusions prèvies, sinó que suggeriren la possibilitat que els esdeveniments presentats en els treballs de Weber no fossin produïts per ones gravitacionals —vegeu, per exemple, els articles de J. L. Levine i R. Garwin [49, 33, 50]. Aquests resultats contradictoris també animaren l'estudi teòric de l'últim límit de sensibilitat d'aquelles antenes resonants d'ones gravitatoris [34, 35], i d'aquí la importància de la temperatura del detector.

Contemporàniament a aquest episodi, lleugerament decebedor, trobem un fet aparentment disconnectat, que va esdevenir amb els anys la següent fita assenyalant la presència d'ones de gravetat a l'Univers: el descobriment del púlsar binari PSR 1913+16 reportat al 1975 per R. A. Hulse i J. H. Taylor [41]. Aquest sistema binari conjuga dues característiques interessants: una estrella de la parella és un púlsar [79], un rellotje natural molt precís, i la seva freqüència orbital (i així doncs, la velocitat relacionada amb aquesta) és força elevada. Per altra banda, es va comprovar que el seu company invisible era un segon estel de neutrons, i d'aquesta manera, camps gravitacionals molt intensos són presents el sistema. Això explica perquè va ser proposat com a un possible laboratori gravitacional astronòmic, pels seus descobridors. Una de les observacions més remarcables va ser la disminució secular en el període de revolució dels estels binaris, el qual podia ser explicat de manera molt acurada (dins un 1% d'error) en termes de les pèrdues energètiques degudes a la radiació gravitacional, d'acord amb les prediccions de la Relativitat General

per a aquest precís sistema [81, 82]. Aquesta s'anomena de vegades *la prova indirecta* de l'existència de radiació gravitacional, però, segons la nostra opinió, el que és realment rellevant a qualsevol prova no és la seva condició de directa o indirecta, sinó la seva correcció i el seu grau de precisió. Així, des del nostre punt de vista, l'existència d'ones gravitacionals a la Natura no es pot continuar considerant una qüestió polèmica.

En qualsevol cas, l'interès en dissenyar i construir una antena operativa d'ones gravitacionals amb l'objectiu de conseguir una evidència *directa* no es va reduir pels resultats derivats de l'estudi del púlsar binari PSR 1913+16, sinó més aviat el contrari. Durant tots aquests anys passats des dels experiments de Weber, altres detectors ressonants a temperatura ambient, com ara el GEOGRAV [18], van ser dissenyats, construïts i operats amb èxit tècnic, però sense donar cap mostra rellevant de la presència de senyals gravitacionals en les dades que enregistraven. Donat que per els grups de recerca experimental, estava ben clar que el soroll termal que afectava el cilindre metàl·lic limitava seriosament la sensibilitat d'aquestes antenes, es concentraren en el disseny dels primers prototips *criogènics* —el detector ALTAIR [15], per exemple, ja era operatiu al final dels anys 70.

Dins d'aquesta nova generació de detectors [10], refredats fins a la temperatura de l'heli líquid, i equipats amb transductors ressonants adaptats i amplificadors basats en efectes quàntics, és on trobem l'antena EXPLORER [6] propietat del grup *ROG* de Roma, però instal·lat dins el recinte del *CERN* a Ginebra. Altres barres ressonants criogèniques es troben operatives a l'actualitat a Legnaro —AURIGA [22]—, Louisiana —ALLEGRO [58]—, Perth —NIOBE [40]—, i Tòquio —el projecte CRAB [80]. També el detector ultracriogènic del grup *ROG* —NAUTILUS [9]— ubicat en els laboratoris de l'*INFN* a Frascati (Roma) opera a l'actualitat amb continuïtat, a una temperatura tant baixa com ara 0.1 Kelvin.

Paral·lelament al creixement dels detectors ressonants la possibilitat de fer servir un interferòmetre de dos braços com a detector d'ones gravitacionals va ser proposada. La idea subjacent és en part similar a la de l'experiment històric de Michelson-Morley, però en comptes de provar d'observar canvis en la velocitat de la llum, aquests nous detectors proven de mesurar les diferències entre la longitud dels braços que una ona gravitacional causaria si creués l'aparell. Diversos prototips *a petita escala*, com ara els de Glasgow i Garching [66], van ser considerats com un pas previ dels nous detectors de mides hectomètriques i kilomètriques, actualment en etapes avançades de construcció: TAMA300

[44], GEO600 [56], LIGO [1], i VIRGO [20].

El futur dels detectors interferomètrics sembla descansar en l'ús de braços encara més llargs, de magnituds astronòmiques —el projecte LISA [25]—, mentre que la nova generació d'antenes ressonants potser que adopti formes esfèriques. La conveniència de l'ús d'una esfera en el nucli d'una antena criogènica d'ones gravitacionals (debat a la millor secció eficaç i a la seva omnidireccionalitat quan es compara amb un cilindre) no és una idea nova [5, 88]. Aquesta possibilitat ha sofert una empenta important recentment, tant el camp teòric [24, 55, 68], com en l'aplicat, amb el detector ultracriogènic GRAIL als Païssos Baixos [32] i els projectes SFERA i TIGA [42, 61, 62].

R.1.2 Motivació

Hem mencionat prèviament que s'accepta generalment que les fonts més intenses de radiació gravitacional es relacionen amb esdeveniments astronòmics catastròfics. La magnitud dels processos que juguen un paper fonamental en l'evolució temporal d'aquests escenaris dramàtics, també prediu la seva curta durada. Això és especialment veritat en el cas de les explosions molt curtes (d'un mil.lisecond) d'energia gravitacional alliberada en l'explosió d'una supernova [84], però també s'aplica als sistemes de binàries compactes que s'apropen en espiral [73], on el mecanisme d'emissió d'ones gravitacionals és més efectiu en els darrers segons, previs a la mateixa coalescència [76, 26].

La gran intensitat, en termes relatius, de les explosions de radiació gravitacional —generades quan un estel massiu colapsa, o en una explosió de raigs gamma [75]—, però també la seva curta durada quan es compara amb les escales de temps característiques dels detectors ressonants (els temps d'esmoreïment de les oscil.lacions mecàniques) fan d'aquests esdeveniments els preferits [34] per a ésser cercats per antenes criogèniques —amb la única excepció digna de menció de la sèrie de detectors CRAB, com explicarem després. De fet, el sistema d'adquisició de dades d'aquests detectors, usualment es dissenya de forma tal que realitza anàlisis *on line*, basats en el procediment conegut com a *lock-in* [14], sobre l'informació enregistrada per l'aparell experimental, amb l'objectiu específic de detectar senyals impulsives. D'aquesta forma, és usual de trobar —vegeu un altre cop, per exemple, [6] o [58]— en els articles que descriuen les primeres etapes de l'adquisició contínua de dades pel detector, una secció dedicada a la discussió dels resultats obtinguts amb aquest procés sistemàtic de filtrat.

Això no vol dir, que no es realitzi cap altra mena d'anàlisi *off-line* en el fluxe de dades emmagatzemades. Noves estratègies de filtrat basades un altre cop en la cerca de coincidències, com aquelles realitzades per Weber, han estat desenvolupades i aplicades quan al menys dos antenes han estat en funcionament de manera simultània [7, 59]. De fet, aquí radica el més important disavantatge de la cerca de senyals provinents d'aquestes fonts de corta durada: la possibilitat de perdre l'esdeveniment més important en molts anys, degut a què cap detector estava treballant amb sensibilitat òptima (o potser, ni tan sols treballant) en aquell precís moment.

Això no passa quan es cerquen ones monocromàtiques. Aquests senyals es generen probablement per la rotació d'estels asimètrics, com ara un púlsar o un estel de neutrons [85]. Com hem mencionat abans, els púlsars es coneixen pel seu moviment estable de rotació, i per tant, són fonts d'ones gravitacionals que radien contínuament durant eons. Aquesta estabilitat, en canvi, també implica que les ones de gravetat emeses no es poden emportar energia a un ritme significatiu, donat que això afectaria al període de rotació de l'estel. La quantitat precisa de fluxe sortint d'energia gravitacional depèn de diverses propietats de la font, però especialment del grau d'asimetria de l'estel giratori, perquè és en aquest paràmetre on es pot trobar un més ampli rang de possibles valors. Les estimacions més raonables de la radiació gravitacional que ens arriba a la Terra de fonts monocromàtiques, inclòs el cas dels anomenats púlsars mil.lisegon [83, 27], donen resultats que estan per sota en alguns ordres de magnitud de les amplituds típiques de les explosions [84].

Tot i això, la més baixa intensitat d'aquestes ones potser àmpliament contrarrestat amb el creixement sense límits els temps d'observació que podem, en principi, aconseguir gràcies a l'esmentada estabilitat de les fonts monocromàtiques. Així doncs ens haurem d'enfrontar amb la complexitat que comporta l'estudi d'aquests senyals durant llargs períodes de temps. Donat que la font és un objecte astronòmic i el nostre detector està collocat sobre la superfície de la Terra, el senyal rebut difereix àmpliament del que en emetre's era monocromàtic: el corrent Doppler degut a la relativa velocitat entre la font i el detector afecta a la freqüència observada de l'ona, i el canvi en l'orientació mútua introduceix variacions en la sensibilitat de l'antena que depenen del temps. Aleshores, s'ha de desenvolupar una estratègia de cerca que compensi aquests efectes destorbants. Dues aproximacions diferents al problema han estat considerades en la literatura de la darrera dècada [51, 31].

La primera opció necessita de coneixement previ sobre la localització de

la font i també sobre la seva freqüència de rotació, donat que el comportament temporal dels efectes anteriorment esmentats depèn fortament d'aquests paràmetres. Quan es disposa d'aquesta informació precisa, és factible treure totes aquestes contribucions en un pas previ, i després aplicar un algoritme de filtrat més estàndard, encaminat a trobar senyals *puramente* monocromàtics [66, 60]. És més, si l'objectiu del procediment de cerca es troba firmement definit, és possible no només afinar l'estratègia de filtrat a les propietats de la font, sinó també la mateixa antena. En aquesta situació trobem tots els detectors CRAB: es dissenyen i es construeixen amb el propòsit de detectar les ones gravitacionals emeses per l'estel de neutrons en rotació ubicat en el mateix centre de la nebulosa del Cranc.

La segona possibilitat, en canvi, implica el disseny d'algoritmes de filtrat que no s'han de veure afectats pel comportament no monocromàtic de l'ona [8, 17]. Això reduirà les seves oportunitats de descobrir senyals còsmics, però donat que no asumeix cap informació sobre la font, qualsevol procediment així implementat serà útil (i necessari) quan es realitzi una cerca de tot el cel. Els mètodes que anem a presentar en aquest treball han de ser inclosos en aquesta categoria.

R.1.3 Sumari d'aquest treball

L'estructura d'aquest texte es descansa en tres pilars fonamentals: l'estudi dels senyals gravitacionals que esperem de trobar, l'anàlisi de l'antena que tenim previst de fer servir per detectar-los, i la descripció dels processos de filtrat que hem desenvolupat amb el propòsit de fer manifesta la seva presència a les dades experimentals enregistrades.

Amb aquest propòsit comencem el Capítol 2 amb una revisió dels aspectes fonamentals de l'aproximació lineal de la Relativitat General: derivem l'equació d'ones, discutim el significat físic de *gauge* transvers i sense traça, i introduïm la fórmula quadrupolar quan calculem la forma d'ona emesa per un el.lipsoide rígid i homogeni en rotació, un model molt senzill per descriure un estel de neutrons. També presentem en aquest capítol l'efecte d'una ona plana en un conjunt de partícules de prova, posposant l'estudi de la interacció entre la radiació gravitacional i els subjectes extensos fins el Capítol 3.

Aleshores, dirigim la nostra atenció cap al problema de la descripció de l'ona que rebrem, tot estudiant els dos principals efectes destorbatius que hem mencionat a la secció prèvia: el corrent Doppler en la freqüència

observada de l'ona, i la sensibilitat en funció del temps del detector. Derivarem les contribucions explícites d'aquests efectes a la forma d'ona de la pertorbació que s'apropa, en termes de la posició astronòmica de la font i la localització geogràfica del nostre detector. D'aquesta manera, l'expressió final que s'obté per a la força gravitacional serà adient, no només per calcular en el Capítol 3 la resposta teòrica de l'antena ressonant a aquesta precisa força externa, sinó en problemes pràctics d'anàlisi de dades, donat que les fórmules poden ser fàcilment restringides a exemples concrets tot usant una simple taula d'efemèrides.

De fet, en el Capítol 3 són descrits tots els aspectes que es relacionen específicament amb l'aparell experimental de detecció: l'antena criogènica ressonant *Explorer*. Veurem, en primer lloc, com un cilindre metàl·lic s'acobla a la radiació gravitacional. Presentem i resolem les equacions que la teoria de l'eslasticitat proporciona per a aquest sistema, i mostrarem com pot ser correctament modelat per un simple oscil.lador harmònic, un resultat aquest ben coneut. Un cop hem raonat que una barra elàstica es pot fer servir com a nucli d'un detector d'ones de gravetat, dissemionem els dos components principals que conformen l'*Explorer*, a més del propi cilindre d'alumini: el transductor capacitiu ressonant, que transforma de manera eficient les vibracions del cilindre a voltatges elèctrics, i el d.c. SQUID, un amplificador electromagnètic basat en efectes quàntics. Després ampliem el model d'oscil.lador harmònic usat habitualment a fi i efecte d'incloure l'acoblament mecànic intencionadament dissenyat, que apareix entre la barra i el transductor. Com hem mencionat abans, trobarem les solucions de les noves equacions que descriuen tot el detector en el cas en què la força externa sigui deguda a una ona gravitacional monocromàtica amb corrent Doppler i amplitud dependent del temps.

També descriurem el sistema d'adquisició de dades de l'antena, el qual enregistra finalment, en forma de fitxers informàtics les referides oscil.lacions de l'extrem de la barra, juntament amb altre informació experimental útil provinent de diferents sensors incorporats a l'*Explorer*: dos sismògrafs, un detector de radiació electromagnètica, i diversos filtres analògics *on line*. Estudiem finalment les presuntes característiques del soroll que amb total certesa afectarà a aquest procés d'adquisició de dades, i per tant serà present a la sortida del detector, amb sort barrejat amb la resposta del detector a la radiació gravitacional que l'affecti.

Aquesta aproximació al tema del soroll pot ser pensada, en certa manera, com un petit prefaci del Capítol 4, on desenvolupem el problema de l'anàlisi

del fluxe de dades experimentals. En aquest capítol és on es troben la major part de les contribucions originals, que al problema de la detecció d'ones gravitacionals, hem presentat en aquest text. Començarem amb la teoria ben establerta del “matched filter”, o filtre adaptat, que determina el millor filtre lineal per un senyal donat, soterrat en soroll amb densitat espectral conejada. En el nostre cas, el procediment de filtrat que s'obté amb aquesta aproximació és equivalent a una simple transformada discreta de Fourier. Després ens enfrontarem a les consecuències que comporta la imposibilitat pràctica de realitzar l'anàlisi de totes les dades recollides d'un sol cop, sinó que ho haurem de fer en diferents blocs. A diferència del procediment usual de promitjar el quadrat dels mòduls de la transformada de Fourier de cada peça, desenvoluparem un mètode que també aprofita la informació relativa a la fase continguda en les diverses porcions de dades procesades, aconseguint d'aquesta manera un procediment de filtrat no lineal.

En un primer pas suposarem que la freqüència del senyal amagat correspon a un únic valor espectral del banc de filtres que apliquem, definit de manera natural per l'algoritme de la transformada ràpida de Fourier. Considerem dos possibles escenaris dependent de la informació de què disposem en relació al soroll: la seva densitat espectral pot ser conejada o bé desconeguda. En tots dos casos es desenvolupa un estudi probabilístic detallat del resultat del filtre i les conclusions que en treiem són comparades amb el resultat obtingut després de l'aplicació del segon algoritme sobre les dades experimentals, amb un senyal extern afegit. Com que el mètode demostra ser efectiu (revela la presència del senyal de control en la sèrie de dades) i funciona d'acord amb les nostres prediccions estadístiques, relaxarem la restricció imposta sobre la freqüència. D'aquesta manera dos nous mètodes de filtrat per freqüències arbitràries es desenvolupen: el primer per sorolls amb espectre conejat, el segon per a espectres desconeguts. Discutim un altre cop el comportament probabilístic dels nostres algoritmes de cerca, el que ens permetrà de fer afirmacions estadístiques en relació als resultats rellevants que obtenim just després de l'aplicació massiva del procediment de filtrat sobre un període de sis mesos de dades enregistrats pel detector *Explorer* l'any 1991.

R.1.4 Notació miscel.lània

- En els objectes tensorials o pseudotensorials, els índexs grecs van de zero fins a tres, mentre que un de llatí ho fa d'u a tres.

- El tensor mètric de l'espai-temps, $g_{\mu\nu}$, té la signatura -+++.
- El conveni d'Einstein de la suma sobre índexs repetits es fa servir per a quantitats tant tridimensional com quatre-dimensionals.
- Les derivades parcials respecte x^μ apareixen en el text amb la forma d'una coma $_{,\mu}$.
- Les derivades parcials respecte la variable x apareixen en el text o bé en la forma $\partial/\partial x$ o bé com ∂_x .
- \square denota l'operador de D'Alembert en l'espai-temps de Minkowski.
- Índex dintre d'un parèntesi expressen l'operació de simetrització respecte ells mateixos, per exemple $\epsilon^{(\mu,\nu)} \equiv (\epsilon^{\mu,\nu} + \epsilon^{\nu,\mu})/2$.
- El barret (^) està sempre collocat sobre els vectors Cartesians unitaris.
- El complexe conjugat de qualsevol quantitat es representa per mitjà d'un asterisc (*).
- Les parts reals i imaginàries d' A són $\Re\{A\}$ i $\Im\{A\}$, respectivament.
- La transformada de Fourier (ja sigui discreta o contínua) d' A la denotarem amb una titlla, \tilde{A} .
- Representarem la freqüència angular relacionada amb f_x per mitjà de ω_x , és a dir, $\omega_x = 2\pi f_x$.
- G és la constat universal de gravitació de Newton, c és la velocitat de la llum en el buit, i K_B és la constant de Boltzmann.

R.2 Les ones gravitatòries

R.2.1 Introducció

Aquest capítol està dedicat a l'estudi dels processos físics que ens hem plantejat de tractar, les ones gravitatòries, amb especial atenció a les monocromàtiques: la seva predicció [29] per la Relativitat General [28], les seves propietats, la

generació d'aquest tipus de radiació [30], la seva propagació i els efectes previsibles que pot arribar a produir en un objecte extens, que actuï eventualment com a detector [64].

Començarem amb l'aproximació lineal de la teoria de la gravitació d'Einstein, on la gravetat es pot pensar com una petita pertorbació mètrica de l'espai-temps pla. Seguirem el procediment estàndard que porta a l'equació d'ones que aquestes quantitats (una mesura de la desviació de la mètrica real respecte de la de Minkowski) han de complir. Veurem, així mateix, com les ones gravitacionals que són descrites per una matriu simètrica amb, en principi, deu termes independents, poden ser totalment (i localment) caracteritzades amb només dues funcions. Mostrarem la forma explícita, sota certes condicions, d'aquestes funcions quan la font és un objecte que gira, com ara un púlsar.

Un cop haurem mostrat quin aspecte té l'ona emesa, ens dirigirem cap al problema que envolta la descripció de l'ona rebuda. El nostre interès es centrarà en el cas en què l'observatori gravitacional està ubicat en una posició fixa sobre la superfície de la Terra, una situació que distorsionarà, des del punt de vista de l'antena, l'ona que arriba [65, 43]. Per una banda, l'existència d'una velocitat relativa entre la font i el detector, causat principalment pels moviments tant orbital com de rotació de la Terra, produirà un corriment en freqüències: el conegut efecte Doppler. Per una altra banda, el propi moviment de rotació del nostre planeta duu com a resultat una variació de l'alignament, respecte de la font, de qualsevol antena direccional. La suma de totes aquestes contribucions serà l'objectiu del nostre procediment de recerca.

R.2.2 Ones gravitatoris

En tota teoria mètrica de la gravitació, com ara la Relativitat General, les forces gravitacionals es tradueixen en geometria, geometria de l'espai-temps [64]. Les ones gravitatoris, aleshores, no són altra cosa que plecs que viatjan per aquest espai-temps i que modifiquen quantitats geomètriques, com ara distàncies pròpies, dels llocs que travessen. Aquesta distorsió de la geometria es veurà reflectida en una tendència envers la modificació de les formes i dimensions dels objectes materials. Aleshores es diu que aquests són afectats per *forces de marea*, en referència a l'efecte que fa pujar i baixar el nivell de les aigües oceàniques.

En aquesta secció recordarem com, en el marc del límit de camp feble de la gravetat d'Einstein, apareix una equació d'ones. Provarem de repassar els

aspectes més fonamentals d'aquest tipus de radiació, incloent-hi un test *a posteriori* del grau d'exactitud de l'aproximació que hem considerat: calcularem l'amplitud de les ones gravitacionals procedents d'un distant objecte rígid que es troba girant *lentament*, i veurem com són de febles. Aquest model per a la font també ens proporcionarà informació explícita de la forma d'ona de la radiació emesa.

Concloureml aquest punt amb un exemple quantitatius de l'efecte d'una ona plana monocromàtica sobre un conjunt de partícules puntuals que no interactuen entre si, fent èmfasi en les similituds i diferències en el seu comportament en funció de la polarització de l'ona.

R.2.3 L'efecte Doppler

Com ja hem dit, estem interessats en la recerca d'ones que originalment són monocromàtiques. És més, les volem *veure* amb una antena gravitacional ubicada a la superfície de la Terra. Aleshores, si l'ona és emesa per un objecte que no està en repòs respecte el detector, la seva freqüència característica es veurà modificada pel clàssic efecte Doppler. Si suposem que la font és un objecte astronòmic que no té cap velocitat peculiar respecte el sistema dels estels fixos (és a dir, no forma part, per exemple, d'un sistema estelar doble) solament haurem de considerar dues contribucions principals que afecten el canvi en la freqüència de l'ona: la rotació de la Terra i el seu moviment orbital al voltant del Sol.

R.2.4 L'orientació

En aquesta secció considerarem el cas d'un cos sólid aproximadament unidimensional, que interacciona amb una ona gravitacional. En aquest cas, les úniques deformacions relevantes induïdes per la pertorbació mètrica són aquelles que proven de canviar la longitud de l'objecte. Així doncs, haurem de considerar només la component de l'acceleració relativa, que apareixerà entre dos punts qualsevol de la *barra*, en la direcció paral·lela amb aquesta.

Òbviament, les variacions al llarg del temps de l'acceleració poden tenir el seu origen en la dependència temporal de la força gravitacional, però també en qualsevol canvi extern de l'orientació, respecte l'ona, del nostre detector amb forma de barra. En el cas d'antenes terrestres, l'agent que provoca canvis en la direcció és simplement la rotació de la Terra. En aquest sentit, el nostre

objectiu és arribar a expresar el vector unitari que marca aquesta direcció en la base pròpia de l'ona plana incident, on la perturbació mètrica es caracteritza mitjançant dues funcions o *polaritzacions*.

R.2.5 La forma global d'ona

Acabarem aquest capítol posant en comú les diferents contribucions a la forma funcional final de la força externa, l'efecte de la qual volem detectar.

R.3 L'antena

R.3.1 Introducció

Desenvoluparem en aquest capítol els aspectes claus relatius al detector: l'antena criogènica ressonant *Explorer* [2, 3, 6].

Començarem amb una descripció general de la forma en què funciona el detector. Hem afirmat en el capítol previ que quan una ona gravitacional interacciona amb un cos extens té tendència a modificar la forma d'aquest objecte, i hem mostrat de manera explícita aquest efecte tot analitzant el comportament d'un conjunt de partícules puntuals que no interactuen entre si, disposades circularment. En el cas que ara ens ocupa, en canvi, l'objecte del nostre estudi és un cilindre metàl·lic i les deformacions que prendrem en consideració són aquelles que fan canviar la seva llargària. Així doncs, usarem la teoria de l'elasticitat aplicada a un medi finit unidimensional, amb l'objectiu de derivar i resoldre les equacions que compleixen els extrems de la barra. És més, mostrarem com el comportament dels esmentats extrems del cilindre elàstic poden ser satisfactoriament descrits mitjançant un model d'oscil.lador harmònic.

Tot i això, la barra metàl·lica no és l'únic component del detector *Explorer*. Les vibracions del cilindre són amplificades i transformades amb variacions de voltatge gràcies a un transductor ressonant [21, 16] col.locat en contacte amb ell. El voltatge elèctric es transforma subsegüentment en flux magnètic amb el que s'alimenta un d.c. SQUID, un aparell superconductor d'interferència quàntica que actua com a amplificador del senyal [19]. Aquest senyal és finalment enregistrat, conjuntament amb més informació útil provenint d'altres sensors de l'antena, en format binari.

Tot aquest procés d'adquisició de dades ha de ser realitzat tot intentant de mantenir el nivell de soroll tan baix com sigui possible. Això si realment volem detectar la presència de les febles pertorbacions que una ona gravitacional hi causaria. Amb aquest propòsit el detector s'aïlla mecànicament del món exterior gràcies a un conjunt de sistemes d'esmorteïment consecutius. És més, la major part dels components de l'antena (la barra, el transductor, el d.c. SQUID...) es refredan fins la temperatura de l'heli líquid, 2.6 graus Kelvin. Això redueix les pertorbacions degudes a les vibracions tèrmiques de les parts constitutives de l'aparell experimental.

Resseguint amb els resultats corresponents al propi cilindre, modelarem el comportament de tot l'aparell físic fent servir un sistema mecànic fet de molles, esmorteïdors i masses. Obtenim les solucions de les equacions derivades del model i aleshores les apliquem al cas en què la força externa prové de la interacció d'una ona gravitacional monocromàtica amb la barra.

Així mateix, dedicarem un temps a l'estudi de l'inevitabile company del senyal en qualsevol mesura experimental: el soroll. Revisarem les contribucions més importants a aquest procés pertorbatiu, i les propietats que hi exhibeix, perquè només amb un coneixement precís dels trets característics d'ambdós, senyal i soroll, serem capaços de distingir l'un de l'altre.

Concloureml el capítol amb una descripció detallada dels continguts dels fitxers informàtics que el sistema d'adquisició de dades de l'antena *Explorer* genera amb la variada informació que el detector registra.

R.3.2 Barres elàstiques i ones gravitatòries

En aquesta secció presentem com una ona gravitacional feble s'acobla amb un objecte elàstic. Donat que el nostre interès es concentra en el comportament dels extrems d'un cilindre d'alumini, dirigirem la nostra atenció cap a l'estudi de les barres elàstiques finites d'una dimensió. És més, el nostre propòsit final és arribar a mostrar com un objecte extens pot ser correctament descrit mitjançant un model d'oscil.lador harmònic, un cop s'han redefinit els paràmetres característics d'una manera adequada. Així doncs, hem seleccionat un sistema relativament net: no hem considerat ni esmorteïment ni acoblament amb altres forces que no sigui l'externa.

R.3.3 L'aparell experimental

Hem vist a la secció prèvia perquè una barra elàstica és un candidat factible (i fàcil de modelar) per ser escollit com a antena d'ones gravitacionals. Al llarg d'aquesta secció anem a descriure amb força detall el detector *Explorer*, l'aparell experimental les dades del qual analitzarem en aquest treball. Com veurem en breu, aquest és una mica més complexe que una simple barra elàstica. L'*Explorer* consisteix en una barra cilíndrica d'alumini equipada amb un transductor ressonant capacitiu connectat a un amplificador d.c. SQUID, via un transformador superconductiu. Tot el conjunt està envoltat per varíes capes concèntriques formant cavitats intermèdies que, o bé s'omplen amb agents refrigerants, o bé són tancs al buit que actuen com a aïllants tèrmics. Així es pot veure a la Figura 3.2.

El detector està ubicat en els laboratoris del *CERN*, 6.1 graus de longitud est, 46.2 graus de latitud nord, i orientat 39.3 graus cap a l'est, respecte la direcció nord local.

R.3.4 L'acoblament dels ressonadors

Presentarem aquí el conjunt d'equacions i la seva solució, que han de complir els desplaçaments petits entre l'extrem de la barra i la placa lliure del transductor. Tal com hem assenyalat a la passada secció, el model ha de tenir en compte els ressonadors mecànics però no l'elèctric. Encara que nosaltres no considerarem cap mena de terme d'acoblament entre els dos tipus de sistemes ressonants, donarem arguments que recolzen el fet que el valor d'alguns paràmetres ve donat a la pràctica per l'amplificador electrònic.

R.3.5 La resposta de l'antena a una ona gravitatòria

Abans de tractar amb ones gravitacionals hem d'assenyalar que degut a la relativa magnitud dels termes que acompanyen les forces que actuen sobre la barra i el transductor haurem de menysprear l'efecte de la radiació gravitatòria en aquest darrer.

El valor apropiat per a la pertorbació externa que actua sobre la barra i que relacionem amb una ona gravitacional plana, surt directament de la banda dreta de l'equació (2.94), amb l'única particularitat remarcable de que hem de substituir ℓ_0 per la longitud efectiva de la barra, ℓ_b , relacionada amb les

veritables dimensions del cilindre elàstic, L_b , mitjançant l'equació (3.25). La resposta de l'antena l'obtindrem primer d'una manera rigurosa i formal, però poc útil; i després d'una manera aproximada però que s'adaptarà de manera exacta a les nostres necessitats.

R.3.6 El soroll

Desafortunadament, el detector dóna resposta no solament a la possible influència d'un senyal gravitacional, sinó que, amb diferent grau, es veu afectat per qualsevol pertorbació interna o externa, [35, 70, 6]. És això el que anomenarem soroll: qualsevol agent aleatori que actui sobre l'antena. Degut a la seva naturalesa estocàstica intrínseca, el soroll no pot ser correctament representat per una funció del temps determinista. Això no significa que no sabem res d'ell. En alguns casos podem preveure no solament la seva presència sinó les seves propietats definitòries. Un bon exemple d'aquesta situació és l'inevitabile soroll tèrmic.

Tots els cossos, degut al senzill fet de mantenir una temperatura per sobre del zero absolut, vibren. El detector *Explorer*, a l'època que va recollir les dades que nosaltres analitzarem, va ser refredat fins una temperatura d'uns 2.6 Kelvin, per així minvar l'amplitud de les pertorbacions tèrmiques que afecten tant al cilindre com al transductor.

A més del soroll que acabem de descriure, haurem de fer front a l'aparició ocasional de soroll no estacionari de múltiple procedència, potser en la forma d'espuris pics esmolats com ara aquells de la Figura 3.5. Haurem de poder diferenciar-los dels veritables senyals gravitatoris basant-nos en les seves propietats distintives.

R.3.7 El sistema d'adquisició de dades

Com hem assenyalat en altres seccions, només a les proximitats dels dos mòduls ressonants tindrem oportunitats de detectar una ona gravitacional. Per tant, és inútil guardar la informació corresponent a l'exterior d'aquest rang de freqüències. L'objectiu dels processos que descriurem en aquesta secció és precisament treure totes les components de Fourier del senyal tret d'aquelles aproximadament compresses entre els 900 i els 927.5 Hz.

La informació així preparada s'emmagatzema juntament amb d'altres paràmetres valuosos del sistema en forma de fitxers informàtics codificats en el

format **R87**, descrit a l'Apèndix B.

R.4 L'anàlisi de dades

R.4.1 Introducció

L'objectiu de l'anàlisi de dades és obtenir la màxima quantitat d'informació referent al senyal tot i l'efecte pertorbatiu del soroll. En el soroll, com s'ha mencionat al capítol previ, es condensa l'acció d'agents incontrolats o incontrolables que afecten al detector d'una manera, en algun sentit unpredictable. Així doncs, aquest no mostrerà un comportament determinista sinó aleatori. En aquest capítol desenvoluparem diverses estratègies amb el propòsit de discernir entre soroll i senyal. Disenyarem els algoritmes a partir de la tècnica ben coneguda en l'anàlisi de dades del "matched filter", o filtre adaptat.

El "matched filter" (el millor filtre lineal que es pot concebre si es donen certes condicions que explicarem àmpliament en el texte) com a qualsevol altre procediment de filtrat digne de confiança necessita d'informació precisa sobre ambdós, senyal i soroll. L'assumpció més rellevant que haurem de fer en el cas d'aquest darrer és que el soroll pot ser modelat satisfactòriament mitjançant un procès estocàstic gaussià, mentre que l'objectiu del nostre procediment de recerca serà, com hem anunciat repetidament, una ona monocromàtica, una funció sinusoidal de freqüència característica constant, però desconeguda. Les consecuències que el corrent Doppler produiran en la forma d'ona si el senyal té un origen astronòmic no es tindran totalment en compte en primera instància, sinó que es consideraran i es corregiran *a posteriori*. Donat que les coordenades celestes de qualsevol possible font seran també desconegudes per nosaltres, disenyarem un procediment de cerca que inclogui tot el cel.

Dos algoritmes principals es desenvolupen al llarg d'aquest capítol dedicat a l'anàlisi de dades, depenen d'un tret particular de la freqüència de l'ona. Qualsevol procés de filtrat no pot comprovar la presència del senyal per tots els possibles valors (un continu, de fet) que la seva freqüència pot prendre, inclòs el cas en què la banda espectral considerada tingui extensió limitada. És per això que només un conjunt finit de freqüències es poden tenir en compte, els valors dels quals vénen dictats pel procediment de la transformada discreta de Fourier. El primer mètode assumeix que la freqüència que realment té l'ona és precisament una de les de l'espectre de Fourier de les dades [52]. S'assoleix

així una millora en el rendiment del filtre respecte de l'algoritme més usual — promitjar el quadrats del mòduls de les transformades de Fourier. Il·lustrarem el bon funcionament de la nostra tècnica tot afegint un senyal de control a les dades reals. També mostrarem el grau de concordància entre les prediccions teòriques i el comportament experimental de l'algoritme.

En canvi, si cap freqüència en el banc de filtres correspon exactament a la pròpia del senyal, el mètode anterior es torna poc útil quan analitzem porcions llargues de dades. Aleshores, disenyarem un segon procediment amb la intenció de relaxar la limitació de freqüències abans descrita i d'estalviar-nos aquest efecte [53]. El preu que haurem de pagar es centra principalment en un nou rendiment del filtre que decreix respecte al que correspon a l'algoritme previ. Les propietats del filtre són investigades un cop més abans que l'algoritme s'apliqui extensivament a sis mesos de dades reals enregistrades pel detector *Explorer* al llarg de l'any 1991.

Després del processat massiu de dades assenyalarem la presència d'uns resultats que difícilment poden ser produïts per la natura aleatòria del soroll. L'origen d'aquests notoris candidats a senyals gravitatoris no serà discussió en aquest treball, limitarem les nostres conclusions a la simple presència d'aquests resultats positius estadísticament rellevants.

Finalment, el lector pot estar interessat en fer una ullada a l'Apèndix C, on podrà trobar el codi font dels programes en llenguatge C que hem dissenyat amb el propòsit d'implementar tots aquests algoritmes, a més d'altres eines informàtiques d'utilitat.

R.4.2 Filtrat de dades

Qualsevol fluxe experimental de dades pot o no contenir la informació justa que ens interessa, allò que genèricament diem *el senyal*, però si realment hi és, estarà indubtablement amagat pel soroll. Com hem mencionat al capítol previ, la presència d'aquest agent pertorbatiu de comportament aleatori a la sortida del detector es troba sempre garantida i, considerant la previsible feblesa de qualsevol mena d'ona gravitacional, i més encara si són monocromàtiques, amenaça seriosament d'emmascarar completament el propi senyal.

D'acord amb això, el primer objectiu de qualsevol procès de filtrat serà donar rellevància al senyal i, simultàniament, disminuir el nivell de soroll en les dades. El resultat d'aquest balanç, usualment mesurat amb l'anomenada *relació senyal-soroll*, determinarà les possibilitats de detecció d'aquell senyal

en particular. En segon lloc, després del procés d'anàlisi haurem de ser capaços d'assegurar no només la presència del senyal a les dades experimentals, sinó els valors concrets dels diferents paràmetres d'aquest, en el nostre cas la freqüència i l'amplitud. Quan més propietats de l'ona, com ara el seu estat de polarització, puguin ésser estimats, l'anàlisi del resultat del filtrat permetrà de calcular la localització al cel de la font de radiació, el primer pas cap a l'astronomia gravitacional.

R.4.3 Els senyals monocromàtics i l'espectre del soroll

Al llarg de les darreres quatre seccions desenvolupem aproximacions successives al problema genèric de detectar un senyal monocromàtic de freqüència fixa però arbitrària immers en un soroll d'espectre també desconegut. Començarem pel cas més senzill en què per una banda suposem que tenim un mitjà accesorí per calcular la densitat espectral del soroll i que, per altra banda, el senyal monocromàtic està contingut en una única component espectral de Fourier, de entre totes les que analitzarem. Un cop dissenyada l'estratègia més adient, i que millora en eficàcia la fins ara més comuna, analitzarem les seves propietats estadístiques més rellevants: densitat de probabilitat del resultat del procés de filtrat en presència o absència de senyal, els seus valors esperats, la relació senyal-soroll, etcètera. El mateix farem amb la resta d'algoritmes que presentarem.

El segon d'aquests resoldrà el problema anteriorment passat per alt de la mesura de les propietats característiques del soroll. El nou mètode estimarà la densitat espectral del soroll per cadascuna de les freqüències i inclourà aquest valor en el propi procés de filtrat. Això permetrà la seva aplicació a dades reals, a les quals hi afegirem un senyal de control per tal de comprovar el funcionament i l'eficàcia del sistema d'anàlisi.

Un cop considerat aquest pas intermig, encetarem la cerca de senyals que es puguin extender per més d'una component espectral. Tornarem a suposar que l'espectre del soroll és conegut, per tal que aquesta complicació afegida no destorbi en el disseny del nou algoritme. Un cop assolit amb èxit el nostre propòsit estudiarem d'afegir un nou estimador de la densitat espectral del soroll inspirat en el presentat anteriorment. El resultat final s'aplicarà de forma extensiva i sistemàtica als sis mesos de dades enregistrades per l'antena criogènica *Explorer* entre els mesos de juny i novembre de l'any 1991.

Gràcies a les eines probabilístiques que, com hem esmentat, desenvolupem

de manera paral·lela als algoritmes de filtrat, serem capaços de treure conclusions estadístiques dels notoris resultats aconseguits un cop el procès massiu ha tingut lloc. En canvi, l'origen d'aquests senyals no serà motiu de discussió en aquest treball, tot i que s'inclouen les amplituds que, segons el nostre mètode, haurien de tenir les ones gravitatoris si en veritat fossin responsables dels senyals detectats.

R.5 Conclusions

Tancarem aquesta exposició amb una revisió general dels temes desenvolupats i dels resultats principals aconseguits.

Aquest treball, tal com revela el mateix títol, està dedicat a la recerca de senyals monocromàtics gravitatoris amb les dades del detector criogènic *Explorer*. Amb aquest propòsit diverses estratègies de filtrat han estat disenyades i aplicades. Amb tot i això, donat que un coneixement detallat de la resposta del detector a l'ona incident és necessari en el desenvolupament d'aquests algoritmes, hem començat la nostra exposició amb un estudi detallat del senyal i de l'antena. De fet, el nostre propòsit final era escriure un texte autoconsistent, abastant la majoria d'aspectes del complex problema que ens hem plantejat. Desitjem que el lector trobi que aquest objectiu ha estat acomplert.

Presentem en aquest apartat final una llista que resumeix la nostra activitat i on hem *enfatitzat* les nostres contribucions principals.

- Hem revisat l'aproximació lineal de la Relativitat General i també hem fet servir la fórmula quadrupolar estàndard per obtenir la forma d'ona de la radiació gravitacional emesa per un cos sòlid en rotació. Hem calculat, aleshores, la forma d'ona rebuda en el cas en què la font és un objecte astronòmic (com ara un púlsar aïllat) i el detector està ubicat a la superfície de la Terra, tot i tenint en compte:
 - el coriment en freqüències causat a l'ona monocromàtica per l'efecte Doppler relacionat amb els moviments orbitals i de rotació del nostre planeta, i
 - les variacions temporals en l'amplitud de l'ona gravitacional degut al canvi en l'orientació del nostre detector direccional, conseqüència d'un altre cop del moviment rotatori de la Terra.

Hem expressat els resultats en termes de paràmetres *geogràfics* (longituds, latituds...) i *astronòmics* (declinacions, ascensions rectes...) típics, i d'aquesta manera poden ser calculats *directament* mitjançant la informació que es pot trobar a qualsevol taula d'efemèrides.

- Hem perfilat la forma en què la pertorbació mètrica s'acobla amb el cilindre ressonant, basant-nos en la teoria de l'elasticitat. També hem descrit la resta de components de l'antena criogènica *Explorer* i hem derivat les equacions que determinen el comportament del detector. Hem resolt aquestes equacions en el cas en que el sistema es vegi afectat per una ona gravitacional monocromàtica originada en una font astronòmica. La resposta del detector va ser obtinguda en primer lloc d'una manera força formal i després recalculada gràcies a un desenvolupament aproximatiu. Aquests *resultats explícits* no es troben a la literatura consultada.
- Hem dissenyat *dos nous algoritmes de filtrat* per detectar senyals monocromàtics *que mostren un millor rendiment* que la tècnica més comú de promitjar mòduls quadrats de transformades de Fourier de sèries experimentals de dades. De fet, la nostra estratègia principal es basa en l'estimació de tant el mòdul *com la fase* del senyal. El primer d'aquests mètodes esmentats s'ha d'aplicar quan la freqüència del senyal és una en el nostre banc espectral, mentre que el segon s'ajusta al cas més general d'un senyal amb freqüència arbitrària, però donada. Donat que en el darrer supòsit no imosem *cap restricció* en els paràmetres de l'ona, la relació senyal-soroll que aconseguim amb el procediment de filtrat associat és lleugerament inferior a la corresponent al primer cas, on hem assolit el *mateix resultat* que hauríem obtingut analitzant tot el conjunt de dades en un únic filtrat.
- Les dues estratègies de filtrat van ser desenvolupades tot i assumint en primer lloc que la densitat espectral del soroll era una quantitat coneguda. Una generalització de tots dos algoritmes amb un *estimador espectral incorporat* va ser implementat fent possible d'aquesta manera la seva aplicació directa quan aquesta informació espectral no és a l'abast per uns altres mitjans. En tots els casos un *ampli estudi probabilístic* dels procediments de cerca va ser realitzat amb el propòsit d'*evaluar i donar significat* els resultats així produïts.



Biblioteca de Física i Química

R.5. Conclusions

183

- L'algoritme per freqüències arbitràries i soroll d'espectre desconegut va ser aplicat extensivament amb l'objectiu de realitzar un filtrat *massiu* de les dades registrades pel detector *Explorer* entre el juny i el novembre de l'any 1991. El resultat d'aquest processat sistemàtic va ser analitzat tenint en compte els possibles efectes que eventualment causarien sobre el senyal el *corriment espectral Doppler*, i aplicant *raonaments probabilístics* basats en el ben conegut criteri de Neyman-Pearson. Fruit d'aquesta cerca, diferents resultats *estadísticament rellevants* van ser trobats. Revelar l'origen d'aquests resultats positius és tema d'un posterior (i més profund) estudi.

